



Institut für Erd- und Umweltwissenschaften
Mathematisch-Naturwissenschaftliche Fakultät
Universität Potsdam



THE ROLE OF EXTENSION DURING THE EVOLUTION OF THE NW INDIAN HIMALAYA

DISSERTATION

zur Erlangung des akademischen Grades
doctor rerum naturalium (Dr. rer. nat.)

in der Wissenschaftsdisziplin

Geologie

eingereicht

an der Mathematisch-Naturwissenschaftlichen Fakultät

der Universität Potsdam

von

Dipl.-Geophys. **Esther Hintersberger**

geboren am 14.07.1979 in Augsburg

Potsdam, Januar 2013

Published online at the
Institutional Repository of the University of Potsdam:
URL <http://opus.kobv.de/ubp/volltexte/2013/6617/>
URN <urn:nbn:de:kobv:517-opus-66179>
<http://nbn-resolving.de/urn:nbn:de:kobv:517-opus-66179>

To the next generation

EIN GROSSES DANKESCHÖN

... an Manfred Strecker, meinem Betreuer, der nie aufgegeben hat, an mich (bzw. an die Fertigstellung dieser Arbeit) zu glauben; der bei den vielen Rückschlägen gerade zu Beginn immer irgendwelche Lösungen und aufmunternde Worte parat hatte; und der mir vermittelt hat, wie spannend Geologie doch selbst für Geophysiker sein kann.

... an Rasmus Thiede, der mich zum ersten Mal mit in den Himalaja genommen hat und mir damit den Zugang zu einer faszinierenden Landschaft und Kultur zeigte, und der auch während der Doktorarbeit durch die Unwegigkeiten von Publikationen und anderen Komplikationen mir immer ein wichtiger und wohlwollender Ratgeber war.

... an Kurt Decker, der in Wien immer wieder Verständnis dafür hatte, wenn ich mal wieder die Doktorarbeit der eigentlichen Arbeit vorzog.

... an Tashi Tsering und Ram Sing Slathia, die mich stets sicher durch die unmöglichsten Situationen während der Geländeaufenthalte führten und all meine ihnen sicher manchmal absonderlich anmutenden Wünsche und Vorstellungen nicht nur geduldig ertrugen, sondern sie auch noch verwirklichten.

... an Frank Scherbaum, Frank Krüger, Christian Haberland und Daniel Vollmer sowie unsere indischen Kooperationspartner Irene Sarkar und Sushil Kumar für ihre Unterstützung bei dem sich im Nachhinein als aussichtslos herausstellendes Vorhaben, ein seismisches Netzwerk in der Grenzregion zwischen Indien und Tibet zu errichten.

... an Stephanie Neuhuber und Angela Landgraf, die fast jedes der Kapitel auf Logik, Schreibfehler und sonstige Ungereimtheiten durchsuchten und die schließlich ganz wesentlich zur Beendigung der vorliegenden Arbeit durch die generöse Überlassung ihres Blockhauses bzw. ihrer Couch und ihres Küchentisches beigetragen haben.

... an Dana, Manu, Reyko, Janek, Helene, Leila, Gela, Nele, Jojo, Taylor, Urs, Gesine, Nina, Sascha, Oli, Berit und Juliane für eure Freundschaft, ungezählte Eisbecher, Abendessen, Klettereien, Schwimmereien, unvergessliche Geländeaufenthalte und Urlaube und all die vielen kleinen, aber abenteuerlichen Dinge, die das Leben lebenswert und meine Zeit in Potsdam unvergesslich machen.

... an die Potsdamer Bürokollegen Gela, Micha, Paolo, Henry, Amoury und Dirk sowie die Wiener Bürokollegen Stefi, Dana, Clemens, Toni, Andras, Andi, Helene, Maria und Eun Young für die gemeinsam verbrachten Arbeitstage, viele Diskussionen über unzähligen Kaffeebechern und Aufmunterungen.

... an Julian für die schöne gemeinsame Zeit und die Unterstützung in einer der schwersten Zeiten meiner Doktorarbeit.

... an Andreas Gaab, ohne den diese Doktorarbeit sicherlich in Word geschrieben worden wäre, für seine inzwischen schon lange zurückliegende Missionarsarbeit in Sachen \LaTeX .

... und an meine Familie für ihre 1000%ige Unterstützung und Zuversicht in all der Zeit.

Abstract

The evolution of most orogens typically records cogenetic shortening and extension. The phenomenon of pervasive normal faulting in an orogen, however, has been related to late syn- and post-collisional stages of mountain building, while shortening is focused along the peripheral sectors of the orogen. While localized extensional processes constitute an integral part of orogenic evolution, the spatiotemporal characteristics and the kinematic linkage of structures related to shortening and extension in the core regions of the orogen are often not well known. The Himalaya and the Tibetan Plateau exemplify these problems very well and this region may serve as an analog for the impact of normal faulting in late-stage evolution of a collisional mountain belt. Related to the India-Eurasia collision, the Himalaya forms the southern margin of the Tibetan Plateau and constitutes the most prominent Cenozoic type example of a collisional orogen. While thrusting is presently observed along the foothills of the orogen, several generations of extensional structures have been detected in the internal, high-elevation regions, both oriented either parallel or perpendicular to the strike of the orogen. In the Sutlej-Spiti river valleys and the Garhwal Himalaya of the NW Indian Himalaya, earthquake focal mechanisms, seismites and ubiquitous normal faulting in Quaternary deposits, and regional GPS measurements reveal ongoing E-W extension in this area. In contrast to other extensional structures observed in the Himalaya, this extension direction is neither parallel nor perpendicular to the NE-SW regional shortening direction.

In this study, I took advantage of this unique setting of obliquity between the trend of the orogen and structures related to E-W oriented extension in order to address the question of the driving forces of E-W extension. Thus, the main topic of this work is whether E-W extension in the NW Indian Himalaya is triggered by processes within the Tibetan Plateau or, similar to arc-parallel and arc-normal extension, originates from the curvature of the Himalayan orogen. In order to document these relationships, I present new fault-kinematic data based on systematic measurements of approximately 2000 outcrop-scale brittle fault planes with displacements of up to several centimeters that cover the region from the Tibetan Himalaya to the southern mountain front in the NW Indian Himalaya. This new data set, as well as field observations including structural cross-cutting relationships, mineral fibers on fault planes, and correlations with deformation structures in lacustrine sediments allows me to distinguish different deformation styles and to establish a relative chronology of deformation styles. One of the main results are that the overall strain pattern derived from this data reflects the regionally important contractional deformation pattern very well, but also reveals significant extensional deformation. In total, I was able to identify six deformation styles, most of which are temporally and spatially linked and represent protracted shortening. The four dominant deformation styles are: (1) shortening parallel to the regional convergence direction between India and Eurasia; (2) arc-normal extension; (3) arc-parallel extension; and (4) E-W extension. This is the first data set where a succession of both, arc-normal and E-W extension have been documented in the Himalaya.

My observations also furnish the basis for a detailed overview of the younger extensional deformation history in the NW Indian Himalaya. In addition to the

fault-kinematic field data, I focused on assessing field and remote-sensing based geomorphic analyses, and generated geochronologic $^{40}\text{Ar}/^{39}\text{Ar}$ data on synkinematic muscovites along normal faults to help elucidate the style and timing of extension in the NW Indian Himalaya. According to my new geochronologic results, widespread extension must have started at approximately 14-16 Ma, if not earlier. In addition, I documented and mapped fault scarps in Quaternary sedimentary deposits using satellite imagery and field inspection. Furthermore, I made field observations of regional normal faults in the Greater Sutlej Region (Spiti, Lahul, Kinnaur) and the Garhwal Himalaya, compiled structures from geological maps and put them in a regional context. Finally, I documented seismites in lake sediments close to the currently most active normal fault in the study area in order to extend the (paleo)seismic record of this particular fault. Taken together, this data sets document that E-W extension is the dominant active deformation style in the internal parts of the orogen. In addition, the combined field, geomorphic and remote-sensing data sets prove that E-W extension occurs in a much more larger region toward the south and west than the seismicity data have suggested.

In conclusion, the data presented in this study reveal the importance of extension in a region, which is still dominated by ongoing collision and shortening. The regional fault distribution and cross-cutting relationships suggest that extension parallel (NW-SE oriented in the NW Indian Himalaya) and perpendicular (NE-SW oriented in the NW Indian Himalaya) to the strike of the orogen are an integral part of the southward propagation of the active thrust front and the associated lateral growth of the Himalayan arc. In the light of a wide range of models proposed for extension in the Himalaya and the Tibetan plateau, I propose that E-W extension in the NW Indian Himalaya is transferred from the Tibetan Plateau due the inability of the Karakorum fault (KF) to adequately accommodate ongoing E-W extension on the Tibetan Plateau. This implies that the KF does not form a primary decoupling horizon for crustal deformation between the Tibetan Plateau and the Himalaya, as proposed previously. Furthermore, in line with other observations from Tibet, the onset of E-W normal faulting in the NW Himalaya may also reflect the attainment of high topography in this region, which generated crustal stresses conducive to spatially extensive extension.

Zusammenfassung

Das gleichzeitige Auftreten von Verkürzung und Extension ist charakteristisch bei der Entstehung der meisten Kollisionsorogene. Eine bis heute gültige These der Orogenese beschreibt ein weit verbreitetes Auftreten von Abschiebungen jedoch erst in späteren syn- bzw. sogar erst in post-kollisionalen Stadien der Gebirgsbildung, während Verkürzung über die gesamte Orogenese an den Gebirgsrändern zu beobachten sei. Während somit räumlich begrenzte Extensionsprozesse einen wesentlichen Bestandteil der Orogenese darstellen, sind sowohl die räumlichen und zeitlichen Abfolge von extensions- bzw. verkürzungsbedingten Strukturen sowie deren kinematische Kopplung nur wenig gesichert. Der känozoische Himalaja, durch die Kollision von Indien und Eurasien entstanden, bildet den südlichen Rand des tibetischen Hochplateaus und stellt einen typischen Vertreter eines Kollisionsorogens dar. Während derzeit an der Peripherie des Orogens Überschiebungen beobachtet werden, können mehrere Generationen an Extensionsstrukturen in den hochgelegenen Regionen des Himalajas dokumentiert werden, die sowohl parallel als auch senkrecht zum Streichen des Orogens verlaufen. Im NW Indiens zeugen Herdflächenlösungen von Erdbeben, weit verbreitet auftretende Abschiebungen und Seismite in pleistozänen Ablagerungen sowie regionale GPS-Daten in dem Gebiet der Sutlej- und Spiti-Flüsse und im Garhwal-Himalaja von aktiver E-W-Extension. Im Gegensatz zu anderen im Himalaja beschriebenen Extensionsstrukturen, ist diese Extensionsrichtung weder parallel noch senkrecht zur NE-SW orientierten regionalen Verkürzungsrichtung.

In der vorliegenden Arbeit nutze ich diesen schrägen Winkel zwischen der Ausrichtung des Orogens einerseits und derjenigen der mit E-W-Extension assoziierten Strukturen andererseits, um die durch Prozesse im Tibet-Plateau ausgelöste E-W-Extension von der parallel bzw. senkrecht zum Himalaja-Bogen orientierten Extension, die bedingt durch dessen Krümmung entstand, sowie von Strukturen, die von der noch andauernden Verkürzung stammen, zu unterscheiden. Um dies zu belegen, präsentiere ich hier einen neuen störungskinematischen Datensatz, der aus systematischen Messungen von ca. 2000 spröden Störungsflächen im Aufschlussmaßstab besteht. Diese Störungsflächen mit Versätzen bis zu mehreren Zentimetern sind über den gesamten Bereich des NW indischen Himalaja vom Tibetischen Himalaja im Norden bis fast zur südlichen Gebirgsfront verbreitet. Zusammen mit Geländebeobachtungen, strukturellen Überschneidungskriterien, Mineralwachstum auf Störungsflächen und der Korrelation von seismischen Ereignishorizonten in Seesedimenten ermöglicht mir dieser neue Datensatz, zwischen unterschiedlichen Deformationsarten zu differenzieren. Die aus diesen Daten abgeleiteten großräumigen Verformungsmuster spiegeln zunächst die regionale Verkürzungsrichtung sehr gut wider. Sie dokumentieren aber auch gleichzeitig signifikante Extensionsstrukturen in einem von Verkürzung dominierten Gebiet. Insgesamt konnten sechs Deformationsarten unterschieden werden, von denen die meisten zeitlich und räumlich verbunden sind und fortschreitende Verkürzung anzeigen. Die vier dominanten Deformationsarten sind wie folgt: (1) Verkürzung parallel zur regionalen Konvergenzrichtung; (2) Extension senkrecht zum Himalaja-Bogen; (3) Extension parallel zum Himalaja-Bogen; und (4) E-W-Extension. Zum ersten Mal konnte in der hier vorliegenden

Arbeit eine Differenzierung von Extension parallel zum Himalaja-Bogen sowie E-W-Extension im Himalaja dokumentiert und eine relative Abfolge zwischen beiden Extensionsrichtungen beschrieben werden.

Ein weiteres Ziel dieser Studie ist es, basierend auf meinen Geländebeobachtungen, einen detaillierten Überblick über die jüngeren Extensionsereignisse im Himalaja von NW Indien zu erhalten. Zusätzlich zu den schon erwähnten störungs kinematischen Daten, erhob ich dabei gelände- und fernerkundungsbasierte geomorphologische Beobachtungen neotektonischer Strukturen und $^{40}\text{Ar}/^{39}\text{Ar}$ -Daten von synkinematisch gewachsenen Muskoviten auf Abschiebungen, um die räumliche Orientierung der jüngsten Extension sowie deren zeitliche Einordnung zu belegen. Ich kartierte zusätzlich Bruchstufen in quartären Sedimentablagerungen, kombinierte eigene Geländebeobachtungen von größeren Abschiebungen im Großraum des Sutlej (Spiti, Lahul, Kinnaur) und im Garhwal Himalaja mit bereits publizierten Strukturen. Schlussendlich konnte ich anhand von Seismiten in Seesedimenten in der Nähe der momentan aktivsten Abschiebung im Untersuchungsgebiet verschiedene paläoseismologischen Ereignissen entlang dieser Störung nachweisen. Mit diesem Datensatz kann ich dokumentieren, dass E-W-Extension in diesem internen Teil des Himalajas die momentan dominante Deformationsart ist, die vor 14-16 Ma begann, wenn nicht noch früher. Darüber hinaus zeigt die Kombination von strukturgeologischen Geländedaten, geomorphologischen und Fernerkundungsdaten, dass E-W-Extension in einem wesentlich ausgedehnteren Gebiet nach Süden und Westen hin auftritt als Erdbebendaten dies vermuten lassen.

Zusammenfassend bezeugen die in der Studie präsentierten Daten die Relevanz von Extension in einer Region, die noch immer von Verkürzung geprägt wird. Die räumliche Verteilung von Störungen sowie Überschneidungskriterien lassen vermuten, dass Extension sowohl parallel als auch senkrecht zum Himalaja-Bogen ein essentieller Teil des südwärts gerichteten Propagierens der aktiven Überschiebungsfrent und des damit assoziierten lateralen Wachstums des Orogens ist. Nach Abwägung der großen Bandbreite an Modellen für Extension im Himalaja und im tibetischen Hochplateau, komme ich zu dem Schluß, dass E-W-Extension im Himalaja NW Indiens ihren Ursprung im tibetischen Hochplateau hat. Der Grund dafür ist, dass der Versatz entlang der Karakorum-Störung nicht ausreichend ist, um die fortdauernde E-W-Extension im tibetischen Hochplateau aufzunehmen. In Übereinstimmung mit anderen Beobachtungen in Tibet ist es außerdem möglich, dass das Einsetzen von Abschiebungen im Zusammenhang mit E-W-Extension im NW Himalaja ebenfalls das Erreichen der hohen Topographie in dieser Gegend widerspiegelt, durch die krustale Prozesse in Gang gesetzt werden, die wiederum zu räumlich ausgedehnten Extensionsprozessen führen können.

Contents

Abstract	I
Zusammenfassung	III
List of Figures	VII
List of Tables	VIII
1 Introduction	1
1.1 Geology of the Himalaya	5
1.1.1 Lithological units	5
1.1.2 Major structures	8
1.2 Models for normal faulting	12
1.2.1 Arc-parallel normal faults	12
1.2.2 Arc-perpendicular normal faults	15
2 Extension during brittle deformation	19
2.1 Introduction	20
2.2 Geological setting of the NW Indian Himalaya	23
2.2.1 Principal structures related to shortening	23
2.2.2 Structures related to extension	23
2.3 Data processing	26
2.4 Paleo-strain results	28
2.4.1 NE-SW (arc-normal) shortening (D1)	29
2.4.2 ENE-WSW shortening (D2)	29
2.4.3 NE-SW (arc-normal) extension (D3)	30
2.4.4 NW-SE (arc-parallel) extension (D4)	31
2.4.5 N-S shortening (D5)	31
2.4.6 E-W extension (D6)	32
2.4.7 N-S extension	32
2.5 Chronology	33
2.5.1 Relative chronology	33
2.5.2 Onset of brittle deformation across the Himalaya based on thermochronology	34
2.6 Tectonic interpretation	38
2.7 Conclusions	42
3 East-west extension in the NW Indian Himalaya	43
3.1 Introduction	44
3.2 Geological Setting of the NW Himalaya	46

3.2.1	Principal structures related to shortening	46
3.2.2	Extensional structures in the Himalaya	46
3.2.3	Seismicity in the NW Indian Himalaya	48
3.3	Methodology	50
3.3.1	Field mapping and analysis of satellite imagery	50
3.3.2	Kinematic analysis of brittle fault data	50
3.3.3	Age determination of normal faulting	50
3.4	Extensional structures in the NW Himalaya	53
3.4.1	Macro-scale normal faults from satellite imagery and field observations	54
3.4.2	Meso-scale and outcrop-scale faults observed in the field	58
3.4.3	Normal faults in sediments and soft-sediment deformation	61
3.5	Paleostrain results	63
3.6	Discussion and conclusions	66
3.6.1	Possible onset of E-W extension in the Higher Himalaya	66
3.6.2	Possible mechanisms for E-W extension in the Tethyan and Higher Himalaya	67
4	Active tectonics in the NW Indian Himalaya	75
4.1	Present-day deformation in the Himalaya and Tibet	76
4.2	Disturbed river profiles	79
4.2.1	Methodology	79
4.2.2	Longitudinal river profiles	80
4.2.3	Transverse river profiles	83
4.3	Paleoseismological records of active normal faulting	85
4.3.1	Soft-sediment records along the Kaurik-Chango Normal fault	85
4.3.2	Evidence for a paleo-earthquake in the Baspa Valley	89
4.4	Conclusions	91
5	General Conclusions	93
	Bibliography	97
A	Overview of paleostrain data	111
A.1	Examples of kinematic field information	111
A.2	Overview of obtained paleo-strain axes	113
B	$^{40}\text{Ar}/^{39}\text{Ar}$ data	117
C	Reports on flash floods in the Sutlej Valley	119
	Selbständigkeitserklärung	122

List of Figures

1.1	Geological map of the Himalaya	6
2.1	Complete data set of all kinematic fault measurements.	22
2.2	Strain axes related to NE-SW shortening.	25
2.3	Strain axes related to E-W shortening.	27
2.4	Strain axes related to NE-SW extension.	28
2.5	Strain axes related to NW-SE extension.	29
2.6	Strain axes related to N-S shortening.	30
2.7	Strain axes related to E-W extension.	31
2.8	Strain axes related to N-S extension.	33
2.9	Evaluation of crosscutting relations observed in the field.	34
2.10	Relative chronology of the major deformation styles.	35
3.1	Structural map of the NW Indian Himalaya	47
3.2	Normal faults southeast of the Tso Morari Lake	51
3.3	Quaternary normal faults in the NW Leo Pargil basin	53
3.4	Normal faults of inferred Quaternary age in the NW Leo Pargil basin	55
3.5	Normal faults in the Lingti Valley	57
3.6	E-dipping brittle normal faults in the Parbar Valley	58
3.7	Plots of $^{40}\text{Ar}/^{39}\text{Ar}$ ages within the footwall of the LPDZ	59
3.8	Brittle fault kinematic data and results of PFPS analysis	60
3.9	Fluviolacustrine sediments in the Spiti Valley affected by normal faulting	61
3.10	Lake sediments in the Spiti Valley affected by soft-sediment deformation	65
3.11	Models for E-W extension observed in the NW Indian Himalaya	68
4.1	Overview of the basin NW of the Leo Pargil gneiss dome.	78
4.2	Schematic longitudinal river profiles.	80
4.3	Longitudinal profiles of rivers crossing normal faults.	81
4.4	Change of valley width of the Pare Chu river crossing normal faults.	83
4.5	Central lake in the basin bounded by normal faulting	84
4.6	Lake sediments along the KCNF showing soft-sediment deformation	86
4.7	Soft-sediment deformation within lake sediments along the KCNF	88
4.8	Lake deposits cut by a normal fault in the Baspa Valley.	89
A.1	Appendix showing stereo plots of all brittle faults	112

List of Tables

2.1	Compilation of age constraints for the NW Indian Himalaya.	37
3.1	Summary of $^{40}\text{Ar}/^{39}\text{Ar}$ data	59
3.2	OSL dating results	64
3.3	Implications of models for E-W extension in the Tibetan Plateau and the Himalaya	72
A.1	List of all calculated paleo-strain axes, sorted by outcrops.	116
B.1	Complete $^{40}\text{Ar}/^{39}\text{Ar}$ data set for sample B270901-3	118
B.2	Complete $^{40}\text{Ar}/^{39}\text{Ar}$ data set for sample B270901-4	118

Chapter 1

Introduction

The Himalayan orogen forms the southern margin of the Tibetan Plateau and has evolved as a result of the Indian-Asian continent-continent collision that started between ~ 65 Ma and ~ 43 Ma (e.g., Patriat and Achache, 1984; Klootwijk et al., 1992; Rowley, 1996; Guillot et al., 1997; Najman et al., 2003; Liebke et al., 2010). It links the Indian subcontinent with the Eurasian plate, and extends over 2500 km from Afghanistan in the west to Myanmar in the east (Molnar and Tapponnier, 1978). The Himalayan orogen is dominated by large contractional fault systems that can be traced almost continuously along the trend of the entire range, accommodating approximately 50% of the NNE directed motion of the Indian plate (Banerjee and Bürgmann, 2002; Zhang et al., 2004). In addition to the important thrust systems to account of its uplift, the gently curved arc of the orogen is characterized by both, arc-parallel and arc-perpendicular normal faults. The arc-perpendicular normal faults constitute approximately N-S striking graben systems (e.g., Burg et al., 1984a, Burchfiel et al., 1992; Hurtado et al., 2001; Guo et al., 2008; Jessup et al., 2008 and references therein). Similar structures have been observed virtually over the entire Tibetan Plateau (e.g., Armijo et al., 1986; Hogdes, 2000; Taylor et al., 2003). The focus of this thesis lies on the origin and the significance of these normal faults as well as on the question whether normal faulting in the Himalaya and the Southern Tibetan Plateau are linked.

The evolution of synorogenic normal fault systems in the overall contractional regimes of active and ancient mountain ranges is still a matter of controversial scientific dispute. Orogens formed by continent-continent collision like the Himalaya-Tibet region (Armijo et al., 1986; Molnar, 1992; Blisniuk et al., 2001; Chen and Yang, 2004; Zhang et al., 2004), and the Alps (Michard et al., 1993; Wheeler and Butler, 1993; Seward and Manckelw, 1994; Selverstone, 2005) may develop extension and normal faulting at higher elevations simultaneously with shortening and thrusting at lower altitudes. Similar extensional fault systems have been documented during the evolution of the Variscides (Schulmann et al., 2005) and the Caledonides (Anderson, 1998). Normal faults have also been documented in subduction orogens like the Andes (e.g., Dalmayrac and Molnar, 1981; Allmendinger et al., 1997; Liu et al., 2002). There, normal faults appear to be late-stage features in the orogenic evolution, are often linked with mafic volcanism, and are restricted to the realm of the high Puna-Altiplano plateau and its margins, where these structures have developed

within the last 5 to 7 Ma (Montero Lopez et al., 2010).

The ubiquitous occurrence of normal faults in these compressive environments suggests that they play an important role in mountain-building processes (e.g. England and Molnar, 1993). Although the mechanisms of normal faulting in orogen interiors is still highly debated, the kinematic change from thrusting to normal faulting or the coeval occurrence of normal and thrust faulting are important mechanisms during orogenesis and reflect fundamental changes in the character and distribution of stresses.

Due to the ubiquitous occurrence and the spatiotemporal characteristics of normal faults, Himalaya-Tibetan orogen is one of the key locations to investigate Cenozoic synorogenic normal faulting (Armijo et al., 1986; Royden and Burchfiel, 1987; England and Houseman, 1989; Molnar and Lyon-Caen, 1989; Burchfiel et al., 1991, 1992; Ratschbacher et al., 1994; McCaffrey and Nabelek, 1998; Blisniuk et al., 2001; Hogdes et al., 2001; Aoya et al., 2005; Murphy and Copeland, 2005; Thiede et al., 2006; Jessup et al., 2008). In addition, the ongoing convergence between India and Eurasia is characterized by a consistent direction and velocity that have prevailed over the approximately last 55 Ma (Klootwijk et al., 1992; Najman et al., 2003; Copley et al., 2010). While the geological framework of shortening in the mountain building process of the Himalaya is well studied, the ultimate driving forces for the observed extensional structures are less clear. In this regard, open questions are:

- Is it possible to decipher several extensional directions within the Himalaya? And if yes, what mechanisms govern the the spatial and temporal evolution of those extensional directions?
- What is the nature of N-S striking normal faults in the internal part of the Himalaya? Are these structures
 - (a) related to tensional stresses related to the formation of the arc-shaped geometry of the orogen (e.g., McCaffrey and Nabelek, 1998);
 - (b) explicable by the subduction process of the Indian plate beneath Eurasia (e.g., England and Molnar, 1993); or
 - (c) linked to the observed E-W extension in the Tibetan Plateau (e.g., Yin, 2000)?
- Does the Karakorum Fault form a strain boundary decoupling deformation within the Western Himalaya from the Tibetan Plateau or is displacement along this strike-slip fault system too small to separate deformation into two independent compartments?

Most previous studies that have addressed normal faulting in the Himalaya present data from the central part of the mountain chain between 81 and 90°E (e.g., Ratschbacher et al., 1994; Kapp and Gynn, 2004; Aoya et al., 2005; Yin, 2006, and references therein). A major disadvantage of this Himalayan compartment is that structures associated with arc-normal extension within the Himalaya due to its arc-shaped geometry run parallel to structures that result from the E-W extension on the Tibetan Plateau due to its eastward movement. Therefore, structures related to both

processes may overlap and their individual origin cannot be unambiguously distinguished. In the NW Indian Himalaya between 75° and 79° E, ongoing E-W extension is documented by earthquake focal mechanisms (Molnar and Lyon-Caen, 1989; Molnar, 1992), normal faults displacing Quaternary deposits (Epard and Steck, 2008), and regional GPS measurements (Banerjee and Bürgmann, 2002). Taken together, these data reflect a regional extensional direction that is neither parallel nor normal to the NW-SE regional trend of the orogen. This environment is well suited to decipher different extensional phases and to evaluate existing models explaining the driving mechanisms for normal faulting within the Himalaya.

By studying the brittle and neotectonic deformation in the NW Indian Himalaya, I took advantage of the obliquity between the regional trend of the orogen and E-W oriented extension in order to test existing models explaining extension within the Himalaya and the Tibet Plateau. This thesis is structured into five main chapters addressing the phenomena of normal faulting using geological field mapping techniques, geochronology, tectonic geomorphology and paleo-strain calculations:

In the introduction (chapter 1), I describe the overall geology of the Himalaya and provide an overview of previously published regional models for arc-normal and arc-parallel extension developed for this orogen. Chapters 2 and 3 correspond to publications in the journals “GSA Bulletin” and “Tectonics”, and present the main findings of my work.

Chapter 2 concentrates on fault-kinematic analysis, based on systematic measurements of hundreds of outcrop-scale brittle fault planes (i.e., dip and dip direction of fault planes, trend and plunge of the associated lineaments and the sense of shear), in order to distinguish between different deformation styles recorded in brittle faults. The overall strain pattern derived from these data documents the regional contractional deformation characteristics very well, but also reveals significant evidence for extensional deformation. I was able to identify six deformation styles, most of which are temporally and spatially linked, and which are associated with protracted shortening. My observations also furnish the basis for a detailed overview of the younger deformation history in the NW Himalaya, which has been characterized by extension overprinting previously generated structures related to shortening. This is the first data set, where a succession of both, arc-normal and E-W extension have been documented in the Himalaya. Importantly, my observations help differentiate E-W extension possibly triggered by processes within the Tibetan Plateau from arc-parallel and -normal extension that may have been forced by the southward convex curvature of the Himalayan orogen.

Chapter 3 presents field observations of young fault scarps using satellite imagery and field observations in the NW Indian Himalaya. In addition, soft-sediment deformation was analyzed in lake sediments close to the Kaurik-Chango normal fault. This new data document that normal faulting is not localized in close vicinity to major structures, such as the normal faults associated with the doming of the Leo Pargil gneiss dome, but rather constitutes an ubiquitous, pervasive phenomenon affecting the Himalaya of NW India as a whole. In addition, new $^{40}\text{Ar}/^{39}\text{Ar}$ age data together with geochronology data, previously published by Thiede et al. (2006) helps to constrain the minimum age of onset of E-W extension in the NW Indian Himalaya

to 14-16 Ma. Taken together, my data help define the spatio-temporal character of extensional deformation and provide valuable information on the causal mechanisms of active normal faulting of this region. Furthermore, since previous models explaining the origin of extension in the Himalaya are generally based on data from the Central Himalaya, my new observations from the NW sector of the orogen can be used to evaluate these models. Based on this evaluation, I favor a scenario in which E-W oriented extension in the NW Indian Himalaya is triggered by extension in the Tibetan Plateau.

The last data chapter 4 provides additional geomorphic evidence for active E-W normal faulting based on river-profile analysis of an inaccessible intermontane basin in the NW Indian Himalaya located in the vicinity of the Indian-Tibetan border. This part of my thesis furthermore provides evidence for paleo-earthquakes associated with N-S striking faults, especially taken into account similar data from the lower Pare Chu River, a tributary of the lower Spiti River (Mohindra and Bagati, 1996; Banerjee et al., 1997). Although dating is only based on regional correlation of sediment strata and landforms, the faulted strata are interpreted to be of Late Pleistocene age. This underlines the recency of E-W extension in the NW Indian Himalaya, which is also manifested in earthquake focal mechanisms and GPS data.

In the final chapter 5, I summarize the main results of the study presented here, and discuss the questions posed earlier in the introduction.

1.1 Geology of the Himalaya

Including the highest mountains on earth, the Himalaya is the result of ongoing India-Eurasia continent-continent collision. After the separation of the Indian Subcontinent from Gondwana during the Lower Cretaceous (~ 130 Ma ago Patriat and Achache, 1984; Stampfli and Borel, 2002), India began moving northward as part of the Australian Plate with about 18-19 cm/yr (Molnar and Tapponnier, 1975; Copley et al., 2010). The collision of Greater India (which entails the about 1500 km more extensive Indian subcontinent before the collision, Ali and Aitchison, 2005) with Eurasia occurred at 15°N between ~ 65 and ~ 43 Ma (e.g., Patriat and Achache, 1984; Klootwijk et al., 1992; Rowley, 1996; Guillot et al., 1997; Najman et al., 2003; Liebke et al., 2010). Since then, the convergence rate between India and Eurasia has slowed down to the present-day motion of ~ 5 cm/yr (Copley et al., 2010).

Some of the most outstanding characteristics of the Himalaya are the structural similarities that show little variations along the strike of the orogen. As consequence, all first-order tectonic units and structures are more or less traceable along the entire length of the Himalayan arc. One of the boundary conditions for this remarkable along-strike similarity is the constant direction and rate of convergence between Eurasia and India since about 55 Ma and the pre-collisional situation of an almost undeformed Indian passive margin (Klootwijk et al., 1992; Najman et al., 2003; Copley et al., 2010).

In the following sections, I describe the most important lithological units and tectonic structures of the NW Indian Himalaya between 75° and 80° E. Since the correlation of lithostratigraphic units along the Himalaya is complex (DiPietro and Pogue, 2004; Yin, 2006), I limit my description to the Greater Sutlej River region and the Garhwal Himalaya, approximately spanning the area of the Indian counties of Himachal Pradesh and Utterakhant in the NW Indian Himalaya.

1.1.1 Lithological units

In a classical sense, the Himalaya is separated into 5 major tectono-stratigraphic units. From north to south these include: the Indus-Yarlong-Suture Zone (IYSZ), the Tethyan Himalayan sequence (TH), the Higher (or Greater) Himalayan Crystalline (HHC), the Lesser (or Lower) Himalayan (LH), and finally the Subhimalayan (Gansser, 1964), separated by large arc-parallel north-dipping fault zones that will be described in the following section.

Indus-Yarlong-Suture Zone (IYSZ)

The IYSZ is the suture zone that forms the boundary between the Indian and Eurasian plates Molnar and Tapponnier (1977). The suture consists of ophiolites and three major rock sequences that represent sediments from the Tethyan ocean and its northern and southern margins (Heim and Gansser, 1939; Molnar and Tapponnier, 1977; Burg and Chen, 1984). Different geochronological studies document an increasing age from west to east (e.g., Rowley, 1996). This pattern in ages has let several authors to propose that the collision of Greater India with Eurasia started in the west and propagated eastward, however, this is still under debate (e.g., Zhu et al., 2005, and references therein).

1.1. GEOLOGY OF THE HIMALAYA

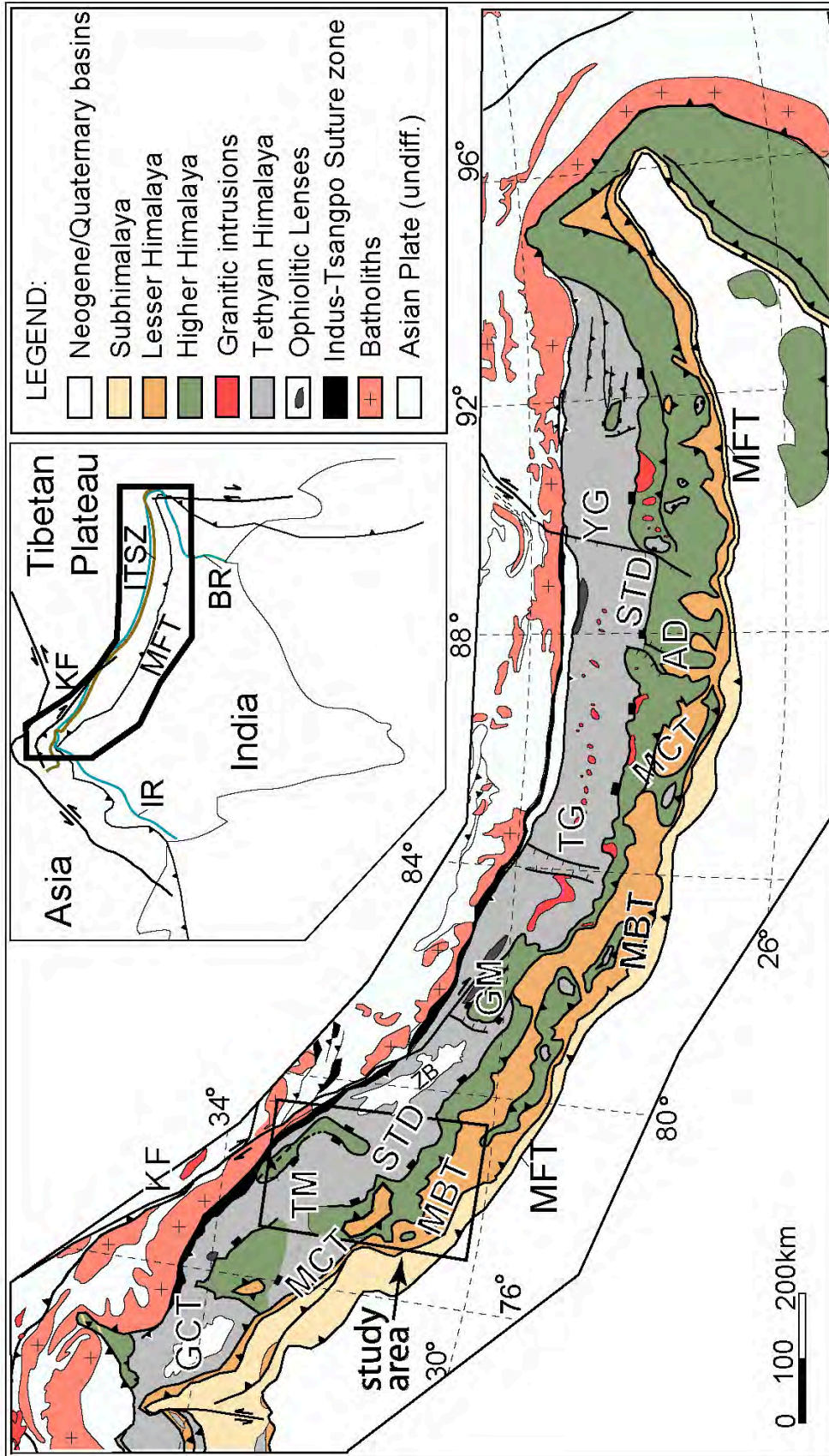


Figure 1.1: (A) Geological map and structural provinces of the entire Himalaya, modified after Yin (2006) and references therein. For the western Himalaya, the structures as mapped by DiPietro and Pogue (2004) are used. AD: Ama Drime massif, BR: Brahmaputra River, GM: Gurla Mandhata gneiss dome, IR: Indus River, ITSZ: Indus-Tsangpo Suture Zone, KEQ: Kinnaur Earthquake, KF: Karakoram Fault, KNF: Karcham normal fault, LPDZ: Leo Pargil Detachment Zone, MBT: Main Boundary Thrust, MCT: Main Central Thrust, MFT: Main Frontal Thrust, MT: Munsiri Thrust, SD: Sangla Detachment, STDS: Southern Tibetan Detachment System, TM: Tso Moriri, TG: Thakkola Graben, YG: Yadong Graben.

Tethyan Himalaya (TH)

The northernmost lithological unit south of the IYSZ, also called “Tibetan Himalaya” (Gansser, 1964), is the relict of the Indian passive margin, consisting of very low and low metamorphic-grade siliclastic and carbonate sedimentary rocks of Paleo-Proterozoic to Eocene age, interbedded with Paleozoic and Mesozoic volcanic rocks. This generally continuous sedimentary sequence comprises a time span of 1840 Ma - 40 Ma and can be subdivided into four subsequences, recording the pre-Himalayan history of the Indian passive margin: a Proterozoic-Devonian pre-rift sequence, a Carboniferous-Lower Jurassic rift to post-rift sequence, the Jurassic-Cretaceous passive continental margin sequence, and the uppermost Cretaceous-Eocene deposits of the early continent-continent collisional stage (Yin, 2006). In the NW Himalaya, in the Zaskar region, the transition between marine and terrestrial sedimentation took place during the Eocene (Gaetani et al., 1986). Intrusive granitic rocks are found at the base of the Tethyan Himalaya along strike of the orogen. In the Greater Sutlej area, the Kinnaur Kailash Granite intruded around 453-477 Ma ago (Kwatra et al., 1999).

Higher Himalayan Crystalline (HHC)

The Higher Himalayan Crystalline is consistently exposed along the Himalayan arc forming the metamorphic core of the orogen. The HHC is bounded by the MCT and the STDS, along which high-metamorphic rocks from mid-crustal levels have been extruded since the Miocene (Le Fort, 1975; Burg and Chen, 1984; Burchfiel et al., 1992; Vannay and Grasemann, 1998; Dèzes et al., 1999). The HHC is composed of Proterozoic to Ordovician paragneisses and orthogneisses (Parrish and Hodges, 1996; DeCelles et al., 2000) with increasing metamorphic grade from amphibolite facies conditions to anatexis close to the top. The paragneisses are of similar characteristics as the low or non-metamorphic overlying Tethyan Himalayan sequences, suggesting that the latter are the protoliths for the HHC paragneisses (Vannay and Grasemann, 1998).

Lesser Himalayan Crystalline (LHC)

The Lesser Himalayan Crystalline is an additional 14-16 km thick medium to high-grade metamorphic sequence between the HHC and the LH that is mainly described in the Greater Sutlej area and the Kullu window north of the Greater Sutlej area (Srivastava and Mitra, 1994; Frank et al., 1995; Vannay and Grasemann, 1998; Wiesmayr and Grasemann, 2002). In its lower part, this unit comprises mainly paragneisses and mica schists, metabasites, quartzite, and granitic gneisses, while the upper part consists of massive granitic augengneiss, the Wangtu Gneiss (Zircon U-Pb 1840 ± 16 Ma, Miller et al., 2000). It is interpreted to be part of the basement onto which the LH sequences were deposited. Some authors propose that the LHC may be correlated with the Munsiri Group in the Garhwal Himalaya (Pêcher and Scaillet, 1989; Metcalfe, 1993) and the LHC in Nepal (Pêcher, 1989).

Lesser Himalaya (LH)

The Lesser Himalaya south of the LHC consists mainly of Precambrian clastic sediments and Proterozoic-Cambrian non-fossiliferous low-grade metasedimentary and

metavolcanic rocks (Heim and Gansser, 1939; Brookfield, 1993; Srivastava and Mitra, 1994; Frank et al., 1995; Miller et al., 2000). It is supposed to represent the Upper Proterozoic - Lower Cenozoic sedimentary cover of the Indian passive margin (Frank et al., 1995). The deposition in the NW Indian Himalaya is dated to 1870 - 850 Ma based on detrital zircons (Miller et al., 2000; DeCelles et al., 2000).

Subhimalaya

The Subhimalaya consists of internally folded Paleocene-Neogene deposits at the southern margin of the Himalaya, also called the Siwalik sequence in the Western Himalaya (Burbank et al., 1996; Schelling, 1992; DeCelles et al., 1998). The Subhimalaya represents the molasse deposits of the Himalaya. It has been partly involved in the orogenesis by being thrust over the youngest deposits in the Ganges plain (Molnar and Tapponnier, 1975). Paleocene-Eocene deposits are sediments of marine origin, whereas Miocene-Pliocene strata consist of terrestrial sediments derived from erosion of the orogen. There is a prominent unconformity between Eocene/early Oligocene and lower Miocene units observed all along the length of the orogen (DeCelles et al., 1998).

1.1.2 Major structures

The first-order structures of the Himalaya are described as arc-parallel north-dipping thrusts, exposed mostly as several-km-thick shear zones with general top-to-the-South slip (e.g., Gansser, 1964). These thrusts are called the Main Central Thrust (MCT), the Main Boundary Thrust (MBT), and the Main Frontal Thrust (MFT) and become younger from north to south. They root all in a common basal thrust, the Main Himalayan Thrust (MHT), which is inferred to be the main interface between the subducted Indian plate and the overthrust Himalayan orogen (e.g., Schelling and Arita, 1991; Nelson et al., 1996). In addition, there are several other large structures that will be explained in the following sections, as they occur from North to South in the NW Indian Himalaya.

Karakorum fault (KF)

The Karakorum fault (KF) forms a 800-km-long, well recognized dextral strike-slip fault system bounding the SW margin of the Tibetan Plateau and accommodating deformation between the Pamir mountains and the Mount Kailash area in the NW Himalaya. The KF is supposed to be a first-order structure associated with plateau deformation and has been proposed to play an important role in the lateral extrusion of the Tibetan Plateau. However, many aspects of the deformation history, fault initiation, as well as the importance for deformation of the Tibetan Plateau are still poorly constrained and debated (e.g., Lacassin et al., 2004; Chevalier et al., 2005; Searle and Phillips, 2007). The onset of movement along the KF is dated by different studies between 24 Ma (Lacassin et al., 2004) and \sim 14-12 Ma (Searle et al., 1998; Phillips et al., 2004). Estimates for the total slip along the KF vary between 120 km (Searle, 1996) and 1000 km (Peltzer and Tapponnier, 1988). Whereas the KF is easily traceable on satellite imagery between the Pamir and Mount Kailas, it is much more difficult to identify its southern continuation. The transfer of slip from the KF either to the Indus-Tsangpo suture zone (e.g., Searle, 1996; Lacassin et al.,

2004) or to the STDS during the late Miocene (e.g., Pêcher, 1991) has been a widely accepted explanation. Alternative interpretations include the termination of the KF either to the N-S trending Pulan basin (Ratschbacher et al., 1994) or further south in the N-S striking Gurla Mandhata detachment system (Murphy et al., 2002).

Great Counter Thrust (GCT)

The Great Counter Thrust (GCT) is the only backthrust, and therefore the only south-dipping thrust encountered in the NW Indian Himalaya, bounding the IYSZ at its southern margin. The backthrust juxtaposes Tethyan Himalayan sedimentary rocks over the melange complex of the IYSZ. Although it can be traced for almost the entire length of the Himalayan arc, it has been recognized independently in different compartments and is therefore known under various names (Yin and Harrison, 2000, and references therein). It has been active between 20 and 13 Ma (Yin et al., 1999), but certainly prior to 9 Ma, accumulating more than 38 km of slip in the western Himalaya (Murphy et al., 2002).

Leo Pargil Detachment Zone (LPDZ) and Kaurik Chango Normal Fault (KCNF)

The LPDZ is described as a system of linked west-dipping, low-angle ductile normal faults at the western flank of the Leo Pargil gneiss dome (Thiede et al., 2006). The onset of activity of this structure is poorly constrained, but extension must have begun during the Miocene between 14-16 Ma (Thiede et al., 2006) and ~23 Ma (Langille et al., 2012). The Kaurik Chango Normal Fault at the western flank of the Leo Pargil gneiss dome is a west-dipping brittle normal fault and overprints the LPDZ (Hayden, 1904; Thiede et al., 2006). Movement on the KCNF is considered as the source for the Kinnaur Earthquake (Jan. 19th 1975, $M_s = 6.8$, Singh et al., 1975; Khattri et al., 1978), demonstrating its recent activity.

Southern Tibetan Detachment System STDS (STDS)

The STDS consists of several arc-parallel, linked low-angle normal faults that strike generally parallel to the major thrusts. The STDS separates the low-grade metamorphic rocks of the Tethyan Himalaya in the hanging wall from the high-grade metamorphic footwall of the Higher Himalaya (Burg et al., 1984a, Burchfiel and Royden, 1985; Burchfiel et al., 1992). In the NW Indian Himalaya, the Sangla Detachment (SD) is the local expression of the STDS in the Greater Sutlej region (Vannay and Grasemann, 1998; Wiesmayr and Grasemann, 2002) as well as the Jahla Detachment in the Garhwal Himalaya (Pêcher and Scaillet, 1989). Crystallization ages related to top-to-the-north shear fabrics range between 21 and 12 Ma are found all along the Himalayan arc (e.g., Schärer et al., 1986; Searle et al., 1997; Hodges et al., 1998). In the Western Himalaya, the STDS has been active at around 21-19 Ma in Zaskar (Dèzes et al., 1999) and at around 23-21 Ma in the Garhwal Himalaya (Searle, 1996), accumulating estimated slip of up to 35 km, but at least 25 km. Some studies have proposed that the STDS has been reactivated as recently as the Quaternary (Hodges et al., 2001; Hurtado et al., 2001). Recent studies north of the Sutlej river suggest that the STDS and the MCT might merge in map view north of the Sutlej Valley (Yin, 2006; Webb et al., 2007).

An overview of models explaining the role of the STDS, its importance in the construction of the Himalaya and the underlying driving forces for the observed arc-perpendicular extension along the SDTS are presented in section 1.2.

Main Central Thrust (MCT)

The MCT overthrusts high-grade metamorphic gneisses and schists of the HHC over non-metamorphic (or low metamorphic) sedimentary sequences of the LH (Heim and Gansser, 1939). However, this lithological contact is not easily defined all along the Himalaya. Therefore, alternative definitions for the location of the MCT have been established, such as abrupt change in metamorphic grade (Le Fort, 1975; Pêcher, 1989), or the top surface of the broad shear zone across the uppermost part of the LH and the lowermost part of the HHC (Arita, 1983; Pêcher, 1989; Searle et al., 2003). During the Miocene, the Higher Himalaya was exhumed during coeval extension along the STDS and thrusting along the MCT (e.g., Burchfiel and Royden, 1985; Grujic et al., 1996; Vannay and Grasemann, 2001).

In the Western Himalaya, the MCT is defined as an up to 10-km-thick mylonitic shear zone (Grasemann and Vannay, 1999) that accommodated a minimum of 140 km of displacement and possibly up to 500 km (Gansser, 1964; Frank et al., 1995; Vannay and Grasemann, 2001). In the Greater Sutlej area and the Garhwal Himalaya, the MCT separates the HHC and LHC (Vannay and Grasemann, 1998). Simple shear deformation along the MCT have been active between 23-14 Ma (Metcalf, 1993; Hogdes et al., 1996; Dèzes et al., 1999). In addition, there is evidence for reactivation of the MCT between around ~ 6 Ma (Metcalf, 1993).

The Karcham Normal Fault (KNF) is a brittle cataclastic normal fault that dips parallel to the MCT and juxtaposes the MCT mylonites. It has been observed only in the Sutlej Valley showing a top-to-the-east displacement and is thought to act as the counterpart of the Munsiri Thrust during the exhumation of the LHC (Janda et al., 2002; Vannay et al., 2004).

Munsiri Thrust (MT)

The MT is a NNE-dipping 1-2 km thick mylonitic shear zone in the Western Himalaya, which separates the LH from the LHC (Vannay and Grasemann, 1998). Top-to-the-SSW shear along the MT occurred approximately between 11 and 6 Ma (Vannay et al., 2004). In comparison with descriptions from adjacent areas, the MT might be part of a duplex-structured MCT and therefore the local expression of the MCT (Kumar et al., 1995; Yin, 2006).

Main Boundary Thrust (MBT)

Generally, the MBT is defined as a steeply north-dipping thrust that juxtaposes the LH sequences over younger sedimentary strata of the Subhimalaya (Heim and Gansser, 1939). However, this definition is very ambiguous, and may not be applicable everywhere (Yin, 2006). Typically, several closely-spaced parallel-striking, north-dipping thrust faults are observed, instead of one larger fault (e.g., Valdiya, 1980; Kumar et al., 2006). Deformation started at around 11 Ma and continued during the Pleistocene, accumulating more than 100 km of slip (Burbank et al., 1996).

Main Frontal Thrust (MFT)

This fault is thought to be the youngest structure, thrusting Neogene Subhimalayan Siwalik strata above Quaternary deposits of the Ganges plain on the Indian plate (Gansser, 1964; Lavé and Avouac, 2001; Kumar et al., 2006). Since surface exposure of the fault trace is sparsely mapped, it is generally mapped as a blind fold-propagation fault (Yeats and Lillie, 1991). Paleoseismological investigations suggest that very large earthquakes ($M_w > 8.0$) were generated along this fault during the last ~ 1000 years (Kumar et al., 2006). This implies that the MFT is the active surface-breaking thrust, where the Himalaya is thrust above the Indian plate.

Main Himalayan Thrust (MHT)

The Main Himalayan Thrust (MHT) is assumed to be the main low-angle fault at the interface between the Indian plate and the overriding orogenic wedge, where all other thrust faults (MCT, MBT, MFT) converge. This concept was first brought up by Schelling and Arita (1991), and confirmed by the INDEPTH seismic reflection profiles (Nelson et al., 1996). However, there is ongoing discussion whether it dips shallowly towards the north (Nelson et al., 1996) or includes a steeper ramp at the transition between the Lower and Higher Himalaya (Pandey et al., 1990; Caldwell et al., 2012, 2013).

North-South trending rifts

In addition to the structures whose strike follow the trend of the Himalayan arc, there are several north-trending rifts and graben systems that intersect this structural fabric. Those graben systems are mainly found in the central Himalaya and Southern Tibet (Molnar and Tapponnier, 1978; Tapponnier et al., 1982; Armijo et al., 1986; Burchfiel et al., 1991; Yin et al., 1999), but more recent field work has provided evidence for young normal faults in the western Himalaya (Thiede et al., 2006; Murphy et al., 2002; Saylor et al., 2009). Deformation along the graben-bounding normal faults started between 14 and 8 Ma (Edwards and Harrison, 1997; Blisniuk and Sharp, 2003; Jessup et al., 2008).

1.2 Models for normal faulting within the Himalaya-Tibet realm

Contemporaneous normal faulting and shortening has been observed at many locations throughout the Himalaya and extension seem to play an important role in the evolution of the Himalaya and the Tibetan Plateau. The realization that there are more than one extensional direction occurring in the Himalaya-Tibet realm occurred during the early 1980s, as the STDS and the southern Tibetan graben systems were mapped independently (Burg et al., 1984a, ; Caby et al., 1983; Seeber and Armbruster, 1984; Armijo et al., 1986). In the following, I will present the most relevant models for both, arc-parallel and arc-perpendicular normal faulting.

1.2.1 Arc-parallel normal faults with the primary representative, the STDS

The first descriptions of north-dipping normal faults in different locations were published in the early 1980s (Caby et al., 1983; Burg et al., 1984a). Since then, increasing field evidence has expanded our view of the role of these structures to a phenomenon observed along the entire length of the Himalaya. Despite local nomenclature, these normal faults are part of the STDS, being is the major representative of arc-parallel normal faults in the Himalaya. Generally, explanations for arc-parallel normal faults along the STDS also relate to the question on the emplacement of the Higher Himalayan Crystalline between the Lesser and the Tethyan Himalaya. Various models have been developed during the last 25 years. The most important ones will be described in the following.

Ramp model

Not only the first detailed field observation, but also the first mechanistic explanation was provided by Burg et al., 1984a. They explain normal faulting along the STDS with a simple ramp model where India is subducted beneath Tibet along a ramp-like structure. The ramp-parallel component of the gravitational energy generated by the overlying 10-km-thick package of Tethyan sediments exceeds the ramp-parallel component of the horizontal compressional shear stress and results in a down-dip movement of the Tethyan sediment package. Already in this early work, kinematic linkage between deformation along the MCT and the STDS was suggested.

Orogenic wedge extrusion

Various authors used the term "orogenic-wedge extrusion" to explain the emplacement of the HHC at its current position. All variations of this model have in common that the HHC is supposed to be part of the Indian plate which is emplaced in its current position by thrusting along the MCT at its base and by normal faulting along the STDS at its top. Importantly, the MCT and the SDTS merge at depth creating an orogenic wedge that is squeezed between the underthrusting Indian plate and the Tethyan Himalaya. Therefore, normal faulting along the STDS is not an expression of syn-orogenic extension in the classical sense, but is associated with relative top-to-the-N movement and the southward extrusion of the HHC.

The differences between models proposed by different authors are twofold and are related to the spatial distribution of deformation and the underlying driving mechanisms. Burchfiel and Royden (1985), for example, postulate a rigid orogenic wedge with the main deformation concentrated along the MCT at its base and along the STDS at its top. They suggest that the increasing potential difference between the rising mountain range and the undeformed Indian foreland results from crustal thickening by underplating of Tibetan crust with partly subducted Indian crust as the main underlying driving mechanism. This process is viewed to have generated a differential stress that, ultimately, exceeded the cohesive strength of the rocks within the upper crust, resulting in the collapse of the mountain front, which is expressed by the extrusion of the orogenic wedge.

Alternative models explain the observed structures by a pervasively deformed wedge with maximal deformation located in the center of the wedge (Thiede et al., 2004; Vannay et al., 2004). Following the latter two author groups, the extrusion of the orogenic wedge is the result of a substantial removal of material by erosion. This explanation is based on the observation that the location of the HHC, i.e. the orogenic wedge in the NW Indian Himalaya, correlates with an area of high erosion and, at present-day, of intensive precipitation.

Channel flow

Based on similar observations as the ductile orogenic wedge model, Grujic et al. (1996) proposed an alternative model, the so-called "channel flow" model. This scenario involves an extruding channel, sandwiched between the rigid underthrusting plate and the overlying rigid orogen (Nelson et al., 1996). Similar to the ductile orogenic wedge, deformation between MCT and STDS is pervasively with the largest amount of deformation in its center. Orogen-parallel normal faulting at the top of the extruding channel is again relative with respect to the overlying plate and not caused by an overall tensional stress regime within the orogen as a whole. In contrast to the orogenic wedge model, however, the MCT and the STDS are subparallel and do not merge at greater depths. This leads to the largest difference with respect to previous models: Here, the material transported within the channel is partially molten Tibetan crust and, therefore, the HHC is of Tibetan origin.

In order to start and maintain such a process, the extrusion of a mechanically weak lower crust and its transfer to the surface is required (e.g., Beaumont et al., 2001). This might be caused by intensified precipitation and erosional removal at the mountain front, similar to the explanation for the ductile orogenic wedge. However, numerical experiments also suggest that channelized flow of the middle and lower continental crust is a viable mechanism for the dissipation of potential energy stored in overthickened crust, even in the absence of lithospheric delamination (Bird, 1991; Royden et al., 1997). Seismic evidence for partially molten lower crust in southern Tibet lends credence to the notion that the lower crust of Tibet is capable of lateral flow Nelson et al. (1996). Furthermore, it has been argued for many years that overthickened, isostatically compensated continental crust has a tendency to flow laterally under its own weight (Fleitout and Froidevaux, 1982; England, 1982; Molnar and Lyon-Caen, 1988; Bird, 1991).

Passive roof thrust model

The orogenic wedge model is again the base for this model here, trying to explain also observations of varying top-to-the-N and top-to-the-S displacement along the STDS. In contrast to the original wedge model, Yin (2006) and Webb et al. (2007) propose that STDS and MCT not only merge at depths (as in the orogenic wedge), but also join up-dip, enclosing the HHC completely. The overlying THS and the HHC start to overthrust the LHS, in such a way that the HHC is intruded between the THS and the LHS. In addition, the THS is thrust over the HHC along the STDS (relative top-to-the-S shear). Later, the intrusion of the HHC is faster than the southward movement of the THS, marked as relative top-to-the-N shear along the STDS. Shear sense along the MCT (contact between HHC and LHS) is constantly top-to-the-S. Therefore, in a later stage, the STDS may be overturned and folded at the leading edge of the HHC, as observed in the NW Himalaya (Webb et al., 2007). Finally, the complete THS sequence on top of the HHC has been eroded without any further normal faulting along the STDS. In consequence, the crust at its extruding edge must be thinned, and the crust at its intruding edge should be thickened (Yin, 2006). Further erosion may explain why the MCT and the STDS do not merge in map view towards the eastern syntax, but diverge (Yin, 2006; Webb et al., 2007).

In addition, the Great Counter Thrust (GCT) may be linked to the STDS, being both the base of the TH. The GCT might be the roof thrust of the tectonic wedge of the Asian Plate. The alternating insertion of the two tectonic wedges could be the cause for the alternating shear on the STDS.

Continental subduction

An increasingly popular model is the continental subduction model by Chemenda et al. (1995, 2000). They propose that the Indian plate has been subducted beneath Eurasia to depths of > 150 km. During this process, the upper part has been moved somewhat slower than the lower lithospheric part of the Indian plate. At a critical point, the crustal part is inferred to have been sheared off and became decoupled from the lower lithosphere. The crustal piece started to move upwards, possibly also triggered by a break-off of the subducted mantle lithosphere.

Modeling of this process shows that low compressional forces and a strong slab-pull are able to subduct a large slice of continental crust to greater depths; after detaching such a piece from the mantle lithosphere, this crustal piece returns fast to upper crustal levels along a north-dipping thrust at its base and a normal fault at its top (i.e., the STDS). In case of high compressional forces and a weak slab-pull, additional erosion above the subduction zone is required in order to initiate the wedge extrusion of the deeply subducted slab, analogous to the models of channel flow.

The continental subduction model would also explain the occurrence of UHP rocks within the Tethyan and Higher Himalaya (Guillot et al., 1997; Epard and Steck, 2008), which would have been produced during the subducting process, and subsequently were transported back to the surface, documenting the critical point where the upward movement started by their peak metamorphic conditions and the associated age. Direct dating of the peak metamorphic phase of the UHP rocks

of the Tso Moriri document that the upward return started at around 50-45 Ma, while the emplacement of the HHC occurred around 25-20 Ma and was triggered by break-off of the subducted Indian continental mantle lithosphere (Guillot et al., 1997; Epard and Steck, 2008).

Change in basal shear stress

In subduction zones, a controlling condition for mountain building processes is the slope that stabilizes the orogenic wedge developing on the overriding plate (Dahlen, 1984). If the basal shear stress of the subducted plate is reduced by slab break-off or slab rollback, arc-parallel extension within the wedge may result (Dahlen, 1984). Similar assumptions can be associated with plateaus showing thrusting and crustal shortening along their margins by reducing the horizontal compressional stress or by changing the boundary conditions (England and Molnar, 1993; Yin, 1989).

1.2.2 Arc-perpendicular normal faults

Explanations for normal faults perpendicular to the Himalayan arc are generally based on the fact that the shape of the Himalaya is arcuate, describing a perfect small circle on the Earth's surface (Bendick and Bilham, 2001). However, the assumed driving forces causing such normal faulting are as variable as the models.

Radial thrusting

This model is based on the observation that not only the Himalaya is curved along a small circle (Bendick and Bilham, 2001), but also that slip at the Himalayan front is oriented radial (e.g., focal mechanisms in Molnar and Chen (1983)). This radial slip implies the occurrence of internal deformation of the overlying parts. In order to keep the arc-shaped geometry of the Himalayan orogen, tangential extension is necessary, either by E-W extension combined with strike-slip components or arc-perpendicular extension (Seeber and Armbruster, 1984).

Oroclinal bending

Klootwijk, 1985 Ratschbacher et al., 1994: This model is based on the observation that the majority of rifts in southern Tibet are confined between the KF and the Yadong-Gulu rift (Klootwijk et al., 1985; Ratschbacher et al., 1994). Due to the observed bending of the orogen, southern Tibet and the central Himalaya is affected by extension oriented N-S. This also could explain the dextral component at the KF and a sinistral component in the east, which, however, is not observed. The model compensates the missing strike-slip component in the east by right-stepping en-echelon arrangement of grabens, as observed at the Yarlung-Gulu rift. The observed opposite shear (dextral in the W, sinistral in the E) probably reflects opposite rotation of crustal blocks at the E and W syntaxes during oroclinal bending.

Focused compression at the Central Himalayan front

Kapp and Guynn (2004) proposed a model that is based on observations that the graben and rifts in the Tibetan Plateau and the Central Himalaya are not trending perfectly N-S but have slight trends towards the E and W. Graben located west of 87°E derive from a purely N-S orientation towards the W, whereas those located

east of 87°E show a tendency towards the E. Elastic modeling of the state of stress reveals that the observed stress pattern responsible for these features can be caused by a limited indenter with lengths between 15° and 40° .

Outward radial expansion of the Himalayan thrust front

One explanation for the existence of arc-perpendicular normal faults is related to the stepwise southward migration of the active thrust zone (Murphy and Copeland, 2005; Murphy et al., 2009). Due to the arcuate shape of the Himalaya, this propagation leads to an increase in length of the orogen. This causes extension parallel to the arc and therefore stretching perpendicular to the trend of the orogen. Since the increase in length is larger for the hanging wall of the MCT, this part experienced the largest amount of arc-parallel extension. The opening of the Zada Basin ($30.921^{\circ}\text{N}/79.651^{\circ}\text{E}$) as well as extension observed at the Gurla Mandhata gneiss dome ($30.250^{\circ}\text{N}/81.167^{\circ}\text{E}$) are interpreted as the manifestation of arc-parallel extension within the hinterland of the MCT (Murphy and Copeland, 2005; Murphy et al., 2009). In addition, the increase of extension towards the hinterland of the thrust zones would also explain the fact that the majority of the orogen-perpendicular normal faults are observed in the Tethyan Himalaya and the Transhimalaya.

Partitioning of oblique convergence

An alternative model derives from observations that interplate thrusting earthquakes along convergent plate boundaries show generally shortening slip directions which are not parallel to convergence directions (e.g., McCaffrey, 1996). The oblique convergence is thus compensated by plate-boundary parallel strike-slip faults and oblique normal faulting in the fore-arc regions or within the orogen's interior (Avé Lallement and Guth, 1990). In the Himalaya, this model of oblique convergence has been used to explain normal faults perpendicular to the Himalayan orogen (McCaffrey and Nabelek, 1998).

Change of boundary conditions along the eastern margin of Asia

N-S trending graben and rifts have been observed in the Himalaya, the Tibetan Plateau and as far north as Lake Baikal. They show similar characteristics in orientation and mode of extension (Yin, 2000). In addition, the larger structures are deeply rooted also in the mantle lithosphere. Furthermore, most of these extension zones were initiated during the late Miocene. Yin (2000) as well as Yin and Harrison (2000) explain them by a change in boundary conditions in East Asia 8-5 Ma ago, which may have been triggered by a protracted backarc extensional process related to large-scale mantle flow beneath Asia.

Convective removal of the mantle lithosphere

Another model linking upper crustal displacement with deep-seated processes within the lithosphere and asthenosphere is based on numerical modeling by England and Houseman (1989). The basic idea is that a thickened lithosphere, due the convergence between India and Eurasia and crustal stacking, will be colder and denser than the surrounding asthenosphere, which then leads to a convective instability and removal of the lower part of the mantle lithosphere, which subsequently will be re-

placed by hot asthenosphere. This “convectonal thinning” would rapidly increase the geothermal gradient of the continental lithosphere and therefore result in a rapid increase of surface elevation, which, in turn, would lead to an increase in potential energy. Thus, deviatoric stresses between elevated and non-elevated regions result in horizontal tension in those regions affected by convectonal thinning and in compression in the marginal areas not affected by this process.

Gravitational collapse of the orogen

A popular theory explaining the occurrence of normal faults within the Himalaya-Tibet region and other orogens is related to gravitational collapse (e.g. Dalmayrac and Molnar, 1981; Molnar and Chen, 1983; Royden and Burchfiel, 1987; Molnar and Lyon-Caen, 1989; Ratschbacher et al., 1994). Gravitational collapse is defined as the gravity-driven ductile flow that effectively reduces lateral contrasts in gravitational potential energy and produces extensional structures perpendicular to the flow direction (Rey et al., 2001). According to this model, the approximately north-trending rift systems within the Tibetan Plateau and the high internal parts of the Tethyan Himalaya are thus the superficial expression of east-directed flow of either a weak lower crust or a partially molten upper mantle (Rey et al., 2001, and references therein). A variation of this concept is the occurrence of extensional structures parallel to the high-elevation margins of plateaus associated with gravitational body forces, which would have its expression in the STDS (Froideveaux and Isacks, 1984).

Chapter 2

The role of extension during brittle deformation within the NW Indian Himalaya

published by Esther Hintersberger, Rasmus Thiede, Manfred Strecker (2011) in *Tectonics*, vol. 30, TC3012, doi: 10.1029/2010TC002822

Abstract

Synorogenic extension has been recognized as an integral structural constituent of mountain belts and high elevation plateaus during their evolution. In the Himalaya, both orogen-parallel and -normal extension has been recognized. However, the underlying driving forces for extension and their timing are still a matter of debate. Here we present new fault kinematic data based on systematic measurements of hundreds of outcrop-scale brittle fault-planes in the NW Indian Himalaya. This new data set, as well as field observations including crosscutting relationships, mineral fibers on fault planes, and correlations with deformation structures in lake sediments allows us to distinguish different deformation styles. The overall strain pattern derived from our data reflects the large regional contractional deformation pattern very well, but also reveals significant extensional deformation in a region, which is dominated by shortening. In total, we were able to identify six deformation styles, most of which are temporally and spatially linked representing protracted shortening. Our observations also furnish the basis for a detailed overview of the younger deformation history in the NW Himalaya, which has been characterized by extension overprinting previously generated structures related to shortening. The four dominant deformation styles are: (1) shortening parallel to the regional convergence direction; (2) arc-normal extension; (3) arc-parallel extension; and finally, (4) E-W extension. This is the first data set where a succession of both, arc-normal and E-W extension have been documented in the Himalaya. Importantly, our observations help differentiate E-W extension triggered by processes within the Tibetan Plateau from arc-parallel and -normal extension originating from the curvature of the Himalayan orogen.

2.1 Introduction

The Himalaya is the type example of a collisional mountain belt, characterized by intense crustal shortening and uplift resulting from ongoing convergence between India and Eurasia (Gansser, 1964; Le Fort, 1975). Along the southern Himalayan mountain front, crustal shortening along major thrust faults is the first-order process accommodating this convergence, which is currently focused on lower-elevation sectors of the Lesser Himalaya and the Siwalik ranges (e.g., Ni and Barazangi, 1984; Wesnousky et al., 1999; Zhang et al., 2004; Kumar et al., 2006). Contemporaneously, syntectonic extension processes at higher elevations have been shown to be an integral part of this tectonic evolution to exhume high-grade rocks to the surface (e.g., Burg et al., 1984a, Burchfiel et al., 1991; Murphy et al., 2000, 2002; Aoya et al., 2005; Murphy and Copeland, 2005; Thiede et al., 2006; Jessup et al., 2008). In fact, in the Higher Himalaya and parts of the Lesser Himalaya, active north-south striking normal faults constitute the youngest brittle structures that overprint all previously generated crustal-scale faults (e.g., Murphy and Copeland, 2005; Jessup et al., 2008; Hintersberger et al., 2010; Leloup et al., 2010). However, the mechanisms and the spatiotemporal relationships of the different kinematic regimes are still poorly understood. This is partly due to the limited availability of timing constraints, as well as the lack of regional kinematic data and unambiguous cross-cutting relationships that could help characterize the principal deformation stages.

Previous tectonic studies in the region have been biased towards the understanding of large orogen-parallel thrusts and detachments in order to decipher the structural evolution of the Himalaya (e.g., Gansser, 1964; Burchfiel et al., 1992; Vannay et al., 2004). Detailed analyses of meso- and small-scale brittle structures have been largely neglected, although such deformation phenomena may furnish important insights into decipher deformation history of orogens, allowing distinguish different kinematic styles during a multi-phased deformation history. For example, regionally focused studies in the vicinity of the Nanga Parbat syntax in the Pakistan Himalaya, using brittle-fault kinematic data sets, have revealed that extensional structures are much more common in this contractile settings than previously thought (e.g., Zeilinger et al., 2000; Burg et al., 2005; Pêcher et al., 2008) and may provide a different perspective of the character of the protracted tectonic processes in the Himalaya. Combined, fault kinematic studies of minor and meso-scale faults and macroscopic structural observations of brittle fault arrays may provide important data to understand the more recent kinematic history of the Himalayan arc. In addition, such data may help decipher the spatial and temporal tectonic relationships between seismically active sectors of the orogen that are characterized by different kinematic regimes.

The Western Himalaya between 74°E and 81°E is particularly well suited for small-scale kinematic studies, because here all first-order structural elements of the orogen are well expressed and access to the transition between the Himalayan and Tibetan structural realm exists. All contractile structures associated with the protracted history of Himalayan mountain building are well exposed (e.g., Thakur, 1998; DiPietro and Pogue, 2004; Vannay et al., 2004). In addition, there are several

generations of normal faults that have affected these sectors during, and subsequent to shortening. One of the main advantages in conducting the kinematic analysis in the NW Indian Himalaya is related to the regionally NW-SE-oriented strike of the orogen providing the opportunity to differentiate between deformation styles related to processes within the Himalaya and its geometry from those features that may have been triggered by deformation of the Tibetan Plateau.

This dichotomy in the distribution of normal and thrust faults in the NW Indian Himalaya described above is also mirrored by earthquakes and GPS data from that region. For example, focal mechanisms of earthquakes with magnitudes up to 8.6 and depths to approximately 30 km indicate NE-SW shortening, perpendicular to the regionally NW-SE striking thrust faults and concentrated along the Main Himalayan Thrust (NEIC Catalog, 2009). On the other hand, closely spaced normal faults offsetting Quaternary deposits, focal mechanisms of earthquakes with magnitudes between 5.2 and 6.8 (Molnar and Lyon-Caen, 1989), and regional GPS measurements (Banerjee and Bürgmann, 2002) reveal ongoing E-W extension in the internal parts of the Higher and Tethyan Himalayas. These observations are in good agreement with previous work, where Thiede et al. (2006) and Hintersberger et al. (2010) documented that active E-W extension is an important part of the long-term geological evolution of this region.

In this study, we document the relative progression of brittle structures related to changes in the kinematic regime during mountain building in the Himalaya. In this context, we recorded fault kinematic data based on fault striations from a new data set comprising 2000 brittle faults, which we measured in a N-S transect between the Spiti Valley in the Tibetan Himalaya in the north and the mountain front in the Garhwal Himalaya (30-33°N/77-79°E, see Fig. 2.1) in the south. This allows us to differentiate several styles of deformation, to document the interplay between shortening and extension, as well as to demonstrate that extension plays a fundamental role during upper crustal deformation and orogenic wedge evolution since the Miocene.

1

¹Figure 2.1:(A) Complete data set of all kinematic fault measurements. Kinematically consistent data sets were extracted to calculate the paleo-strain axes shown in Figs. 2-8. Structural map of the NW Indian Himalaya, modified after Thiede et al. (2005) and references therein. Earthquakes, shown as red dots, are taken from the NEIC catalog. The shaded relief map in the background is obtained by using a SRTM image. (B) Geological map and structural provinces of the entire Himalaya, modified after Yin (2006) and references therein. For the western Himalaya, the structures as mapped by DiPietro and Pogue (2004) are used. Black box marks the area of (A). Abbreviations: AD - Ama Drime Massif, BR - Brahmaputra River, GM - Gurla Mandhata gneiss dome, IR - Indus River, ITSZ - Indus-Tsangpo suture zone, KF - Karakorum fault, KNF - Karcham normal fault, LPDZ - Leo Pargil detachment zone, MBT - Main Boundary thrust, MCT - Main Central thrust, MFT - Main Frontal thrust, MT - Munsiri thrust, SD - Sangla detachment, STDS - Southern Tibetan detachment system, TM - Tso Morari, TG - Thakkola graben, YG - Yadong graben, ZB - Zada Basin.

2.2 Geological setting of the NW Indian Himalaya

2.2.1 Principal structures related to shortening

Deformation at the southern front of the NW Himalaya is dominated by south-vergent thrust systems that have been accommodating the underthrusting of India under Eurasia which started between ~ 65 Ma and ~ 43 Ma (e.g., Patriat and Achache, 1984; Klootwijk et al., 1992; Rowley, 1996; Najman et al., 2003). These large along-strike fault systems, traceable almost continuously along the length of the entire orogen, separate the Himalaya into five principal lithologic-tectonic provinces, including the Sub-Himalaya, the Lesser Himalaya, the Higher Himalaya, the Tethyan Himalaya, and the Transhimalaya (Gansser, 1964; DiPietro and Pogue, 2004). These structures are interpreted to accommodate approximately 30 to 50 % of the present-day NNE-directed motion of the Indian plate with respect to stable Asia (Le Pichon et al., 1992; Banerjee and Bürgmann, 2002; Zhang et al., 2004). This process has been furthermore associated with a stepwise southward migration of thrust systems, from the Main Central Thrust (MCT, since 23 -20 Ma; Hogdes et al., 1996), to the Munsiri Thrust (MT, since 11-6 Ma Vannay et al., 2004) and the Main Boundary Thrust (MBT, since 11 -9 Ma; Meigs et al., 1995), and to the currently active Main Frontal Thrust since the Pliocene (MFT; Molnar, 1984; Wesnousky et al., 1999; Kumar et al., 2006). All those major thrust faults are suggested to root into a low-angle detachment, the Main Himalayan Thrust (MHT, e.g., Schelling and Arita, 1991). Based on the overall strike of these structures, recent GPS data and earthquake focal mechanisms, a general radial shortening direction perpendicular to the strike of the orogen is observed, both on geological time scales as well as in the present-day active tectonics. In the NW Indian Himalaya, the regional NE-SW shortening direction, expressed by the regional NW-SE oriented strike of the large thrust faults, is not only confirmed by GPS data (Banerjee and Bürgmann, 2002), but is also reflected by large NW-SE trending open folding of the Tethyan Himalaya sequences (Wiesmayr and Grasemann, 2002; Neumayer et al., 2004) and by an orogen-parallel band of seismicity (NEIC Catalog, 2009). Fault-plane solutions of larger earthquakes indicate radial shortening parallel to the strike of the faults (Seeber and Armbruster, 1981; Molnar and Chen, 1983; Molnar and Lyon-Caen, 1989). The most important events in the NW Indian Himalaya associated with thrusting are the Kangra (4 April 1905, $M(\text{estimated})=8.6$, Middlemiss, 1910), Uttarkashi (20 October 1991, $M_w = 6.8$, Kayal et al., 1992), and Chamoli earthquakes (29 March 1999, $M_w = 6.6$, Rastogi, 2000), all generated most probably along the MFT (Wesnousky et al., 1999).

2.2.2 Structures related to extension

The protracted, ongoing overall radial shortening in the NW Indian Himalaya is coeval with several styles of extension. The most important extensional structures are arc-parallel, linked normal faults associated with the Southern Tibetan Detachment System (STDS). The STDS strikes parallel to the MCT and separates the low-grade metamorphic rocks of the Tethyan Himalaya in the hanging wall from high-grade metamorphic footwall units of the Higher Himalaya (Burg et al., 1984a, (Burchfiel

and Royden, 1985; Burchfiel et al., 1992)). During the Miocene, the Higher Himalayan rocks were exhumed during coeval thrusting along the MCT and extension along the STDS. There is a controversial discussion of the underlying mechanics and the role of the STDS during the extrusion of crustal material along the MCT. It is debated whether or not these structures facilitate extrusion of the crust via channel flow from underneath the Tibet Plateau (e.g., Grujic et al., 1996; Beaumont et al., 2001) or if extension along the STDS may simply be the surface response of a ramp-like geometry of the main subduction horizon (Lavé and Avouac, 2001). In addition, the level of activity of the STDS is debated. This involves the question as to whether the STDS has been reactivated during the Holocene (e.g., Hogdes et al., 2001; Hurtado et al., 2001) or if it has been inactive for the last 13 Ma (e.g., Jessup et al., 2008; Leloup et al., 2010). In the NW Indian Himalaya, the ductile Sangla Detachment (SD) and the Zaskar shear zone (Dèzes et al., 1999) constitute an integral segment of the STDS associated with regional NE-SW oriented extension. However, neotectonic activity has not been observed in this region (Vannay and Grasemann, 1998; Wiesmayr and Grasemann, 2002). Along to the Sutlej Valley, an additional extensional fault is observed at the level of the MCT. The Karcham Normal Fault (KNF) is an east-dipping extensional brittle fault that crosscuts the MCT mylonites at the base of the Higher Himalaya (Jessup et al., 2008). In earlier studies, it has been inferred that the KNF may act as the counterpart of the MT during the tectonic exhumation of the Lesser Himalayan Crystalline (e.g., Vannay et al., 2004).

Another extensional detachment zone, the Leo Pargil Detachment Zone (LPDZ) farther north is more obliquely oriented with respect to the orogen (Fig. 2.1). Thiede et al. (2006) describe the LPDZ as a system of linked west-dipping, low-angle ductile normal faults at the western flank of the Leo Pargil gneiss dome. The onset of activity of this structure is poorly constrained, but extension must have begun during the middle Miocene (~16 Ma, Thiede et al., 2006).

An important group of extensional structures constitute active N-S striking normal faults. In the NW Himalaya, several N-S striking normal faults are documented in the vicinity of the Gurla Mandhata Dome (e.g., Murphy et al., 2000), the Kaurik-Chango normal fault (KCNF) at the western flank of the Leo Pargil gneiss dome overprinting the LPDZ (Hayden, 1904; Thiede et al., 2006), the Tso Kar, the Tso Morari, and the Eastern Tso Morari normal faults north of the Spiti Valley, as well as the recently discovered N-S striking faults in the Lingti Valley and north of the Leo Pargil gneiss dome (e.g., Steck et al., 1993; Fuchs and Linner, 1996; Epard and Steck, 2008; Hintersberger et al., 2010). These structures have affected either Quaternary alluvial or colluvial deposits and have generated fault scarps that are easily identified on satellite imagery (Epard and Steck, 2008; Hintersberger et al., 2010). These structures belong to the youngest tectonic phase reflecting ongoing E-W extension. Neither one of these extensional faults are parallel nor perpendicular to the regional NW-SE shortening direction. However, the orientation of those faults aligns perfectly with a group of shallow earthquakes with depths < 15 km between 78°E and 78.5°E (Molnar and Lyon-Caen, 1989, NEIC catalog, 2009). This swath of seismicity stretches from the Tso Morari in the north close to the MCT in the south.

The largest earthquake in this seismic belt was the Kinnaur Earthquake (Jan. 19th 1975, $M_s = 6.8$, Khattri et al., 1978), which ruptured the KNCF close to the Leo Pargil gneiss dome (Singh et al., 1975). Importantly, since the installation of the worldwide seismic network in the 1960s, several similar major earthquakes have been located in the Sutlej region, with focal mechanisms providing additional evidence for ongoing E-W directed extension associated with these fault systems (e.g., Molnar and Chen, 1983).

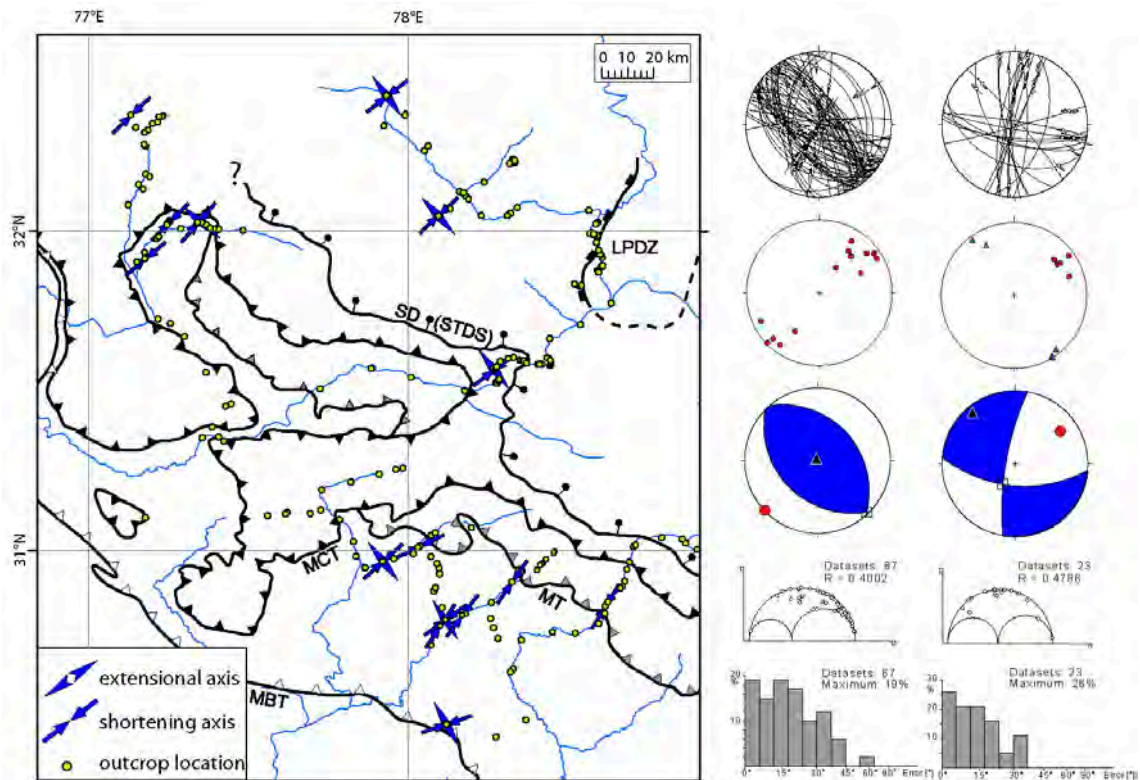


Figure 2.2: Strain axes related to NE-SW shortening. Arrows indicate the horizontal component of the extensional or shortening axes for each outcrop location (green dots). Green dots without arrows are places without any observations related to NE-SW shortening. The structural map is the same as in 2.1. For abbreviations see caption to 2.1. On the right side from top to bottom: stereo plot of compiled data from all outcrops showing respective shortening, separated into strike-slip (left) and reverse faulting (right); extensional (blue triangles) and shortening axes (red dots) for each outcrop (also plotted in the map); paleo-strain calculation for the complete data set shown in the stereo plot on the top (NDA method); Mohr circle for the paleo-strain calculation; misfit plot for the paleo-strain calculation.

2.3 Data processing

Here, we describe the collection of fault-kinematic data, how the data was processed, and how the paleo-strain estimates were obtained. We collected fault-kinematic data of approximately 2000 brittle faults, including measurements of fault-plane dip and dip direction, trend and plunge of fault-plane striations, mostly slickenlines, as well as the sense of shear. Given this information for a cogenetic set of faults, the associated strain axes can be determined (Bott, 1959). For coaxial deformation, these obtained kinematic strain-axes can be used as an approximation for paleo-stress axes. In the case of brittle faulting, the condition of coaxial deformation is met for fault planes outside of prominent brittle shear zones. Therefore, we concentrated on outcrop-scale brittle faults between the Tibetan Himalaya and the southern Himalayan mountain front, typically showing a displacement of up to several centimeters. The quality of the fault-kinematic data was documented with respect to well developed lineation and unambiguous indicators for the sense of shear. This provided the basis for classifying the data into four categories (1 -very good, 2 -good, 3 -weak, 0 -no shear sense). Crosscutting relationships were scarce, we therefore also noted the minerals creating the slickenlines, and if there was any ductile part of deformation along the fault planes, in order to obtain more insight concerning the relative chronology of the different deformation styles. Most data has been collected along road cuts, where dynamite blasting is common during construction work. However, features associated with blasting are easily distinguished in field, mainly by containing traces of sulfur or by their radial occurrence around a blasting site, and not considered within this study.

In order to obtain strain axes, we separated the fault kinematic data into cogenetic homogeneous subsets. For the separation and calculation of paleo-strain axes, we used the program *TectonicsFP* (Ortner et al., 2002), which also allows us to include data sets only containing the orientation of the lineation, but no information about the sense of shear. We started by plotting the data for every outcrop and singled out those outcrops dominated by a single deformation style. For these outcrops, we calculated the associated paleo-strain axes by using the kinematic P/T-axes method (Turner, 1953). Information from outcrops with more complex deformation histories was sorted by compatibility with the paleo-strain axes. We then added the missing sense of shear for those kinematic fault data sets where possible. The extracted kinematic information related to the different deformation styles in each outcrop was then used to finally calculate the pseudo fault-plane solutions using the numeric dynamic analysis (NDA, Spang, 1972; Sperner, 1996). The angle between the fault plane and its P axis varies between 30, 45, and 60 degrees, depending on the best fit to the data. This ultimately resulted in a total of about 1700 measured fault planes with associated lineations, distributed over approximately 150 outcrops (see Figs. 2.2-2.8).

In order to exclude the influence of one single deformation zone, we gathered the kinematic data from outcrops in the same tectonic unit (e.g., all data collected between the MCT and the MT). Those data subsets were defined by the vicinity of the outcrops to large structures and are called "outcrop subsets" in the following.

As an example for all those outcrop subsets, we describe the outcrops and the detailed analysis for the Bhagirati Valley (see dotted profile box in Fig. 2.1). The Bhagirati Valley in the Garhwal Himalaya provides a natural cross section through the major structures related to NE-SW shortening, from the hanging wall of the MBT to the hanging wall of the SDTS. The high data density, as well as the well developed overprinting criteria in this particular valley provide detailed insight into the development of brittle deformation in relation to the larger thrust faults such as the MCT, MT, and MBT. We gathered data from three outcrops on average and extracted the faults related to different deformation styles. In general, two or three different deformation styles were identified per outcrop subset. However, variations of the identified deformation styles to the single-outcrop analysis are negligible.

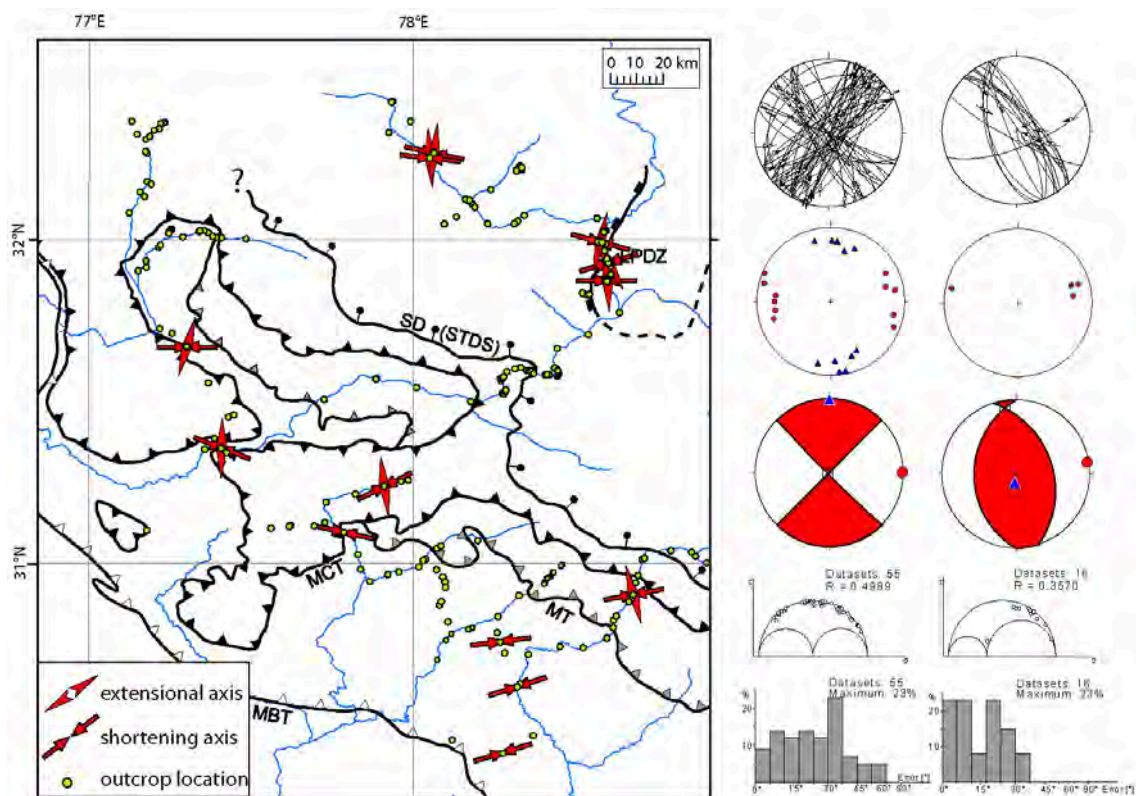


Figure 2.3: Strain axes related to E-W shortening that is mainly expressed by strike-slip faults. For details see Fig. 2.2

2.4 Paleo-strain results

Our data show 6 separate, yet related kinematic styles. As a general trend, we observe protracted shortening throughout the part of the Himalaya that is dominated by the large thrust zones in the footwall of the STDS (in the following named "thrust belt"). However, structures associated with shortening are superposed by features related to extension with varying directions. In addition, strike-slip faulting is an ubiquitous phenomenon associated with shortening in this environment. Shortening expressed by both, reverse and strike-slip faulting, is supposed to be possible in case of similar size of the intermediate and the extensional axes. As other mountain belts, the Himalayan orogen is a highly dynamic region, and thus, different styles of deformation may act contemporaneously. Therefore, a differentiation of the observed deformation styles into "older" and "younger" phases is only partly possible, and perhaps locally applicable, and will be further specified below. This is the reason why we prefer to use "styles" over the term "phases", since coeval activity of different styles in adjacent areas, or even in the same area, cannot be completely ruled out.

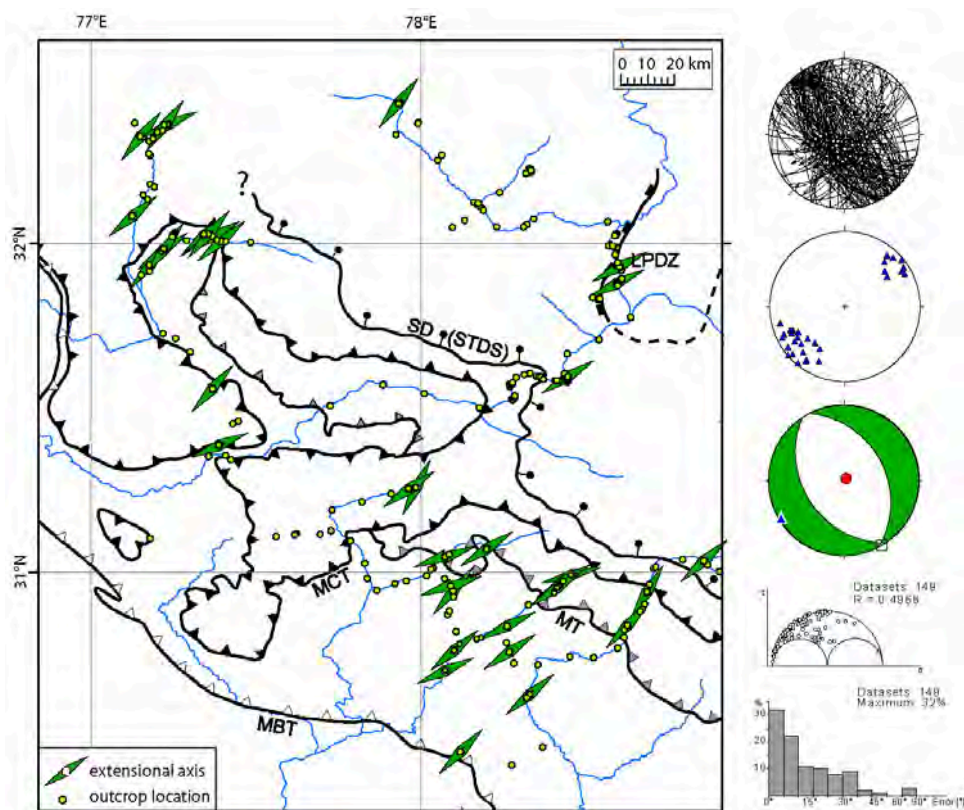


Figure 2.4: Strain axes related to NE-SW (arc-normal) extension. For details see Fig. 2.2.

2.4.1 NE-SW (arc-normal) shortening (D1)

Parallel to the present-day regional shortening direction, NE-SW oriented shortening is reflected by generally NW-SE striking brittle reverse faults associated with steeply plunging mineral lineations (Fig. 2.2). Such faults are mainly concentrated in the thrust belt and were generated within the ductile-brittle transition zone. In the Tethyan Himalaya, however, this deformation style is only occasionally observed and represented by strike-slip faults, which generally form in conjugate sets of WNW-ESE striking left-lateral, and NNE-SSW striking right-lateral faults.

2.4.2 ENE-WSW shortening (D2)

Another group of lineations, but much less frequent, indicate ENE-WSW oriented shortening (Fig. 2.3). The majority of them are subhorizontal lineations on conjugate sets of steeply dipping NE-SW striking right-lateral and NW-SE striking left-lateral strike-slip faults, respectively. Interestingly, a high concentration of faults related to this style of deformation is found close to the LPDZ. Rarely, but consistently, lineations associated with oblique fault motion on NW-SE striking, steeply dipping reverse faults are observed only within the thrust belt, indicating the generation of the described strike-slip faults during shortening. In addition, the reverse faults seem to reactivate the previously generated faults.

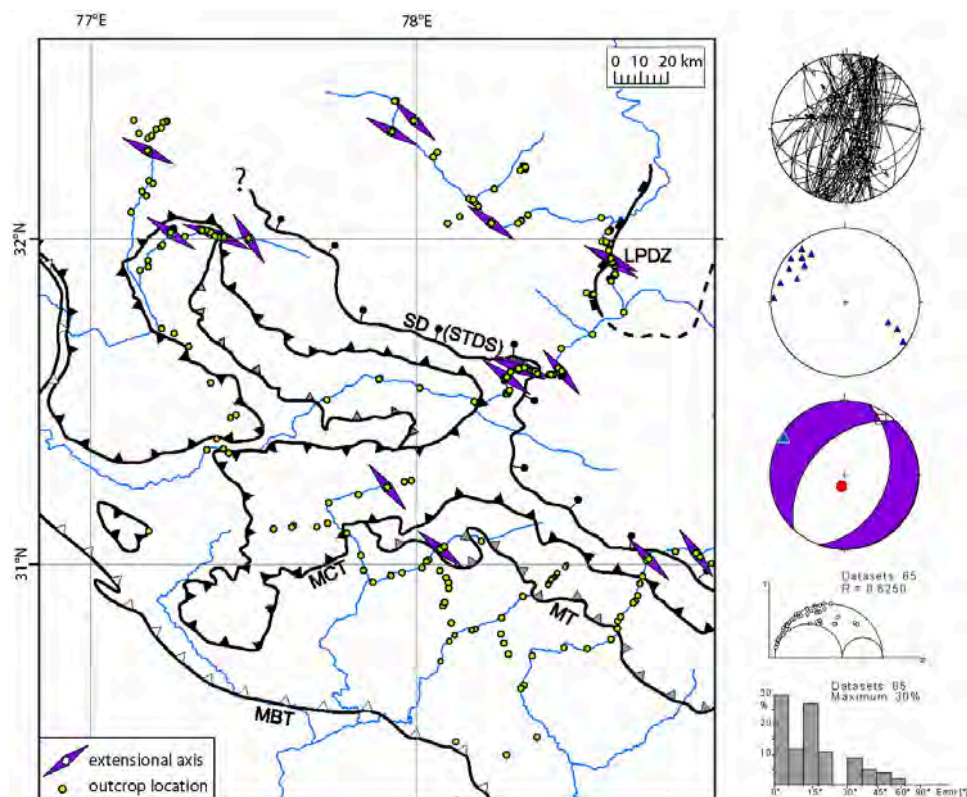


Figure 2.5: Strain axes related to NW-SE (arc-parallel) extension. For details see Fig. 2.2.

2.4.3 NE-SW (arc-normal) extension (D3)

Lineations, consisting mainly of quartz and mica mineral fibers, plunge steeply on NW-SE striking normal faults that are related to NE-SW oriented, arc-normal extension (Fig. 2.4). Conjugated sets of NW-SE striking, steeply dipping joints, as well as parallel quartz-filled veins traversing basement rocks emphasize the dominant character of this deformation. Importantly, the normal faults are neither limited to the Higher Himalaya nor are they associated with larger regional-scale structures, such as the MCT and the STDS. Instead, normal faults are closely spaced and have pervasively affected the rocks of the thrust belt. In the Tethyan Himalaya, features related to NE-SW extension are mainly found close to the LPDZ. Crosscutting relationships observed in the field show that this kinematic style is clearly younger than the NE-SW shortening. However, the orientation of faults related to each of those deformation styles is very consistent. Taking this observation into account, it appears likely that reverse faults generated during NE-SW shortening were reactivated as normal faults during NE-SW extension. This would also explain the low degree of preservation of kinematic records related to NE-SW shortening.

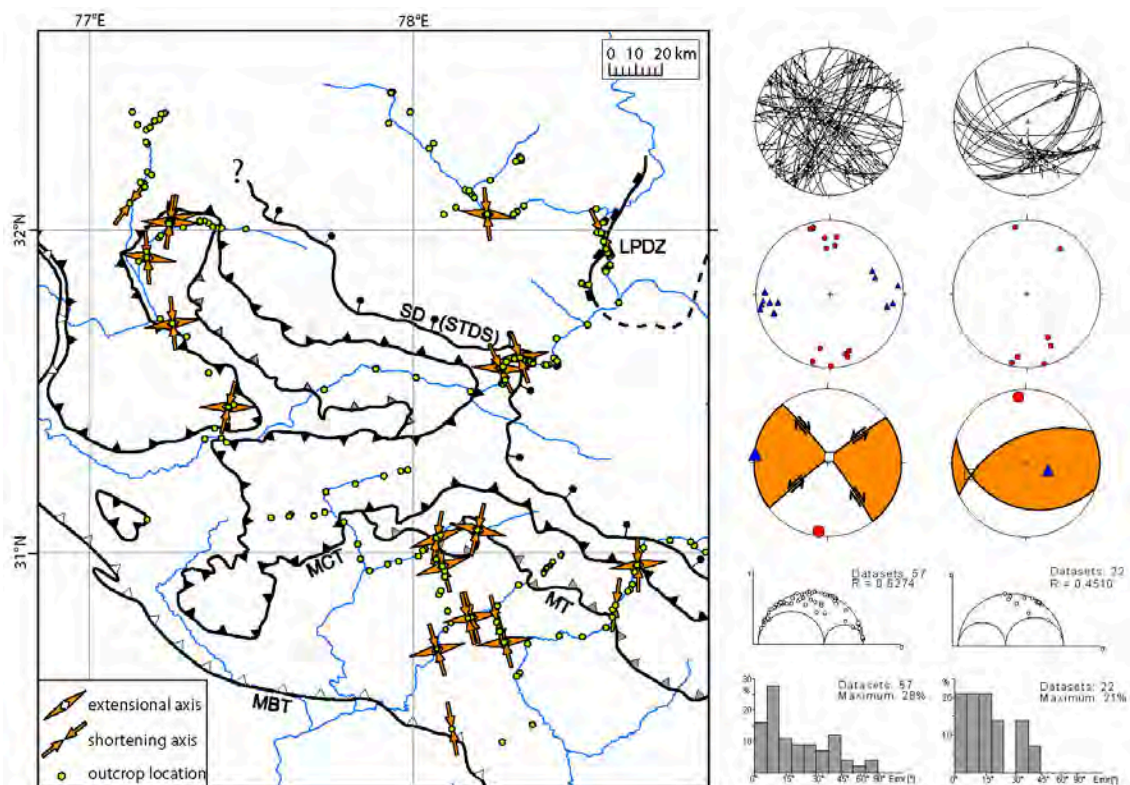


Figure 2.6: Strain axes related to N-S shortening that is mainly expressed by strike-slip faults. For details see Fig. 2.2.

2.4.4 NW-SE (arc-parallel) extension (D4)

Most of the fault planes associated with NW-SE (arc-parallel) extension are striking N-S to NNE-SSW with oblique lineations (Fig. 2.5). The faults seem to be partly reactivated strike-slip faults, most probably generated during NE-SW shortening (D1). This is emphasized by the kinematic records related to this direction of extension, which are only observed in the hinterland of the MT. Around the Leo Pargil gneiss dome and close to the STDS, in the Sutlej Valley between the villages of Rekong Peo and Pooh, NW-SE extension is the most dominant brittle deformation. In this region, lineations associated with this deformation style are steeply dipping slickenlines on NE-SW striking normal faults with varying dip angles.

2.4.5 N-S shortening (D5)

Again, this deformation style is dominated by strike-slip faulting on NW-SE striking right-lateral and NE-SW striking left-lateral steeply dipping faults, respectively (Fig. 2.6). A small number of NE-SW and WNW-ESE striking reverse faults dipping moderately toward the S is also observed. This deformation style is mainly recorded in the thrust belt, suggesting that it might be a mere adjustment to slight variations within the strain pattern.

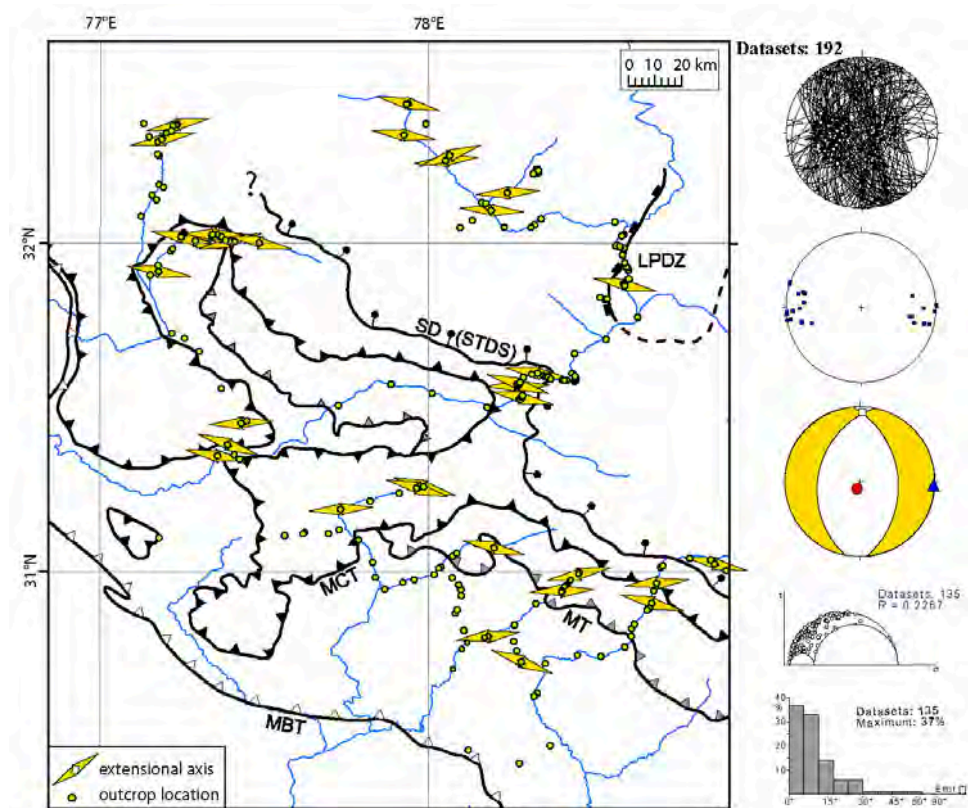


Figure 2.7: Strain axes related to E-W extension. For details see Fig. 2.2.

2.4.6 E-W extension (D6)

Structures related to E-W extension in the thrust belt are commonly associated with clayey fault gouges and poor preservation of lineations. This is generally observed on reactivated NW/NNW-SE/SSE or NE-SW striking faults, which are characterized by oblique striations (Fig. 2.7). Interestingly, those structures often occur with a large number of N-S striking joints. In addition to the small-scale structures, further evidence for E-W extension within the thrust belt is provided by an approximately 5-m-wide brittle fault with a clayey fault gouge. This fault strikes NNW-SSE and has clayey lineations indicating normal fault movement. The amount of displacement cannot be determined. In the Tethyan Himalaya, mostly carbonatic slickenlines indicating E-W extension are found on a variety of fault planes, mostly exhibiting oblique normal faulting (see stereo plot in the upper right corner of Fig. 2.7 and stereo plots related to D6 in Appendix A.1). This fact, together with observations of N-S striking normal faults affecting Quaternary alluvial terraces, suggest that E-W extension is currently overprinting all other kinematic styles that were previously generated. However, close to the STDS, we also found quartz-filled N-S striking tension gashes where the Quartz minerals are oriented perpendicular to the rim. This implies that E-W extension close to the STDS is either a longer-lasting phenomenon, generating the tension gashes and cataclastic faulting, or have occurred during different time spans.

2.4.7 N-S extension

Observed only at a few outcrops within the thrust belt, E-W striking normal faults with steeply plunging lineations and NW-dipping normal faults with slightly oblique lineations occur in this region (Fig. 2.8). Unfortunately, there are no crosscutting relationships to other deformation styles. Due to this fact and to its limited occurrence, we suggest that it is unlikely that this deformation style has any regional relevance.

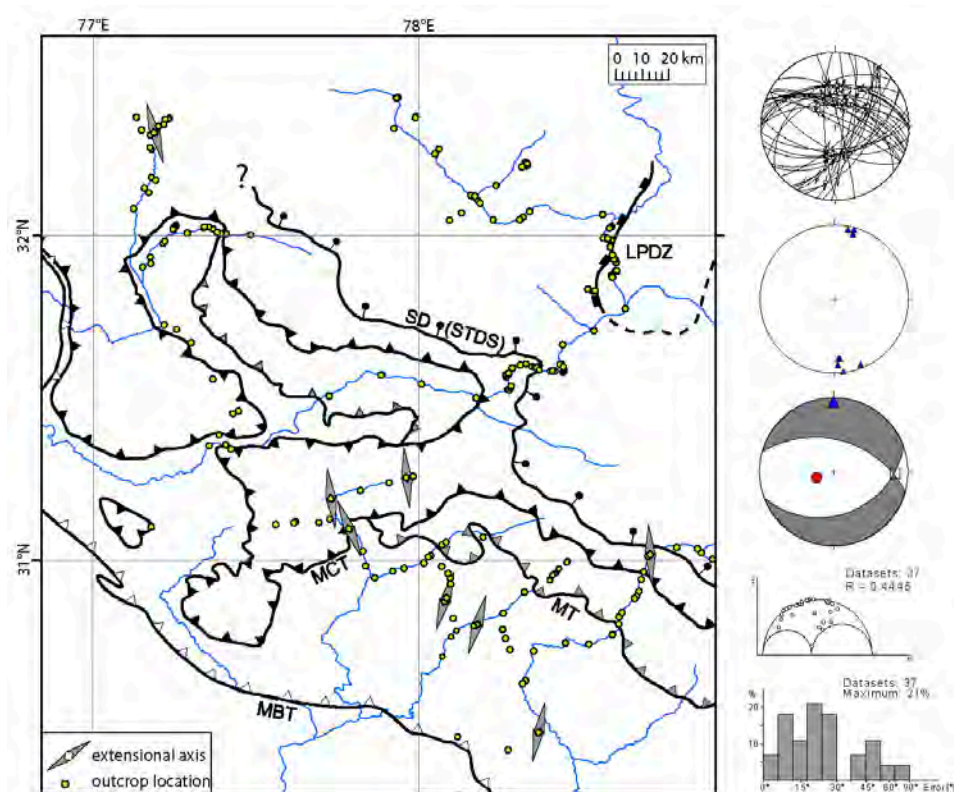


Figure 2.8: Strain axes related to N-S extension. For details see Fig. 2.2.

2.5 Chronology

2.5.1 Relative chronology

The relative chronology of the deformation styles is based on cross-cutting relationships observed in the field, such as overprinting slickenlines or faults that are crosscut by other structures (Fig. 2.9). However, these criteria are not always well expressed. Therefore, we used the following arguments to arrange the deformation styles in the relative order shown in Fig. 2.10.

Faults related to NE-SW shortening (D1) were generated within the brittle-ductile transition zone. Nevertheless, ductile motion along the large thrusts such as the MCT, MT and MBT is also characterized by NE-dipping schistosity and mineral lineations indicating a similar shortening direction (Vannay and Grasemann, 2001; Vannay et al., 2004), consistent with our observations of NE-SW shortening inherited from the brittle deformation history. Therefore, we consider NE-SW shortening to be the oldest brittle deformation style.

There is no clear age correlation between D1 and D2. However, lineations associated with D2 are only observed showing oblique movement on NW-SE striking reverse faults that are assumed to have been generated during D1. Therefore, we suggest that D2 is younger than D1. This fits well with the observations of Neumayer et al. (2004), who describe NE-SW extension in the Tethyan Himalaya of the Spiti Valley postdating SW-vergent folding associated with D1.

Figure 2.9: Evaluation of crosscutting relations observed in the field. The younger deformation phase is on the vertical line, the older one on the horizontal line. Numbering of the deformation styles follows same order as shown in 2.10. Colors are in accordance with those of Figs. 2.2-2.8.

OLDER \ YOUNGER	D6	D5	D4	D3	D2	D1
D6						
D5						
D4						
D3						
		4 insights	3	2		1
				3		2
			1			
				3		

E-W extension (D6) is generally associated with red clay-rich cataclastic fault zones, which are considered to be generated at low temperatures below 200°C (McNulty, 1995). Together with other observations of N-S striking normal faults cutting alluvial-fan deposits and terraces (Hintersberger et al., 2010), as well as fault-plane solutions of recent earthquakes in the hinterland of the Tethyan Himalaya (Molnar and Lyon-Caen, 1989), we consider E-W extension to be the most recent deformation style in the NW Indian Himalaya.

In addition, E-W extension is mostly associated with oblique slickenlines on a variety of fault planes (see uppermost stereo plot in Fig. 2.7 and stereo plots associated with D6 in Appendix A.1), which might be explained as reactivation of fault planes generated during former deformation styles.

Quartz-filled veins associated with NW-SE striking joints generated during D3 point towards a higher temperature during this deformation style. Therefore, we consider it to be older than D6, which is also supported by a limited number of cross-cutting relationships.

Slickenlines associated with NNW-SSE shortening (D5) consist mainly of mafic and quartz mineral fibers. Therefore, D5 must be older than the clay-rich cataclastic faults of D6.

2.5.2 Onset of brittle deformation across the Himalaya based on thermochronology

In the following, a compilation of thermochronologic studies (e.g., Metcalfe, 1993; Lal et al., 1999; Jain et al., 2000; Wiesmayr and Grasemann, 2002; Vannay et al., 2004; Thiede et al., 2005) will be used to constrain the onset of the deformation styles in different tectonic compartments in the NW Indian Himalaya (Table 2.1). Thermochronologic age constraints such as $^{40}\text{Ar}/^{39}\text{Ar}$ cooling ages and fission track ages provide insight concerning the time when the host rocks were passing through specific temperature ranges. Especially the closure temperatures for biotite ($\sim 300^\circ\text{C}$) and white mica ($\sim 450^\circ\text{C}$, Vannay et al., 2004) coincide with the transition to ductile deformation within a temperature range between 250 and 400°C. Below these tem-

peratures rocks behave in a brittle manner. In addition, the annealing temperature for zircon fission tracks (ZFT, $\sim 290^{\circ}\text{C}$, Vannay et al., 2004) helps to temporally pinpoint the transition between brittle-ductile and entirely brittle behavior of the rocks. Apatite FT (AFT) ages indicating annealing temperatures of approximately 110°C (Vannay et al., 2004), however, define a temperature range during which most of the generated faults show mostly pure cataclastic behavior with fault breccia and clay gouges. Obviously, the limitation of this approach is that the age determination of the host rocks only shows that they were "cold" enough to behave in a brittle manner, but the timing of fault initiation cannot be determined. Therefore, those ages must represent the upper limit of deformation processes. Also, in certain segments of the orogen with young $^{40}\text{Ar}/^{39}\text{Ar}$, ZFT, AFT cooling ages in the range of $< 6\text{Ma}$, $< 4\text{Ma}$, $< 2\text{Ma}$, respectively, thermochronology provides narrow bounds for brittle deformation such as in the Higher Himalaya, while other segments with old cooling ages such as the Tethyan Himalaya only provide very little additional constraints. Thus, future dating of synkinematically grown minerals on fault-plane surfaces would help pinpoint the timing of certain deformation styles.

The Upper Proterozoic to Eocene sedimentary rocks in the Tethyan Himalaya of the Spiti Valley have never been exposed to more than lower-greenschist conditions (e.g., Draganits et al., 2001). Ages of recrystallized illites in cleavage domains related to D1 indicate that folding in the Tethyan Himalaya was active at around 42-46 Ma (Wiesmayr and Grasemann, 2002). Therefore, since conjugated dextral and sinistral strike-slip movement on NNE/NE-SSW/SW and NW/WNW-SE/ESE striking fault planes compensating D1 and D2 shortening do not show any sign of being folded, those structures should have been initiated after this time (Figs. 2.2, 2.3 and Appendix A.1). The preservation of the illites also indicates that at least since this time, the main part of the Tethyan Himalaya deformed under non-metamorphic conditions. Therefore, the construction of a more detailed absolute time frame for the sedimentary rocks of the Tethyan Himalaya is not possible at present. However, we outlined in a previous study that E-W extension (D6) is a continuous process that has been overprinting all other structures until today. In the Tethyan Himalaya, this

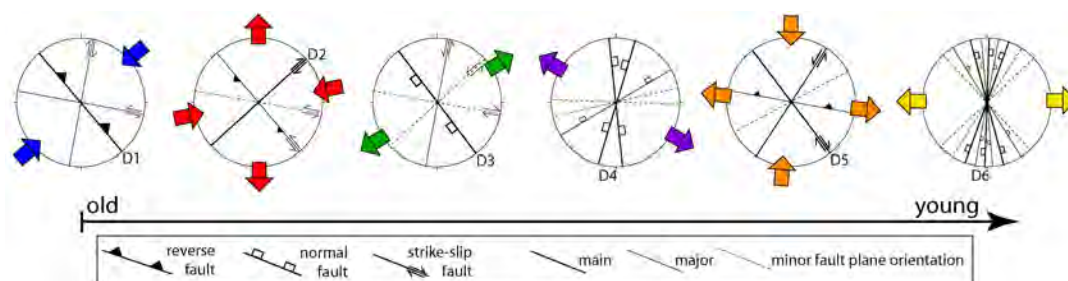


Figure 2.10: Relative chronology of the major deformation styles. For each deformation style, a representative fault pattern is shown. Labeled thick lines show the main fault plane orientation and movement along those faults during the indicated deformation style. Other major faults are marked with solid lines, minor reactivated faults with dashed lines. Reactivation of fault planes of former deformation styles is common and not marked especially. Colored arrows show shortening and/or extension axes. Colors are in accordance with those of Figs. 2.2-2.9.

is documented by N-S striking normal faults offsetting Quaternary fluvio-lacustrine sediments, fluvial terraces, and alluvial fans (Hintersberger et al., 2010).

The areally limited exhumation of the Leo Pargil gneiss dome constitutes a local perturbation within the Tethyan Himalaya. Therefore, age constraints from this part of the orogen may tell a separate history. While deformation in the hanging wall in this region (within the Tethyan Himalaya) occurred under brittle conditions, $^{40}\text{Ar}/^{39}\text{Ar}$ dating shows that the exhumed rocks in the footwall reached the brittle-ductile transition zone at around 14 to 15 Ma (Thiede et al., 2006; Hintersberger et al., 2010). Synkinematically grown white micas on W-dipping normal faults in the hanging wall of the Leo Pargil as well as ductile mineral stretching lineations observed in the footwall of the Leo Pargil indicate that E-W extension close to the Leo Pargil has been active since at least 16 Ma (Thiede et al., 2006; Hintersberger et al., 2010). Focal mechanisms of earthquakes recorded during the last 35 years, and especially the 1975 Kinnaur Earthquake (Molnar and Lyon-Caen, 1989, Harvard CMT catalog, 2009) document the continuity of this deformation style until the present day.

Close to the STDS, however, the situation within the Tethyan Himalaya is slightly different from the general picture. Based on $^{40}\text{Ar}/^{39}\text{Ar}$ dating of white micas, the Kinner Kailash Granite (KKG) at the base of the sedimentary rocks reached the brittle-ductile transition zone between 17-19 Ma (Vannay et al., 2004, Table 2.1.). ZFT ages are only slightly younger, between 13 - 16 Ma (Vannay et al., 2004), and mark the upper time limit for the onset of the brittle behavior of the KKG, in the Sutlej Valley and therefore also the onset of cataclastic brittle faulting related to NE-SW extension (D3). During D5, brittle strike-slip faults related to D5 are associated mostly with clay gouges, while young joints were formed related to D6. Both types of faults are characteristic for very cold rocks, e.g. in the temperature realm related to AFT ages. In the Tethyan Himalaya, close to the STDS, we therefore assume that D5 and D6 have been active at least since approximately 5 Ma (Vannay et al., 2004; Thiede et al., 2005).

The Higher Himalaya is the compartment of the orogen, where most thermochronologic data is available (Table 2.1 and references therein). The distribution of ages resulting from different dating techniques has lead to a similar pattern as observed in the KKG, but slightly younger. The brittle-ductile transition zone is reached here at around 15-17.5 Ma, where D1 and D2 deformation changed from ductile to brittle deformation. Protracted brittle deformation started between about 11-12 Ma. Cohesive deformation during D6, indicated e.g. by clay gouges, has been active at 4 Ma, based again on apatite FT ages (Vannay et al., 2004; Thiede et al., 2004, 2006).

In the LHC between MT and MCT, there are no reliable zircon FT data available. $^{40}\text{Ar}/^{39}\text{Ar}$ ages, however show very young ages of about 4-7 Ma for the greater Sutlej Valley area (Vannay et al., 2004; Thiede et al., 2005), indicating that the LHC has experienced a very short brittle phase, where NE-SW extension (D3) is the most prominent deformation style.

The Lesser Himalaya between the MT and the MBT is most probably the most complicated part of the Himalaya in respect of regional dating of the different brit-

Region	$^{40}\text{Ar}/^{39}\text{Ar}$	Zircon FT	Apatite FT	Author
TH (Sutlej Valley)	17 - 19 Ma (wm)	13.6 - 16.3 Ma	2.6 - 5 Ma	Vannay et al. (2004)
TH (Sutlej Valley)			2.7 - 4.6 Ma	Thiede et al. (2005)
TH (Baghirati Valley)	17.0 Ma (wm), 18.0 Ma (biotite)		1.5-2.4 Ma	Sorkhabi et al. (1996)
HHC (Sutlej Valley)	15.4 - 17.6 Ma (wm)	10.7 - 12.2 Ma	3.0 - 4.1 Ma	Vannay et al. (2004)
HHC (Sutlej Valley)	14.9 - 17.3 Ma (wm)		1.2-3.7 Ma	Thiede et al. (2005)
HHC (Sutlej Valley)		1.5 Ma	1.0 - 2.0 Ma	Jain et al. (2000)
LHC (Sutlej Valley)	4.3 - 6.6 Ma (wm)			Vannay et al. (2004)
LHC (Sutlej Valley)	4.3 - 6.7 Ma (wm)		0.6-5.0 Ma	Thiede et al. (2005)
LHC (Sutlej Valley)			4.5 Ma	Jain et al. (2000)
LHC (Rotang Pass)			2 - 4 Ma	Lal et al. (1999)
Spiti Valley (D2)	42-45 Ma (illites)			Wiesmayr and Grasmann (2002)
Bhagirati Valley	19 Ma (hornblende), K/Ar (wm)			Metcalf (1993)

Table 2.1: Compilation of age constraints for the NW Indian Himalaya. TH: Tethyan Himalaya (base), HHC: Higher Himalayan Crystalline, LHC: Lower Himalayan Crystalline. For the $^{40}\text{Ar}/^{39}\text{Ar}$ ages, the mineral used for dating is given in brackets (wm = white micas).

tle deformation styles. The metasedimentary rocks were deposited between 1.9 and 1.8 Ga and have never been heated up above greenschist-facies conditions (Miller et al., 2000). This implies that these rocks have behaved either purely brittle or at least in a ductile-brittle manner since ca. 1.8 Ga. Considering the fact that the northern margin of India has been mostly a passive continental margin with limited deformation, it is likely that deformation generated during the Indo-Eurasian collision might dominate the records. This is mainly visible in the Garhwal Himalaya, where all deformation phases have been recorded, except for D4. However, limited vestiges of pre-collision deformation may have survived. One example could be the limited amount of fault planes indicating N-S extension that are mostly found in the Lesser Himalaya and do not show any crosscutting relationship to other deformation phases. Those could be evidence for much older deformation prior to the shortening related to the collision (D1).

2.6 Tectonic interpretation

In the following section, we put the different brittle deformation styles into the larger geodynamic framework of the Himalaya and present models for the generation of the brittle structure within the evolution of the NW Indian sector of the orogen. Documented by small faults with displacements within the range of centimeters and decimeters, the most prominent brittle deformation styles (D1, D3, D4, D6) are represented by a large amount of ubiquitous structures within the study area. Since we consider those four structural styles to represent important steps in the evolution of brittle deformation of the NW Indian Himalaya, we will discuss them in detail, especially the extensional styles D3 and D4. Nevertheless, it is necessary to keep in mind that the data base presented here consists of small-scale faults with limited displacement, so they rather represent a measure for changes in strain orientation than for fault displacement.

The brittle deformation structures associated with **NNE-SSW oriented shortening direction (D1)** are in good agreement with the orientation of the present-day regional shortening direction as shown by the focal mechanisms of earthquakes (Molnar and Lyon-Caen, 1989). Faults generating these earthquakes and faults displaying corresponding kinematics and deformation features thus represent shortening related to the ongoing convergence of India and the southern margin of Eurasia at present day. In contrast, the hinterland of the active thrust belt, the low-grade Tethyan Himalayan sedimentary sequence, displays only limited or regionally localized shortening associated with reverse faults, such as the Great Counter Thrust (Heim and Gansser, 1939). Instead, the shortening seems to have been accommodated by large open folds with NW-SE striking fold axes, which are the dominant structures in the Spiti Valley (Wiesmayr and Grasemann, 2002; Neumayer et al., 2004). This situation is reflected also in our data, where D1 within the Tethyan Himalaya is only rarely observed, and mainly represented by strike-slip faults instead of reverse faults.

E-W shortening (D2) is mainly associated with strike-slip movements in the immediate vicinity of the Leo Pargil gneiss dome, suggesting a causal relationship with the emplacement of the dome. Corresponding faults related to this deformation are observed in the hanging and footwall of this structure. Scarce pure reverse faulting in the thrust belt might be explained by locally slightly rotated shortening axes which are nonetheless related to D1.

NE-SW extension (D3) is the most dominant deformation style observed in the thrust belt and less commonly in the hinterland. Our observations show that during this deformation style, reverse faults of D1 were most probably reactivated as normal faults. Since the extensional faults are reactivating the D1 fault planes with almost pure dip-slip lineations (Fig. 2.4, Appendix A.1), D3 reflects arc-normal extension in the NW Indian Himalaya.

Various mechanisms have been invoked to explain along-strike normal faulting associated with arc-normal extension. This normal faulting, with the Southern Tibetan Detachment System (STDS) as the principal fault system (Burg et al., 1984; Burchfiel et al., 1992), has been explained by processes associated with channel flow

or extrusion of the orogenic wedge (e.g., Grujic et al., 1996; Nelson et al., 1996; Beaumont et al., 2004; Vannay and Grasemann, 2001) or caused by a ramp-like structure of the subduction interface (Burg et al., 1984a, Burchfiel et al., 1992). Other explanations include the increase of gravitational potential energy in the orogen due to a significant build-up of high topography, followed by collapse (e.g., Royden and Burchfiel, 1987; Buck and Sokoutis, 1994; Hogdes et al., 2001); basal shear produced by southward crustal flow below the Himalaya (Yin, 1989); and more recently, a passive roof thrust model (Yin, 2006; Webb et al., 2007). However, these models mainly account for observed crustal-scale ductile deformation phenomena in the Himalaya and generally focus on arc-normal extension limited to the Higher Himalaya. Our observations unambiguously show, however that arc-normal extension within the upper crust is also pervasive in the Lesser Himalaya and occurs as far south as the MBT (Fig. 2.4). Assuming that arc-normal extension within the Himalaya, both on a crustal scale and the brittle deformation within the upper crust, is caused by one process, the ramp model (Burg et al., 1984a, Burchfiel et al., 1992) may provide a plausible explanation for our observations of structures related to D3. Accordingly, the part of the Himalaya that advances southward over a crustal ramp is bent and generates normal faults. Such a process may thus be expressed by along-strike brittle normal faulting. Since the movement over the ramp is part of the ongoing collision process and may have been continuous over long time scales, the area affected by arc-normal extension is shifted toward the south as rocks move over the ramp-flat-hinge over time (or toward the southwest in the NW Indian Himalaya) and a new area is deformed during successive motion over the ramp.

Brittle deformation related to **NW-SE oriented extension (D4)** is pronounced in the hinterland of the thrustbelt and decreases toward the MBT (Fig. 2.5). Compared to the regional NNE-SSW shortening direction (D1) and the NW-SE oriented trend of the NW Indian Himalaya, D4 represents arc-parallel extension. A number of models have been developed to explain arc-parallel extension in the Central Himalaya, including (1) oroclinal bending (e.g., Rosenberg et al., 2004; Robinson et al., 2007); (2) radial expansion (e.g., Armijo et al., 1986; Molnar and Lyon-Caen, 1989; Seeber and Armbuster, 1984); (3) oblique convergence (e.g., Avé Lallement and Guth, 1990; McCaffrey, 1996; McCaffrey and Nabelek, 1998); (4) southward propagation of the subduction front (Murphy and Copeland, 2005); (5) compression focused at the Central Himalayan front (Kapp and Guynn, 2004); (6) change of boundary conditions along the eastern margin of Asia (Yin, 2000; Yin and Harrison, 2000); (7) convective removal of the mantle lithosphere (England and Houseman, 1989); and finally, (8) those models linked with escape tectonics in the course of the continental collision process (e.g., Molnar and Tapponnier, 1978; Tapponnier et al., 1982; Molnar and Chen, 1983; Royden and Burchfiel, 1987). Murphy et al. (2009) evaluated all these models comparing model predictions with field observations in the Gurla Mandhata area (see Fig. 2.1). They concluded that radial expansion due to the southward migration of the active zone of overthrusting is the most viable mechanism. In this case, the increase in length of the Himalayan arc over time and associated arc-parallel extension in the hinterland is a necessary process in order to adjust to the length of the southern margin of the orogen Murphy et al.

(2009). We agree with this assessment and propose that southward propagation of the active thrust zone and the resultant relaxation in the hinterland are the causes for arc-perpendicular NE-SW extension. Having one tectonic event causing both arc-parallel and arc-perpendicular extension, both deformation styles should occur contemporaneously. Indications for the existence of such a scenario would be that mineralizations on fault-planes related to both extensional directions are very similar. Interestingly, it seems that arc-parallel extension (D4) cannot be observed south of the MCT (Fig. 2.5), while arc-normal extension (D3) is observed as far south as to the MBT (Fig. 2.5). If both extensional styles show a protracted southward movement, as also proposed by Murphy and Copeland (2005), this would support our field results based on crosscutting relationships that arc-normal extension is slightly older than arc-parallel extension.

Alternatively, arc-parallel extension observed close to the Leo Pargil gneiss dome may be the expression of vertical axis rotation of structures generated during E-W extension and subsequent clockwise rotation. This interpretation of those structures is supported by evidences for ongoing E-W extension in the vicinity of the Leo Pargil gneiss dome since at least 14-16 Ma (Thiede et al., 2006; Hintersberger et al., 2010).

N-S shortening (D5) is mostly expressed by strike-slip faulting along steep NE-SW or NW-SE striking fault planes. This deformation style is mainly observed in the thrust belt (Fig. 2.6) and may represent an adjustment related to the bending of the orogen in this area. Alternatively, D5 might be the expression of structures related to ongoing NE-SW shortening that were rotated after their generation. Especially the third stereoplot related to D5 shown in Appendix A1b might be an indication for rotation within the Lesser Himalaya. In any case, these faults clearly show that there is overall and continuous shortening due to the ongoing collision of India and Asia. Therefore, D5 might not be temporally limited by D4 and D6, but rather be an intermediate or contemporaneous deformation to both extensional deformation styles.

E-W extension (D6) is observed in the entire study region. This deformation style is not limited by the STDS or to areas north of it, nor is it limited to the close vicinity of the Leo Pargil gneiss dome (Fig. 2.7). In a recent study, it has been shown that E-W extension in the NW Indian Himalaya is the youngest deformation style, overprinting or reactivating structures of all other deformation phases (Hintersberger et al., 2010). Earthquake focal mechanisms and faulting of Quaternary deposits emphasize the recency of this deformation in the NW Indian Himalaya. Therefore, we conclude that this deformation may be related to ongoing extensional tectonism observed within the Tibetan Plateau. Alternatively, at first sight normal faulting may be explained by processes associated with the activity of the Karakoram Fault. Displacement rates along the Karakorum fault, one of the large strike-slip faults delimiting the Tibetan Plateau towards the southwest, are controversially discussed (e.g., Lacassin et al., 2004; Chevalier et al., 2005; Searle and Phillips, 2007). In addition, we demonstrated earlier that the Karakorum fault is not decoupling normal faulting observed within the plateau from the Himalaya, as earlier suggested by others, since structures related to E-W-extension are also documented to the SW of this major fault zone. Therefore, we rather suggest that

part of the E-W-extension documented within the Tibet Plateau is transferred into the Himalaya (Hintersberger et al., 2010).

Taken together, we propose that the different deformation styles have affected the individual tectonic compartments in the order proposed here. Yet these styles cannot be considered to reflect tectonic phases that were separated in time and they rather present the result of continual deformation, geometric constraints related to it and the build-up of topography and associated space problems. Since active thrusting has been propagating southward from the MCT toward the Indian foreland in the course of the Himalayan orogeny, the spatiotemporal characteristics associated with the deformation styles observed in our study probably also follow the overall evolution of contractile deformation in a successive manner.

2.7 Conclusions

Analysis of fault kinematic data provided by hundreds of outcrop-scale brittle faults, of satellite imagery and of younger structures in the NW Indian Himalaya reveals that the derived strain pattern reflects the large-scale regional deformation pattern both in space and time very well. Shortening in the upper crust is mainly accommodated by strike-slip faulting and folding instead of reverse faulting, particularly in the Tethyan Himalaya.

However, despite the ongoing overall shortening in the mountain belt along its southern front and at deeper crustal levels, syntectonic extension in the upper crust generally characterizes deformation within many compartments of Himalaya in the recent geologic past. This is also emphasized by the fact that extension in the Himalayan upper crust is not only limited to large structures such as the STDS, or several dome and graben structures along the High Himalaya, but can rather be observed as pervasively exposed brittle, lower-order, closely spaced normal fault systems across the entire orogen. NE-SW (arc-normal) extension in the upper crust seems to be related to a ramp-like geometry of the underthrusting zone along the MHT and the motion of Himalayan rocks over such a ramp. Structures related to arc-parallel (NW-SE) extension seem to be younger than faults accommodating arc-normal extension. Our field observations support the model of Murphy et al. (2009), where southward propagation of the active mountain front and the associated widening of the Himalayan arc are responsible for the presence of arc-parallel extension. Normal faults related to E-W extension overprint structures generated during prior extensional phases, and their generation may be associated with deformation processes originating within the Tibetan Plateau (Armijo et al., 1986; Molnar, 1992; Yin, 2000; Hintersberger et al., 2010). Importantly, E-W extension can be clearly differentiated from arc-parallel (NW-SE) and -normal (NE-SW) extension. In addition, arc-normal and E-W extension are not mutually exclusive, but can occur subsequently within the same region, thus illustrating the change of deformational processes within the orogen since the beginning of the Miocene.

Acknowledgements

This work was financially supported by the Deutsche Forschungsgemeinschaft (DFG) Graduate School 1364 at the University of Potsdam, Germany and the DFG Leibniz Center for Surface Process and Climate Studies at the University of Potsdam. We want to thank Kurt Decker for his support during the interpretation of structural field data and Tashi Tsering for excellent logistical support during fieldwork. In addition, we are grateful to two anonymous reviewers for their detailed comments that helped improve the manuscript.

Chapter 3

East-west extension in the NW Indian Himalaya

published by Esther Hintersberger, Rasmus Thiede, Manfred Strecker, Brad Hacker (2010) in GSA Bulletin, vol. 122 (9/10), p. 1499-1515

Abstract

Explaining the presence of normal faults in overall compressive settings is one of the most challenging problems in understanding the tectonics of active mountain belts. The Himalayan-Tibetan orogenic system is an excellent setting to approach this problem because it preserves one of the most dramatic records of long-term, contemporaneous shortening and extension. Over the past decades, several studies have described extensional features, not only in the Tibetan plateau, but also in the Himalaya. For long time, the favored model explained the function of the Southern Tibetan Detachment System (STDS), a major fault zone in the Himalaya, as a decoupling horizon between the regime of crustal shortening forming the Himalayan wedge to the south and the extensional regime of the Tibetan Plateau to the north. However, in recent years, increasing evidence has shown that N-S trending normal faults in the Central Himalaya crosscut not only the STDS, but also the Main Central Thrust (MCT). Here, we present new structural data and geologic evidence collected within the NW Indian Himalaya and combine them with previously published seismic datasets documenting pervasive E-W extension accommodated along N-S trending faults extending as far south as the footwall of the MCT. We conducted kinematic analysis of fault striations on brittle faults, documented and mapped fault scarps of Quaternary sedimentary deposits using satellite imagery, and made field observations in the Greater Sutlej Region (Spiti, Lahul, Kinnaur) and the Garhwal Himalaya. Studying extensional features within the regionally NW-SE trending NW Indian Himalaya provides the advantage that arc-parallel and E-W extension can be separated, in contrast to the Central Himalaya. Therefore, our observations of E-W extension in the Indian NW Himalaya are well suited to test the applicability of current tectonic models for the whole Himalaya. We favor an interpretation of the E-W extension in the NW Indian Himalaya as a propagation of extension driven by collapse of the Tibetan Plateau.

3.1 Introduction

The mechanistic principle governing the spatio-temporal evolution of normal fault systems in active mountain belts is still a matter of dispute (e.g., Kapp and Guynn, 2004; Selverstone, 2005; Murphy et al., 2009). Observations in Cenozoic orogens related to continent-continent collision like the Himalaya-Tibet region (Armijo et al., 1986; Molnar, 1992; Chen and Yang, 2004; Zhang et al., 2004), the Pamir (Burtman and Molnar, 1993; Strecker et al., 2007), or the Alps (Michard et al., 1993; Wheeler and Butler, 1993; Seward and Manckelow, 1994; Selverstone, 2005; Sue et al., 2007) document that extension and normal faulting at higher elevations occur contemporaneously with shortening and thrusting at lower elevations.

Various mechanisms attempting to explain this high-elevation normal faulting have been proposed. In the transition between the Himalaya and Tibet region, the generation of normal faults parallel to the trend of the orogen, with the Southern Tibetan Detachment System (STDS) as the principal representative (Burg et al., 1984a, ; Burchfiel et al., 1992), has been explained by processes associated with channel flow or extrusion of the orogenic wedge (e.g., Grujic et al., 1996; Nelson et al., 1996; Beaumont et al., 2004; Vannay and Grasemann, 2001). Other explanations include the increase of potential gravitational energy, followed by collapse due to excess elevation (Royden and Burchfiel, 1987; Buck and Sokoutis, 1994; Hogdes et al., 2001), basal shear produced by southward crustal flow below the Himalaya (Yin, 1989), and, more recently, a passive roof thrust model (Yin, 2006; Webb et al., 2007).

Models that have been invoked to explain orogen-perpendicular grabens of the Himalaya and the southern Tibetan Plateau include an additional variety of mechanisms. The most prominent ones include (1) radial thrusting (e.g., Seeber and Armbruster, 1984; Armijo et al., 1986; Molnar and Lyon-Caen, 1989); (2) oroclinal bending (e.g., Ratschbacher et al., 1994; Kapp and Yin, 2001; Robinson et al., 2007); (3) partitioning of oblique convergence into thrusting and normal faulting components (e.g., McCaffrey, 1996; McCaffrey and Nabelek, 1998); (4) southward propagation of the subduction front (Murphy and Copeland, 2005); (5) concentrated compression at the Central Himalayan front (Kapp and Guynn, 2004); (6) change of boundary conditions along the eastern margin of Asia (Yin, 2000; Yin and Harrison, 2000); (7) convective removal of the mantle lithosphere (England and Houseman, 1989); and finally, (8) those models linked with escape tectonics in the course of the continental collision process (e.g., Molnar and Tapponnier, 1978; Tapponnier et al., 1982; Molnar and Chen, 1983; Royden and Burchfiel, 1987). In general, these models can be combined into two major groups: the first one contains all models where extension is related to processes within the Himalaya and the arcuate shape of the orogen, such oroclinal bending, and radial thrusting. The second group relates extension to deeper-seated processes, mainly within the Tibetan Plateau.

The Himalayan collision zone, characterized by ongoing shortening due to the convergence of India and Eurasia, hosts major active normal fault systems that strike approximately perpendicular to the trend of the orogen (Armijo et al., 1986; Royden and Burchfiel, 1987; Molnar and Lyon-Caen, 1989; Burchfiel et al., 1991;

Ratschbacher et al., 1994; McCaffrey and Nabelek, 1998; Hogdes et al., 2001; Murphy et al., 2002; Aoya et al., 2005; Thiede et al., 2006). GPS measurements and fault-plane solutions of earthquakes indicate approximately radial shortening in the Himalaya and E-W extension in the Tibetan Plateau (Zhang et al., 2004; Molnar and Lyon-Caen, 1989). However, in the central part of the Himalaya between 84 and 92°E longitude, tectonism does not conform to this first-order kinematic differentiation. In this high-relief region with mean elevations of approximately 3000 m, numerous N-S striking extensional fractures, closely spaced normal faults, and linked graben systems document that extensional processes are not limited to the Tibetan plateau and the internal parts of Himalaya, but also affect the high Himalayan realm farther south. Cross-cutting relationships indicate that these extensional structures cut all pre-existing deformation fabrics and structures, including older, orogen-parallel normal faults. This is documented by observations in the vicinity of the Gurla Mandhata gneiss dome and around the Ama Drime Massif (e.g., Murphy and Copeland, 2005; Jessup et al., 2008). Whether the driving forces for their generation are rooted in the geometry of the Himalaya or in the eastward motion of the Tibetan Plateau is still an open question, mainly because in the Central Himalaya, both extensional directions are oriented approximately E-W.

In this paper, we take advantage of the regionally NW-SE oriented strike of the orogen in the NW Indian Himalaya to differentiate between extension triggered within the Himalaya and extensional processes triggered by deformation of Tibetan Plateau. We present new field evidence from structural mapping, analysis of satellite imagery (ASTER, GoogleEarth, LandSat), and new fault kinematic data from brittle faults from the NW Indian Himalaya. We document that normal faulting is not simply localized in close vicinity to major structures, but rather is an ubiquitous, pervasive phenomenon affecting the Himalaya of NW India as a whole. Our new data help define the spatio-temporal character of the extensional deformation and provide valuable information on the causal mechanisms of active normal faulting of the studied region. Our data set shows that extension is not limited to the higher parts of the Himalaya, but is also found in the lower-elevation region with average elevations of around 1500 m in the foreland of the Main Central Thrust (MCT).

Because previous models explaining the origin of extension in the Himalaya are generally based on data from the Central Himalaya, we used our new observations from the NW sector of the orogen to evaluate those models. Based on this evaluation, we favor a scenario where E-W oriented extension in the NW Indian Himalaya is triggered by extension in the Tibetan Plateau.

3.2 Geological Setting of the NW Himalaya

3.2.1 Principal structures related to shortening

In the NW Himalaya, the curved orogen trends dominantly NW-SE and can be separated into five principal lithologic-tectonic provinces, including the Sub-Himalaya, the Lesser Himalaya, the Higher Himalaya, the Tethyan Himalaya, and the Transhimalaya (Gansser, 1964). These tectonic provinces are fault-bounded and accommodate ~ 30 -50 % of India-Eurasia plate convergence (Banerjee and Bürgmann, 2002; Zhang et al., 2004). The NW Himalaya accommodates SSW directed shortening and thrusting caused by the underthrusting of India beneath Eurasia since the collision at around 50 Ma (Klootwijk et al., 1992). This process has been associated with a stepwise southward migration of thrust systems, from the Main Central Thrust (MCT, since 23 -20 Ma; Hogdes et al., 1996) to the Main Boundary Thrust (MBT, since 11 -9 Ma; Meigs et al., 1995) to the Main Frontal Thrust that has been active since the Pliocene (MFT; Molnar, 1984; Wesnousky et al., 1999). In addition to these structures, in the NW Himalaya, the ductile, north-dipping Munsiri Thrust (MT) between the MCT and the MBT separates the Lesser Himalayan crystalline sequence from the Lesser Himalayan paragneisses (Fig. 3.1B, Vannay et al., 2004).

3.2.2 Extensional structures in the Himalaya

Contemporaneous with crustal shortening along the southern mountain front, large regions of the Himalaya are characterized by activity along orogen-parallel and orogen-perpendicular normal faults (e.g., Le Fort et al., 1982; Burchfiel et al., 1992; Wu et al., 1998). One of the extensional hallmarks of the Himalaya is the system of orogen-parallel, linked normal faults associated with the Southern Tibetan Detachment System (STDS). The STDS strikes parallel to major thrusts and separates the low-grade metamorphic rocks of the Tethyan Himalaya in the hanging wall from the high-grade metamorphic footwall of the Higher Himalaya (Burg et al., 1984a, ; Burchfiel and Royden, 1985; Burchfiel et al., 1992). During the Miocene, the Higher Himalaya was exhumed during coeval extension along the STDS and thrusting along the MCT. Some studies have proposed that the STDS has been reactivated as recently as the Quaternary (Hogdes et al., 2001; Hurtado et al., 2001).

In the NW Indian Himalaya, the Sangla Detachment (SD) is the local expression of the STDS in the Greater Sutlej region (Vannay and Grasemann, 1998; Wiesmayr and Grasemann, 2002). This structure is well recognized in the field, however, evidence for neotectonic activity has not been observed by us or by several earlier investigations (e.g., Vannay and Grasemann, 1998). Recent studies in the vicinity of the Kullu Valley (Fig. 3.1B) suggest that the STDS and the MCT merge in map view, which the authors explain with a passive roof-thrust model for the development of the STDS (Yin, 2006; Webb et al., 2007). In the Sutlej Valley, the brittle Karcham normal fault crosscuts the MCT mylonites, showing a top-to-the-east displacement and is assumed to be the counterpart of the MT during the exhumation of the Lesser Himalayan Crystalline (Janda et al., 2002; Vannay et al., 2004). Other extensional detachments comprise the Leo Pargil Detachment Zone (LPDZ, Thiede et al., 2006) farther north and the Gurla Mandhata Detachment Zone (GMDZ, Murphy et al.,

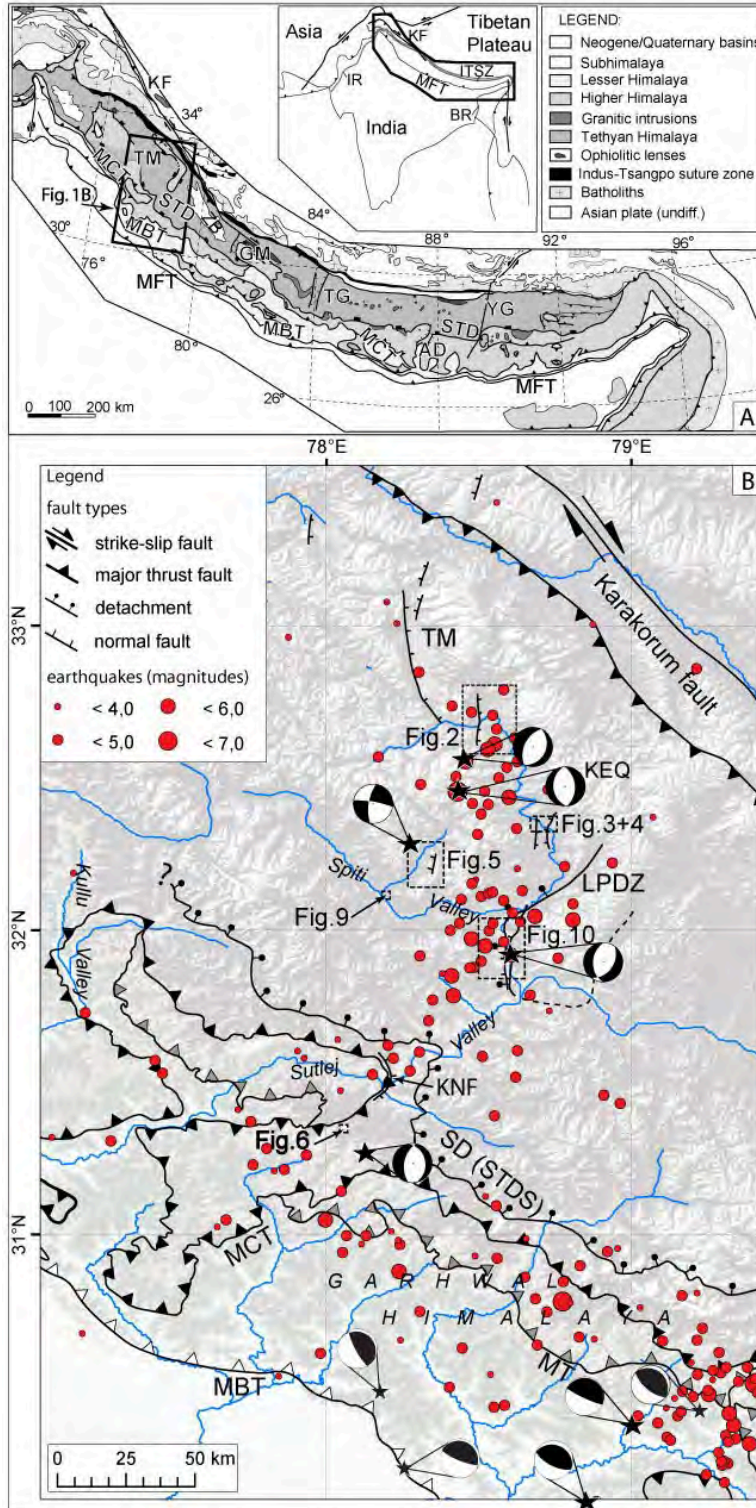


Figure 3.1: (A) Geological map and structural provinces of the entire Himalaya, modified after Yin (2006) and references therein. For the western Himalaya, the structures as mapped by DiPietro and Pogue (2004) are used. (B) Structural map of the NW Indian Himalaya, modified after Thiede et al. (2005) and references therein. Earthquakes, shown as red dots, are taken from the NEIC catalog, fault-plane solutions for the larger earthquakes from the Harvard CMT catalog. The Kinnaur Earthquake (KEQ) is labeled explicitly. Dotted rectangles represent the locations of figures shown later in the text. Locations of Figs. 3.3 and 3.4 are too close to each other to be separated on this map scale, therefore they are represented by one box. The base map shows elevations taken from a SRTM image. AD: Ama Drime massif, BR: Brahmaputra River, GM: Gurla Mandhata gneiss dome, IR: Indus River, ITSZ: Indus-Tsangpo Suture Zone, KEQ: Kinnaur Earthquake, KF: Karakorum Fault, KNF: Karcham normal fault, LPDZ: Leo Pargil Detachment Zone, MBT: Main Boundary Thrust (white triangles), MCT: Main Central Thrust (black triangles), MFT: Main Frontal Thrust, MT: Munsiari Thrust (gray triangles), SD: Sangla Detachment, STDS: Southern Tibetan Detachment System, TM: Tso Morari, TG: Thakkola Graben, YG: Yadong Graben.

2000, 2002) farther east (Fig. 3.1), forming the low-angle ductile normal faults of two major domes exhumed during the Miocene in the Tethyan Himalaya.

A second group of extensional structures comprises N-S striking normal faults. In the NW Himalaya, several N-S striking, high-angle brittle normal faults are documented in the vicinity of the Gurla Mandhata Dome (Murphy et al., 2000, 2002), the Kaurik-Chango normal fault at the western flank of the Leo Pargil dome (Hayden, 1904; Thiede et al., 2006), and the Tso Kar and Tso Morari normal faults north of the Spiti Valley (e.g., Steck et al., 1993; Fuchs and Linner, 1996; Epard and Steck, 2008). Also in the central Himalaya, between 83 and 90°E, several large-scale, Neogene normal faults strike perpendicular to the orogen. These include structures bounding the Thakkola Graben (Le Fort et al., 1982; Garzzone et al., 2000; Hurtado et al., 2001; Garzzone et al., 2003), structures close to the Ama Drime Massif (Jessup et al., 2008; Cottle et al., 2009) in Nepal, and the southern end of the Yadong Graben in Bhutan (Wu et al., 1998; Guo et al., 2008). Several of these offset the STDS, especially the N-S striking normal faults bounding the Ama Drime massif in the Central Himalaya, which displace the STDS for several kilometers, and thus represent the youngest deformation phase (Jessup et al., 2008). However, the southern and the northern terminations of those normal faults are not yet fully documented. This raises the question of whether the N-S striking grabens in the Central and Southern Tibetan Plateau are linked to the extensional processes observed within the Himalaya, or if they represent an entirely different, but possibly coeval process that generates very similar structures and geomorphic features that have their origin in the Tibetan Plateau.

3.2.3 Seismicity in the NW Indian Himalaya

Fault-plane solutions derived from seismicity in the Himalaya-Tibet region reflect first-order deformation patterns and provide insight into the characteristics of the present-day regional stress field (Fig. 3.1). In the southern Tibetan Plateau, fault-plane solutions document pure normal faulting indicating E-W extension, both at shallow crustal levels (< 15 km) and at greater depths of 80 - 95 km (Molnar and Chen, 1983; Molnar and Lyon-Caen, 1989). In contrast, earthquakes in the Himalaya with NE-SW oriented thrusting focal mechanisms and magnitudes of up to 8.0 are located at depths between 20 and 40 km, and are primarily related to the underthrusting of India beneath Eurasia (Seeber and Armbruster, 1981; Ni and Barazangi, 1984). We have extracted all seismic events of magnitude 3.2 to 6.5 recorded between 77.5 and 79°E within the NW Indian Himalaya from the global seismicity catalogs (NEIC and Harvard Catalogs, 2009). This subset of seismic events can be separated into two groups. The southern Himalayan front is characterized by one group of large earthquakes with magnitudes up to $M = 8.6$ and dominant NE-SW shortening (Fig. 3.1B). Some of the most prominent examples are the Kangra (4 April 1905, $M(\text{estimated})=8.6$, Middlemiss, 1910), Uttarkashi (20 October 1991, $M_w = 6.8$, Kayal et al., 1992), and Chamoli earthquakes (29 March 1999, $M_w = 6.6$, Rastogi, 2000). The second group is characterized by shallow earthquakes with depths < 15 km, and occupies a narrow swath between 78 and 78.5°E, stretching from the Tso Morari dome in the north to close to the MCT in the south (Fig. 3.1B).

The Kinnaur Earthquake (Jan. 19, 1975, $M_S = 6.8$), with its epicentral zone close to the Leo Pargil gneiss dome, was the most prominent event of this group (fault-plane solution KEQ see Fig. 3.1B). Fault-plane solutions for this event and other major earthquakes in the Sutlej region provide additional evidence for ongoing E-W extension (e.g., Molnar and Chen, 1983). The degree of activity in the Sutlej region is much higher than that recorded along other N-S striking structures in the Himalaya, such as the Thakkola graben in Nepal, where only microseismicity with magnitudes < 4 is observed (Pandey et al., 1990).

3.3 Methodology

3.3.1 Field mapping and analysis of satellite imagery

Previously, structures related to E-W extension have been only described around prominent morphologic features such as graben or dome systems. We were interested whether these extensional structures are restricted to these features or if normal faulting is more pervasively distributed across the orogen. To explore this question, we collected structural field data on recent normal faults and interpreted satellite images from the Lesser and Higher Himalaya of NW India. We focused on an area extending from the Tso Morari dome in the north to the Garhwal Himalaya in the south, covering the region shown in Fig. 3.1B. We determined the kinematics of brittle faults in basement rocks and sedimentary strata, such as lake deposits and fluvial-terrace conglomerates. To better understand recent fault displacement, we analyzed fluvial terraces and paleo-surfaces affected by Quaternary faulting (section 3.4.1 and Figs. 3.2-3.5). We used satellite imagery (LandSAT, ASTER, and GoogleEarth), where the border-region between India and China did not permit direct field access. Detailed investigations of the fault inventory in river terraces were undertaken, such as in the immediate vicinity of the Leo Pargil gneiss dome and in the Spiti Valley (section 3.4.3 and Figs. 3.9, 3.10).

3.3.2 Kinematic analysis of brittle fault data

To obtain a better image of the distribution of paleo-strain axes in the study area, we collected fault kinematic data. We measured the strike and dip, slip direction, and sense of slip for major and minor brittle faults from the Spiti and Sutlej Valleys, the Kullu Valley, and the Garhwal Himalaya (see Fig. 3.1B). We selected only the youngest structures, which were mainly normal faults, and analyzed them with TectonicsFP (Ortner et al., 2002). For coaxial deformation, derived kinematic strain-axes can be interpreted carefully as paleo stress-axes. In the case of brittle faulting, the condition of coaxial deformation is met for fault planes outside of prominent shear zones. Therefore, we concentrated on outcrop-scale brittle faults with displacements of up to several centimeters. We used the kinematic P/T-axis method (Turner, 1953), as well as the numeric dynamic analysis (NDA, Spang, 1972; Sperner, 1996) to cross-check differences introduced by the underlying assumptions. To compare our results with seismicity data, we generally assumed an angle of 45° between a fault plane and its P axis for the determination of P and T axes. The differences observed in the resultant extension and shortening directions from both methods are negligible, as they are mostly within the limit of error.

3.3.3 Age determination of normal faulting

We were able to constrain the minimum age for onset of normal faulting at three sites using the $^{40}\text{Ar}/^{39}\text{Ar}$ and OSL (optically stimulated luminescence) techniques. South of the Leo Pargil gneiss dome, synkinematic micas on a fault plane were dated by the $^{40}\text{Ar}/^{39}\text{Ar}$ technique at the University of California in Santa Barbara. The mica separates were wrapped in Cu foil, sealed in a quartz vial, and irradiated at the TRIGA reactor at Oregon State University for 8 MWhr. Ratios of reactor-produced

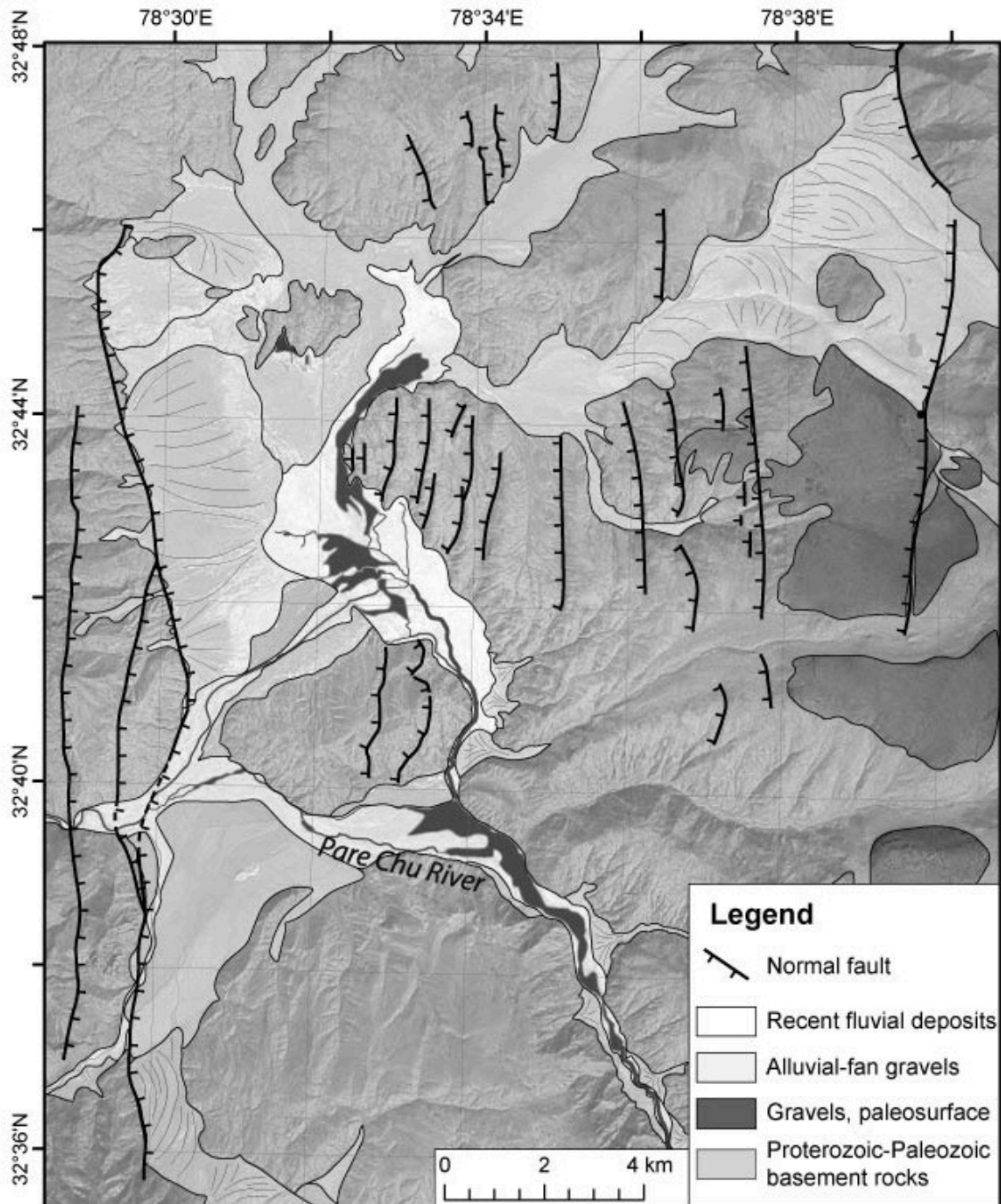


Figure 3.2: Normal faults mapped on a LandSat7-image of the region southeast of the Tso Morari Lake. In the west, the large east-dipping normal faults deform older alluvial fans. In the east, several smaller, antithetic normal faults dip toward the west and also affect an older paleosurface (dark gray). Both groups of normal faults have produced a half-graben system that influences the drainage system of the Pare Chu River.

3.3. METHODOLOGY

Ca- derived isotopes were established by analyzing CaF₂ included in the irradiation vial. Sanidine from the Taylor Creek rhyolite, with an assumed age of 27.92 Ma, was used as a neutron flux monitor to determine irradiation parameter, *J*. The samples were analyzed using a double-vacuum Staudacher-type resistance furnace in 12 to 15-min heating steps. Gas was gettered continuously during extraction with two SAES ST172 Zr-V-Fe getters. The collected gas was analyzed with an MAP-216 spectrometer with a Baur-Signer source and Johnston MM1 electron multiplier operating in static mode with a room temperature SAES ST707 Zr-V-Fe getter. Peak heights at the time of gas introduction into the mass spectrometer were determined by extrapolating the evolved signal size using a linear regression. Resistance furnace m/e 40 blanks varied from 2×10^{-16} moles at 800°C to 6×10^{-16} moles at 1400°C. Complete ⁴⁰Ar/³⁹Ar dating protocol is placed in Appendix B.1 and B.2.

In addition, we took samples from Quaternary sedimentary deposits affected by normal faulting or layers subjected to soft-sediment deformation that may have been caused by coeval activity along nearby faults. These samples, collected in 20-cm-long, opaque tubes, were dated with the OSL technique. The analysis of the OSL samples was carried out by the Sheffield Centre for International Drylands Research (UK). The samples were prepared under subdued red lighting to extract and clean quartz following the procedure outlined in Bateman and Catt (1996). The remaining pure quartz with grain sizes between 90-250 μm was mounted as 4 mm diameter aliquots and checked with infrared stimulated luminescence for feldspar contamination, which was not given. All OSL measurements were carried out using an upgraded DA-15 Risø luminescence reader system, equipped with a calibrated ⁹⁰Sr beta source and blue LEDs for stimulation. The OSL signal was measured through a Hoya-340 filter. All samples were analyzed using the single aliquot regenerative (SAR) approach (Murray and Wintle, 2000), where the last measurement replicated the first one. Aliquots were excluded from further analysis if the ratio of first and last dose point exceeded ± 10 % of unity. To remove unstable signals, the samples were preheated prior to OSL measurements using a preheat temperature of 180°C for 10 seconds.

3.4 Extensional structures in the NW Himalaya

Here, we report on different phenomena related to normal faulting in the northwestern Indian Himalaya, where the deeply incised Sutlej and Spiti rivers provide an excellent and easily accessible natural transect through the entire mountain range. Apart from the structures already mentioned above and described in literature, we document pervasively distributed young normal faults related to E-W extension at the km-scale based on the analysis of satellite imagery and field work, and at the outcrop-scale between the southern Himalayan mountain front and the Indian-Chinese border. Additionally, we assess normal faulting in fluvio-lacustrine sediments, including soft-sediment deformation. In the following sections, we use the term **macro-scale** to describe faults traced over distances of hundreds of meters and up to several kilometers, **meso-scale** for faults with several meters of fault-zone observed in outcrops that can be traced over several meters, and **outcrop-scale** for faults and fault-planes visible at a scale of a few centimeters and up to a few meters.

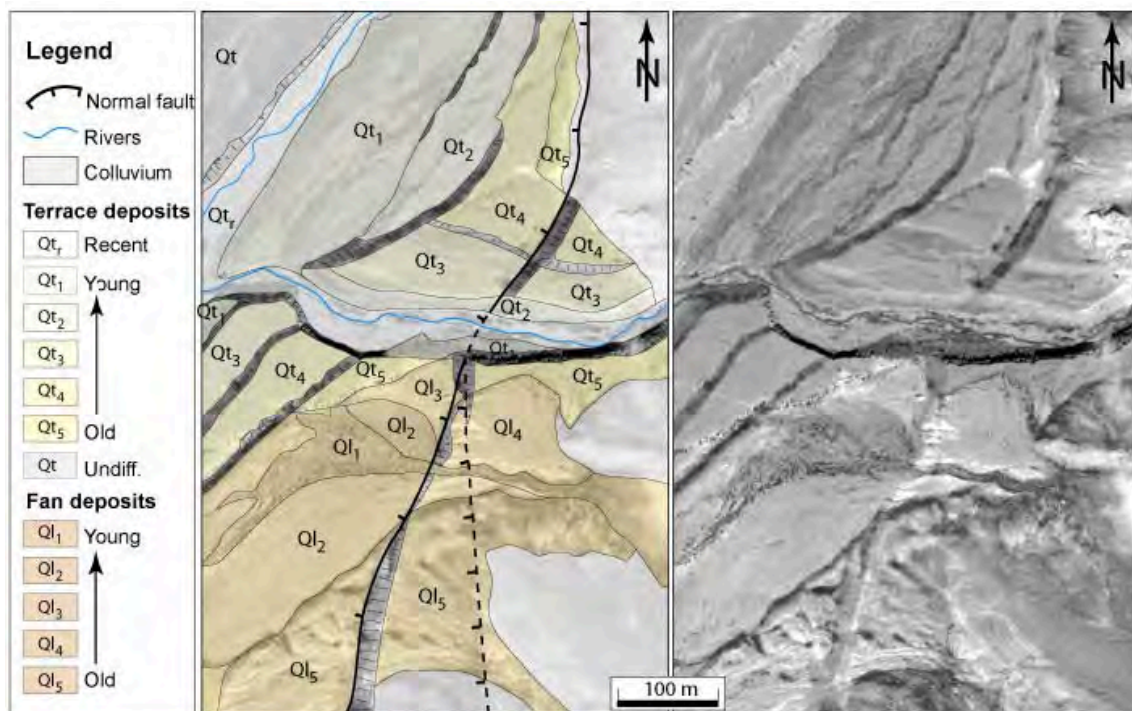


Figure 3.3: Example of Quaternary normal faulting in the NW Leo Pargil basin, where a normal fault displaces fluvial terraces (northern part) and alluvial fans (southern part). Terrace risers are marked as white areas; lines indicate the approximate slope direction. Uninterpreted GoogleEarth air-photo of this region is shown on the right.

3.4.1 Macro-scale normal faults from satellite imagery and field observations

Area southeast of Tso Morari

In addition to the 40-km-long Tso Morari normal fault (see Fig. 3.1), there is a second en échelon set of parallel east-dipping normal faults to the southeast, which we term the eastern Tso Morari fault system (Fig. 3.2). The two fault strands are exposed for 20 and 10 km, respectively, and are spaced ~ 2 km apart. In the central sector of the eastern fault, the fault diverges into a lozenge-shaped segment, which converges with the main fault approximately 5 km south. The eastern Tso Morari fault system separates sedimentary rocks of Neoproterozoic and Cambrian age and Ordovician granites in the footwall from fan gravels of inferred Quaternary age that constitute a large, contiguous bajada adjusted to the Pare Chu River. The alluvial fans in the hanging wall of the easternmost fault, as well as fluvial terraces parallel to the Pare Chu River that crosses the fault, are apparently not displaced by the fault (Fig. 3.2).

Approximately 6 km east, the landscape is dissected by numerous W- to WNW dipping normal faults (Fig. 3.2). The fault scarps are less pronounced compared to the eastern Tso Morari fault system but strike N-S. These faults clearly show evidence for top-to-the-west normal faulting. Similar to the larger east-dipping faults on the west, the fluvial deposits of the Pare Chu River and its tributaries are not displaced by these west-dipping faults, and therefore postdate faulting in this region (Fig. 3.2). However, the normal faults offset gently inclined erosion surfaces that were sculpted into the Proterozoic to Paleozoic basement rocks (see eastern part of Fig. 3.2). These surfaces are interpreted to represent a pediment surface that was formerly adjusted to a higher base-level of the Pare Chu River, but became subsequently abandoned due to base-level lowering.

Normal faulting north of Leo Pargil

One of the most striking preserved young features affected by normal faulting is an extensive, originally contiguous gravel-covered paleo-surface with ubiquitous erosional remnants in a formerly closed sedimentary basin northwest of the Leo Pargil gneiss dome (for location see Fig. 3.1). The basin is bounded by E- and W-dipping normal faults. In the center, the paleo-surface consists of large, gently NE-tilted segments that are incised by small streams. The geomorphic character of the surface remnants and their lower eroded sectors is similar to features observed in the Zada Basin of the upper Sutlej River, southeast of the Leo Pargil gneiss dome. Based on similar outcrop and geomorphic characteristics, we infer that this surface constitutes the remnant of extensive gravel-covered lacustrine marls that once filled the basin before the current rivers started incising and eroding the basin fill due to headward erosion. Based on the degree of preservation of the fault scarps, what we infer to be the oldest normal faults occur at the eastern and western margins of the basin. Movement along these structures created accommodation space for the sedimentary fill, which is now being incised and evacuated. Farther basin-ward towards the east, there are also morphologically younger N-S striking faults that

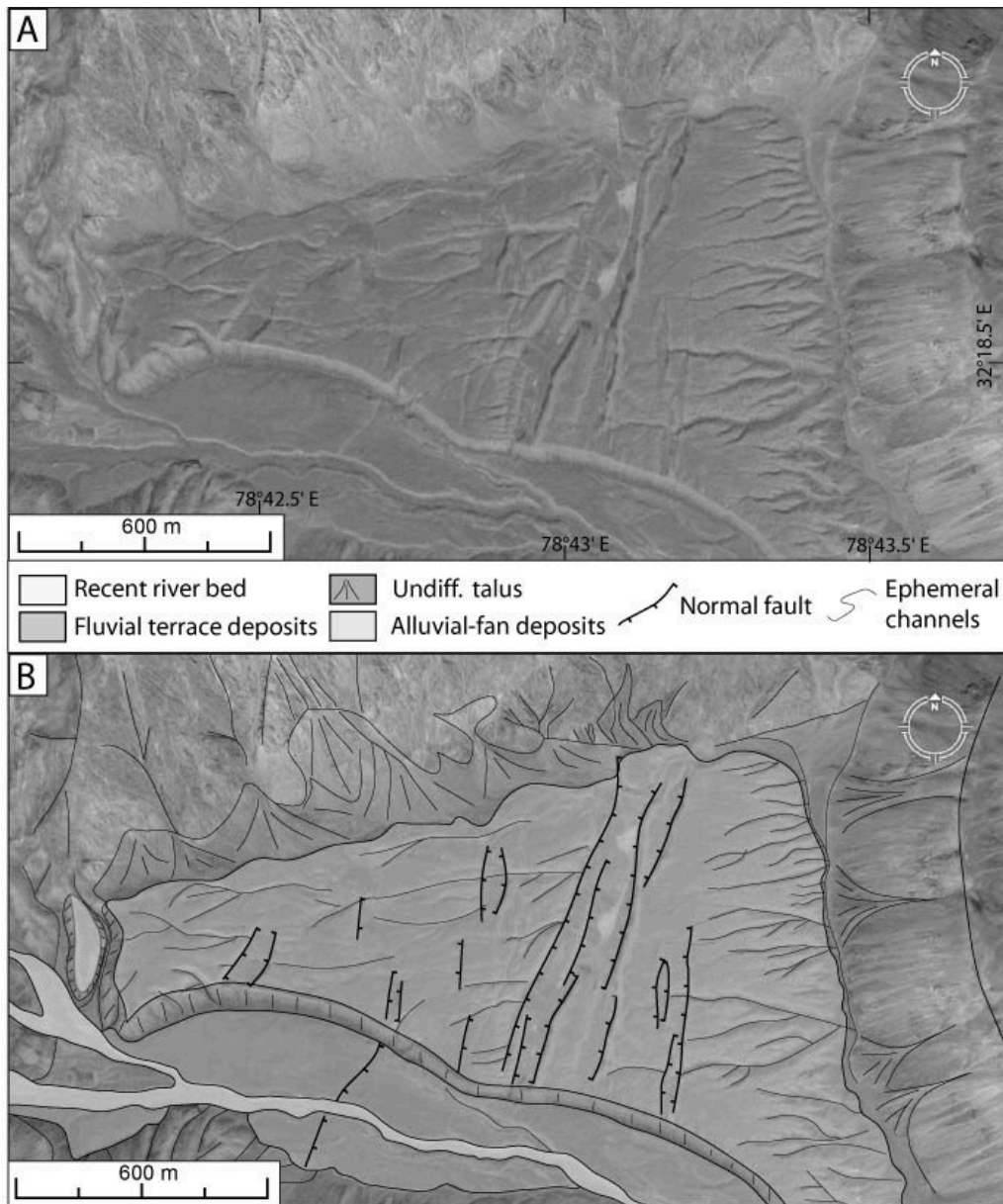


Figure 3.4: Normal faults of inferred Quaternary age in the NW Leo Pargil basin. E- and W-dipping faults displace an alluvial fan and a younger fluvial terrace (image source: GoogleEarth). Ephemeral channels are affected by normal faulting and were used to determine the dip direction of the normal faults.

offset fluvial-terrace and alluvial-fan surfaces that have prograded into the basin fill in the course of down-cutting. These surfaces thus postdate the extensive basin fill and are located at a lower elevation than the top of the surface that forms the youngest part of the basin-fill unit. However, the youngest alluvial-fan deposits in this area cover the faults and clearly postdate tectonic activity along these older normal faults (Fig. 3.3).

The western margin of the basin is delimited by east-dipping normal faults, which

are readily identified on satellite imagery. The normal faults constitute a sharp boundary between the basement rocks in the footwall and the sedimentary cover in the hanging wall. Several terrace levels in the northern part of the basin indicate that the paleo-surface was displaced by normal faulting. In contrast, multiple extensive terraces observed along most of the larger rivers in the southern part of the basin are not displaced and thus also postdate activity along the border faults. More recent normal faulting affecting an alluvial fan of inferred Quaternary age and sub-recent fluvial terrace deposits is observed within the basin center (see Fig. 3.4). This has resulted in a horst-and-graben morphology, which indicates that normal faulting is still active.

Lingti Valley

In the Lingti Valley between the Tso Moriri Lake in the north and the Spiti Valley in the south, prominent N-S striking normal faults can be identified on satellite imagery (Fig. 3.5A). The most prominent normal fault is exposed east of the Lingti River and can be traced for ~ 8 km. Our field observations confirm that this fault dips to the west with a vertical displacement of several hundred meters (Fig. 3.5C). An undated erosional paleo-surface sculpted into Jurassic carbonates and preserved at an average elevation of 4700 m within the hanging wall is displaced by this fault and subsidiary structures. Furthermore, there are brittle normal faults arranged in book-shelf manner on the western border of the Lingti River that affect the same erosional paleo-surface (Fig. 3.5B). These latter structures dip WNW. A minimum vertical displacement on each fault strand of approximately 20 m can be inferred from correlating the layers across the fault planes (Fig. 3.5B). In the lower parts of the valley, steeply dipping brittle faults striking N-S are observed. Limited striations on these fault planes plunge down-dip, and therefore fit into an overall E-W extensional regime.

Our observations in this area are consistent with mapping of normal faults by Neumayer et al. (2004) at different length and displacement scales, ranging from meso-scale features to several-kilometer-long structures in the southernmost part of the valley. Similarly, these authors related the normal faults to E-W extension and interpreted them as representing the youngest tectonic movements in the region.

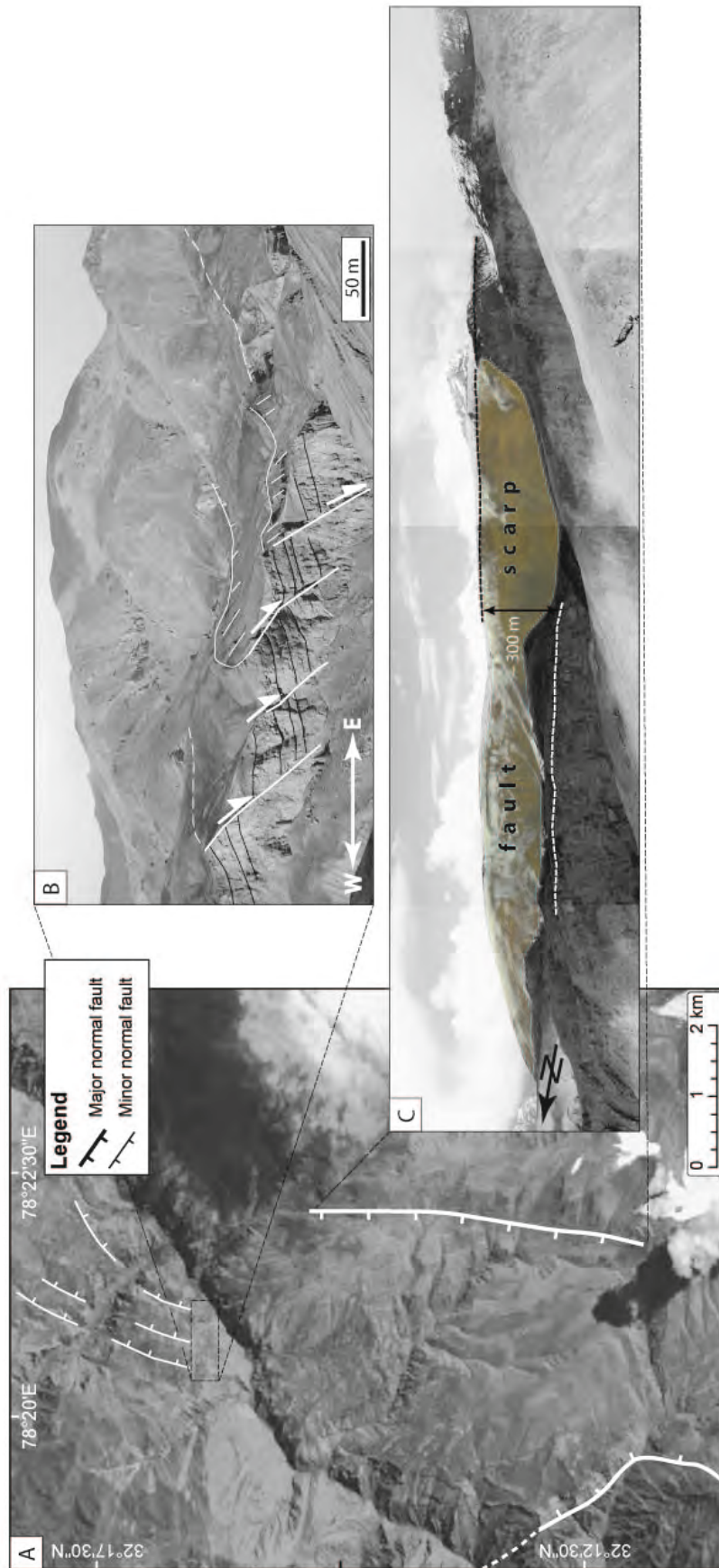


Figure 3.5: Normal faults in the Lingti Valley. (A) Overview of the Lingti Valley with normal faults and locations of panels B and C (image source: ASTER). (B) Normal faults dipping to the ENE arranged in bookshelf manner. A minimum vertical displacement on each fault strand of 20 m can be inferred from correlating the layers across the fault planes. (C) Normal fault with a fault scarp dipping to the W; dotted line denotes 300 m normal offset of gravel-covered erosion surface in Jurassic basement.

3.4.2 Meso-scale and outcrop-scale faults observed in the field

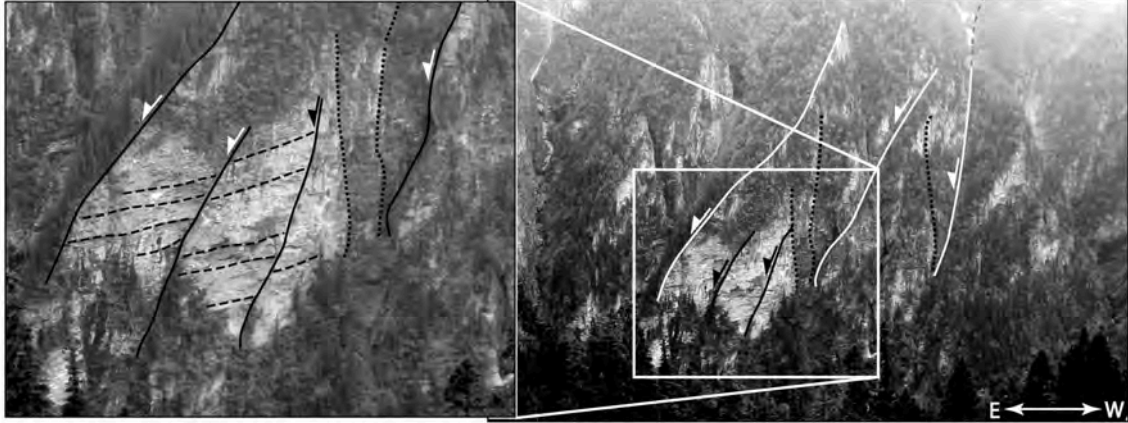


Figure 3.6: Roughly E-dipping brittle normal faults in the granitic gneisses of the Higher Himalaya close to the Main Central thrust observed in the Parbar Valley (Garhwal Himalaya). Solid lines mark the fault traces; dashed lines show foliation orientation. Dotted lines mark the trend of possible Riedel-shear planes. See Figure 1B for location.

Meso-scale and outcrop-scale brittle normal faults are ubiquitous in the area surrounding the Tso Morari-Leo Pargil seismic zone and document the extent of active normal faulting in the Higher Himalaya and also south of the STDS (Fig. 3.6). Our field observations reveal a network of small-scale normal faults that cannot be detected on satellite imagery. Between the Spiti River in the north and the MBT in the south, numerous steeply dipping N-S striking normal faults and extensional fracture zones form a dense network, with surface disruptions virtually every 15 to 20 m (Fig. 3.8A). Identical to the large-scale structures described above, these faults result from E-W extension and cross-cut all older structures. Taken together with all other sites visited in the field, these structures thus represent the most recent phase of deformation in this part of the Himalaya.

In addition, prominent N-S striking normal faults with gouge zones up to 3 m wide dominate a diffuse band between 78°E and 78.5°E . They are typically associated with steeply plunging striations indicating dip-slip faulting and E-W extension. In most cases, smaller, parallel, brittle fault planes are observed in their vicinity. Because none of these faults are overprinted by any other structure, we infer that they also reflect the youngest phase of deformation in the region. Synkinematic micas on fault planes and within fault gouges indicate that these faults were associated with deeper-seated processes and originated in the brittle-ductile transition zone, but have been exhumed since. Consequently, the faulted basement rocks exposed at surface today were initially deformed by E-W extension at greater depths, suggesting that this style of deformation has been sustained over long timescales. In the exhumed orthogneisses of the footwall of the southernmost sector of the Leo Pargil detachment zone, we found synkinematically grown muscovites on a west-dipping fault (strike/dip: $178/83\text{W}$, see marked location in Fig. 3.8B) associated with a steeply dipping lineation (trend/plunge: $280/82\text{W}$). $^{40}\text{Ar}/^{39}\text{Ar}$ dating of these mi-

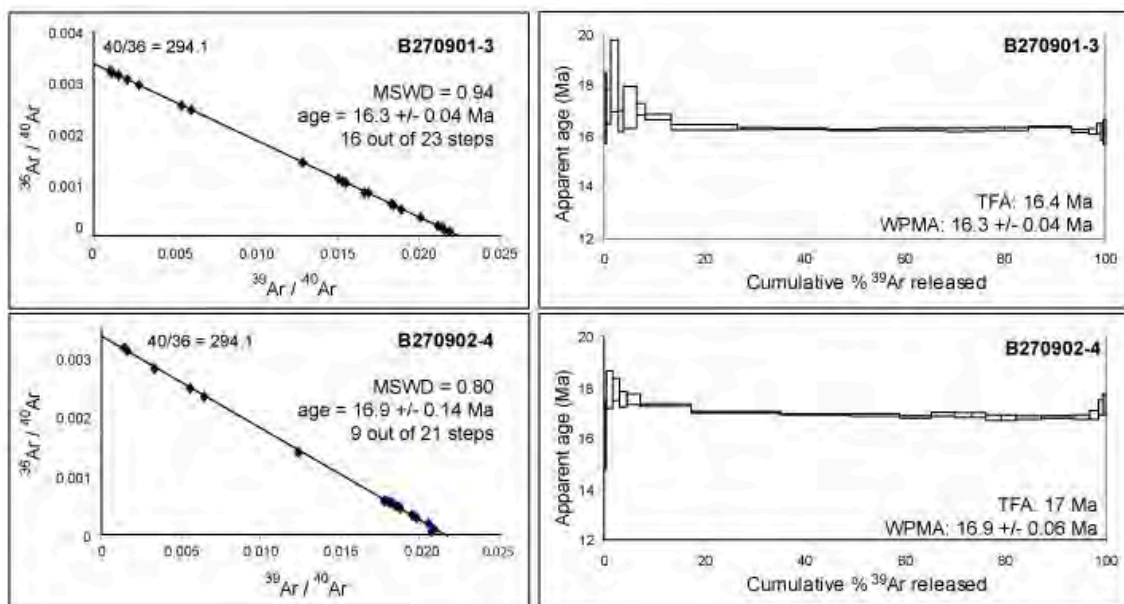


Figure 3.7: The $^{40}\text{Ar}/^{39}\text{Ar}$ ages in inverse isochron and spectra diagrams measured on white mica from rocks within the footwall of the Leo Pargil detachment zone. Increments indicate number of temperature steps considered for the age termination with the isochron plot. Both samples yield well-constrained plateau ages of 16.3 and 16.9 Ma. TFA: total fusion age; WMPA: weighted mean plateau age; MSWD: mean square of weighted deviation.

cas provides ages of 16.3 ± 0.04 Ma and 16.9 ± 0.04 Ma (see Table 3.1, and Fig. 3.7). This age coincides with the onset of exhumation of the Leo Pargil gneiss dome at 16-14 Ma, also derived from $^{40}\text{Ar}/^{39}\text{Ar}$ mica cooling ages farther north (Thiede et al., 2006). Therefore, it is possible that normal faulting in the hanging wall of the Leo Pargil detachment zone had already started before this time. However, the $^{40}\text{Ar}/^{39}\text{Ar}$ age presented here can be considered as a lower boundary for the onset of E-W extension in the NW Himalaya.

Sample	Weight (mg)	TFA (Ma)	WMPA (Ma, $\pm 2\sigma$)	IA (Ma, $\pm 2\sigma$)	Steps used (total steps)	% ^{39}Ar
B270901-3	3.2	16.4	16.3 ± 0.04	16.3 ± 0.04	8 - 23 (23)	87
B270902-4	3.3	17	16.9 ± 0.06	16.9 ± 0.14	8 - 16 (21)	39

Table 3.1: Summary of $^{40}\text{Ar}/^{39}\text{Ar}$ data (age uncertainties include error in irradiation parameter J). TFA: total fusion age; WMPA: weighted mean plateau age; IA: isochron age. Detailed information is available in Appendices B.1 and B.2.

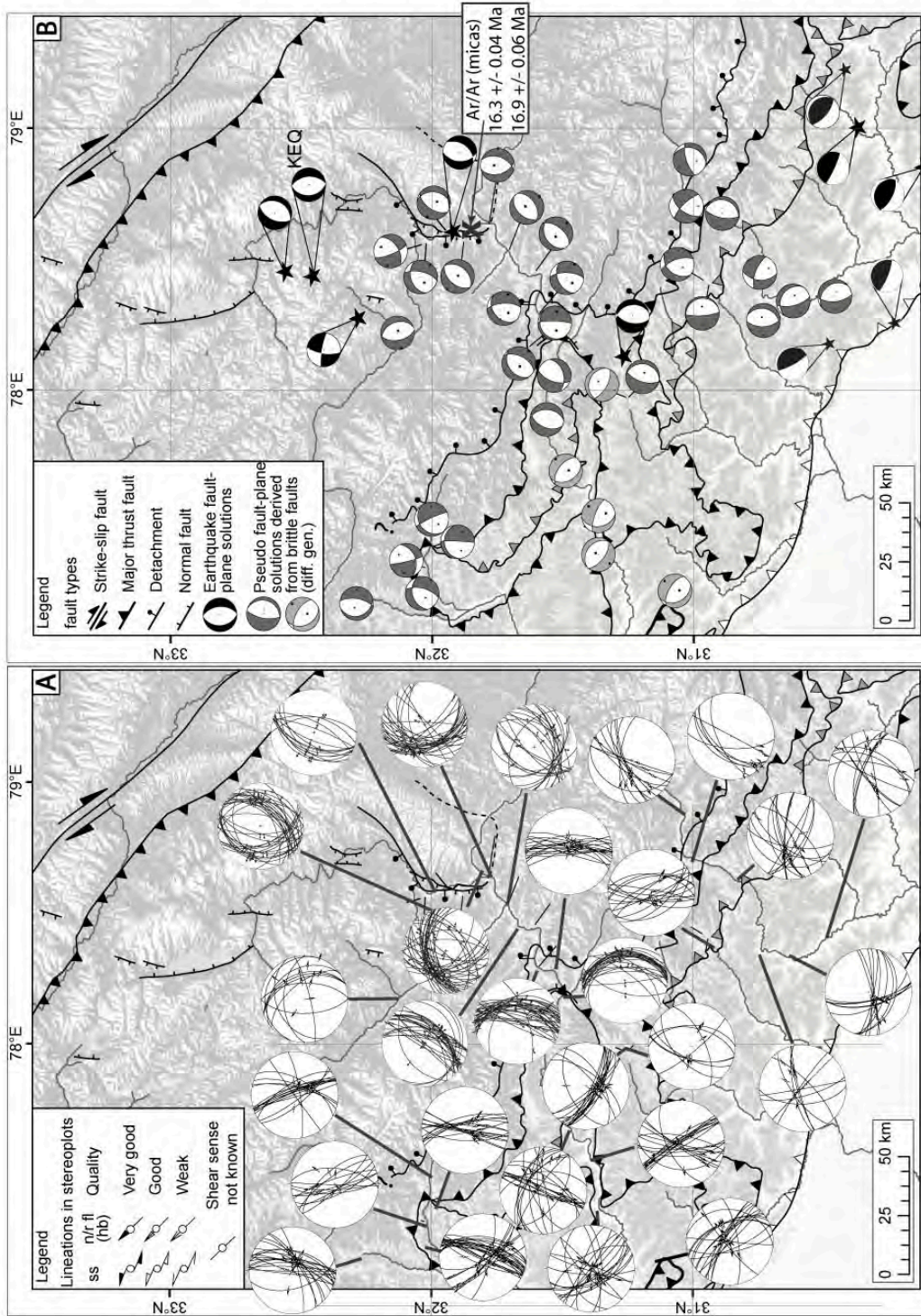


Figure 3.8: (A) Combined kinematic information of brittle deformation (fault planes and striations) in the NW Indian Himalaya. Data close to the Leo Pargil dome were previously published by (Thiede et al., 2006). (B) Synopsis of the pseudofault-plane solutions shown in different gray colors based on the data shown in A. For details for obtaining the pseudofault-plane solutions, see text. For details about the $^{40}\text{Ar}/^{39}\text{Ar}$ ages, see text and Tables 3.1, B.1, and B.2. Structural map and base map showing elevation are the same as in Fig. 3.1.

3.4.3 Normal faults in sediments and soft-sediment deformation

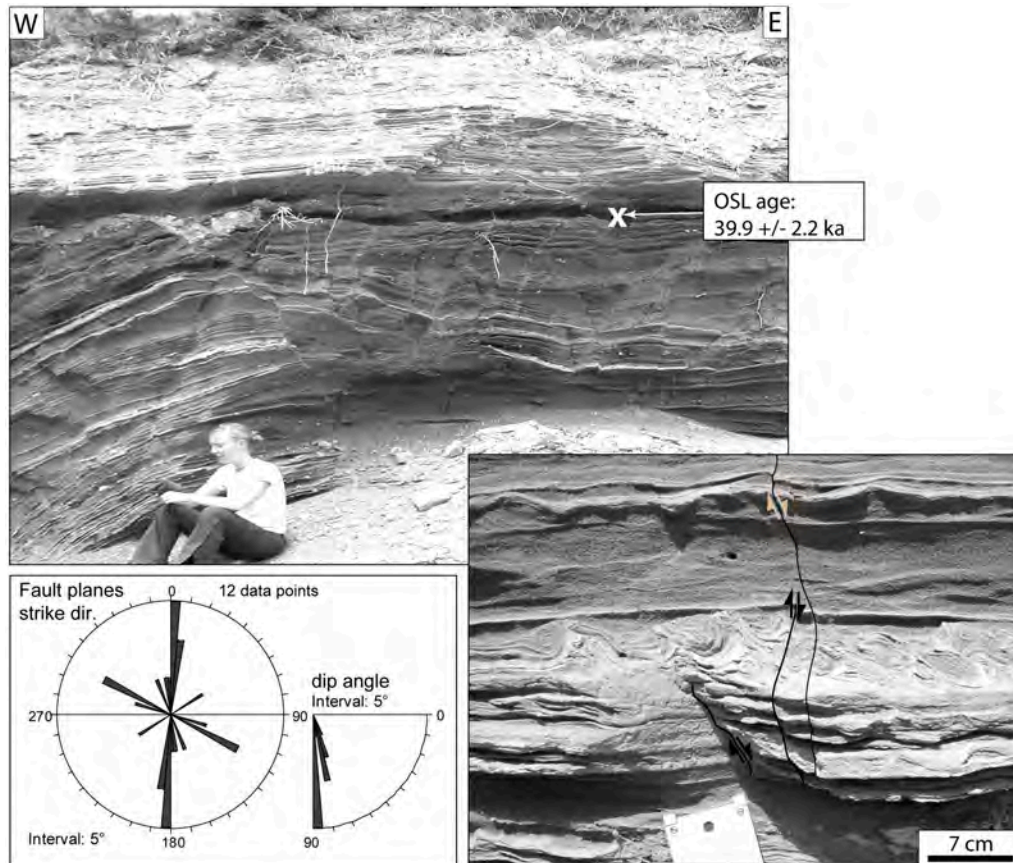


Figure 3.9: Fluvio-lacustrine sediments in the upper Spiti Valley, at the junction to the Lingti Valley. The sediments are affected by normal faulting. The two fault populations strike N-S and 105/285. Some of them terminate in layers with soft-sediment deformation typically associated with deformation during earthquakes (lower-right inset).

With the exception of the spatially limited Quaternary basin fills described above, mostly Paleozoic basement rocks are affected by normal faults in the Higher and Tethyan Himalaya due to the virtual absence of Cenozoic deposits at these high elevations. Hence, it is difficult to unambiguously constrain onset and duration of extensional processes in this region. In places, weathered conglomeratic gravel of unknown age overlying basement rocks is affected by extensional fractures and normal faults. In particular, at the junction of the Spiti River and its tributary, the Lingti River, approximately 2 m of fine-grained gray alluvial-fan sediments are overlain by 1.5 m of laminated sandy-silty lake sediments (Fig. 3.9). Both units are displaced by several N-S striking normal faults. A slightly older generation of NW-SE striking normal faults is systematically displaced by the N-S striking faults, supporting our inference that N-S striking normal faulting reflect the youngest phase of deformation in the NW Himalaya. However, because the NW-SE striking normal

faults are approximately parallel to the trend of the regional slope, it may be possible that this fault set is not tectonic in origin, but instead results from gravity sliding. In contrast, the N-S striking faults are oblique to the regional slope; a gravitational origin can thus be excluded. Interestingly, some fault planes end in layers that have flame structures, typically associated with deformation during earthquakes (Fig. 3.9). This observation suggests a possible seismogenic origin of these faults. OSL dating of these deposits provides a burial age of 39.9 ± 2.2 ka for the interface between the alluvial-fan sediments and the lake sediments, illustrating the recent nature of seismogenic processes in the Tethyan Himalaya, which is in line with the instrumentally recorded seismicity in this region (e.g., Molnar and Chen, 1983).

Evidence for soft-sediment deformation of lacustrine sediments is also observed farther east, along the lower Spiti River near the western flanks of the Leo Pargil gneiss dome, where lake deposits reach a thickness of up to 100 meters. They extend along the valley for approximately 8 km and are located between 10 and 100 m above the recent river bed (Fig. 3.10). The sediments are mainly composed of clay with intercalated thin sandy or silt layers between 0.5 and 10 cm thick. In several locations within the lacustrine sediments, we identified soft-sediment deformation phenomena, such as flame structures, neptunic dikes, and intruded lenses of conglomerates (Fig. 3.10). All these soft-deformation phenomena can be traced laterally up to 50 m. OSL dating of the sandy layers above the strata affected by soft-sediment deformation provides ages of 29.2 ± 1.6 ka at point B and 31.7 ± 3.9 ka at point D, indicating that the sedimentary deposits at those outcrops are related to the same lake. The OSL ages at points A and C are given as 5.61 ± 0.48 ka and 21.3 ± 1.1 ka, respectively, showing that there are several generations of lake deposits in this region. Details of the OSL dating results are given in Table 2. Interestingly, soft-sediment deformation within different lacustrine sedimentary bodies is found mainly in the vicinity of the Kaurik-Chango normal fault. Given this proximity to the regional active tectonic structures, the soft-sediment deformational structures could be seismogenic. The last large earthquake on this fault (Kinnaur earthquake, Jan. 19th, 1975, $M=6.5$, fault-plane solution labeled with KEQ see Fig. 3.1B) produced surface ruptures on the order of 0.5 m (Singh et al., 1975; Bhargava et al., 1978). Due to the absence of a present-day lake in the source area of the 1975 Kinnaur earthquake, a comparison between recently produced seismogenic features and our inferred older, possibly earthquake-induced soft-sediment deformation features is not possible. However, although other mechanisms could be invoked locally, the close relationship between normal faults and various types of soft-sediment deformation features in lake sediments in the immediate vicinity of the seismically active belt between the Tso Morari Lake and the Leo Pargil gneiss dome suggests a cogenetic origin.

3.5 Paleostrain results

We collected fault kinematic information at approximately 100 outcrops between the Tso Morari dome in the north and the Lesser Himalaya in the south. We focused on the southern continuation of the Tso Morari-Leo Pargil seismicity zone and the area between the Leo Pargil gneiss dome in the east and the Kullu Valley in the west. We only considered brittle faults that could be clearly assigned to the youngest deformation phase in the area. The striations on the mainly N-S striking normal faults related to this deformation phase are typically steeply dipping. However, there are several instances where older fault planes were reactivated as oblique normal faults. In total, we selected approximately 30 outcrops, where we had sufficient data related to the youngest deformation phase in the local context. For these measurements, we calculated pseudo fault-plane solutions (Fig. 3.8B).

The majority of the pseudo fault-plane solutions show chiefly E-W extension. In the vicinity of the Leo Pargil gneiss dome, the extension direction is NW-SE. In the southwest of the study area, the extension direction is NE-SW, and thus perpendicular to the strike of the orogen (light grey pseudo fault-plane solutions in Fig. 3.8B). Clear crosscutting relationships between fault planes associated with these different extension directions are rare. Observations at a single outcrop indicate that fault planes related to the NE-SW extension are locally overprinted by faulting during E-W extension.

Diffuse E-W oriented extension is observed in virtually the entire the study area. However, the density of fault planes dipping steeply W or E in the region associated with the N-S seismicity belt is much greater, and enhanced seismicity between the Tso Morari Lake and the Leo Pargil gneiss dome is much more pronounced compared to other regions of the study area. Nevertheless, at present, we have no data to test if this zone of preferred seismicity is a temporary, short-lived feature, or if it is important over longer geologic timescales.

Sample	Location		Depth (m)	Dose rate analysis				OSL dating results				
	Latitude (°N)	Longitude (°E)		U (ppm)	Th (ppm)	Rb (ppm)	K (%)	Moisture (%)	Aliquots meas. (used)	Paleodose (Gy)	Dose rate ($\mu\text{Gy}/\text{yr}$)	Age (ka)
Point A	32.0151	78.5764	3	1.6	7.0	43.1	0.66	0.3 \pm 5	14 (11)	9.9 \pm 0.7	1756 \pm 79	5.61 \pm 0.48
Point B	31.9575	78.6001	50	4.57	17.9	112	1.57	0.3 \pm 5	13 (9)	120 \pm 3.1	4103 \pm 202	29.2 \pm 1.6
Point C	31.9560	78.5990	2	3.15	12.9	102	1.44	0.6 \pm 5	16 (14)	73 \pm 1.6	3414 \pm 159	21.3 \pm 1.1
Point D	31.9925	78.5840	75	3.9	16.1	88.5	1.34	0.6 \pm 5	3 (1)	113 \pm 13	3576 \pm 170	31.7 \pm 3.9
Lingti	32.1088	78.1829	1.5	4.46	21.7	103	1.50	0.4 \pm 5	12 (12)	180 \pm 5.6	1221 \pm 64	39.9 \pm 2.2

Table 3.2: OSL dating results. Location of sample: sample refers to map points in Fig. 3.10, Lingti is related to the contact of alluvial-fan and lacustrine deposits in Fig. 3.9. Dose rate analysis: Content of naturally occurring potassium (K), thorium (Th), rubidium (Rb), and uranium (U) within the sample material, which are the main contributors of dose to sedimentary quartz. OSL daing results: total dose rate is attenuated for grain size, density, and moisture.

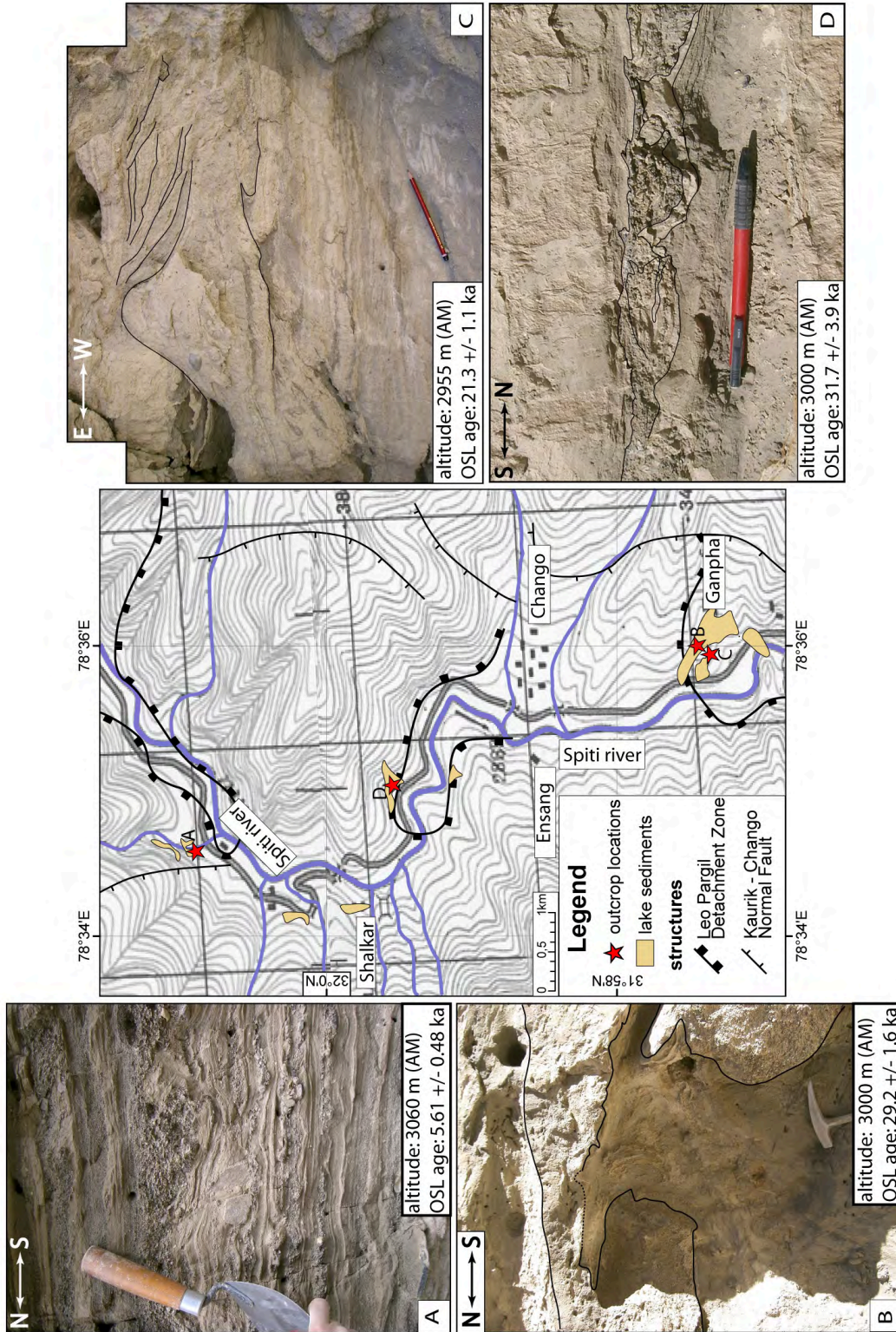


Figure 3.10: Lake sediments in the lower Spiti Valley affected by soft-sediment deformation. Thin black lines delimit layers of fine sandy layers, coarse sandy layers, and/or clay layers. Location of the field photos are marked in the central map. Geological information was taken from Thiede et al. (2006); topographic map is an amplified Russian map with an original scale of 1:100,000.

3.6 Discussion and conclusions

The new data we presented, including map-scale normal faults identified on satellite imagery and in the field, meso-scale faults, outcrop-scale fault-kinematic data, and fault-cut Quaternary sediments document ongoing normal faulting extending from the Greater Sutlej river region to the Garhwal Himalaya. The different observations record E-W oriented extension over a diffuse, approximately N-S striking swath between 77.5 and 79°E. Below, we first address the possible onset and/or ages of the different evidences for deformation, and secondly discuss their origin and possible underlying driving mechanisms.

3.6.1 Possible onset of E-W extension in the Higher Himalaya

A comparison of our own newly derived $^{40}\text{Ar}/^{39}\text{Ar}$ and OSL ages with already published studies in the NW Himalaya allows us to estimate the possible ages of the onset of normal faulting and its continuation to the present day. The following discusses the possible timing for the different types of extensional features, where available.

Brittle faulting on meso- and outcrop-scale

Synkinematic micas on fault planes and within fault gouge and quartz-filled tension gashes suggest that at least part of the brittle faulting related to E-W extension has its origin in the brittle-ductile transition zone. This zone broadly coincides with depths where temperatures are around 350°C. $^{40}\text{Ar}/^{39}\text{Ar}$ cooling ages of micas recording a closure temperature of approximately 350°C, have age ranges between 14 and 19 Ma for the Higher Himalaya, and 4.3 to 6.7 Ma for the Lesser Himalayan Crystalline between the MT and MCT, respectively (Vannay et al., 2004; Thiede et al., 2005, 2006). These ages can be thus considered as the older limit of brittle deformation behavior of the rocks. The age obtained for synkinematic muscovites on a fault plane in the footwall of the Leo Pargil gneiss dome in our study provides a similar age constraint of about 16 Ma (see Figs. 3.7 and 3.8). Because those micas area synkinematically grown on a fault that fits kinematically in the E-W extensional stress field, we infer that E-W extension was already active in the Higher and Tethyan Himalayas at that time. In addition, ductile mineral stretching lineations observed in the footwall of the LPDZ along the western flank of the Leo Pargil also indicate E-W extension at lower structural levels between 14 to 16 Ma (Thiede et al., 2006). Combining all of these observations, we suggest that E-W extension was initiated at least around 4 Ma in the Lesser Himalaya and between 14 and 16 Ma in the Higher and Tethyan Himalayas.

Large-scale normal faults on satellite imagery

Age constraints on the large-scale normal faults that we evaluated mainly from satellite imagery are essentially non-existent. The age of the faulted paleo-surface in the Tso Morari area and in the Lingti Valley is unknown, but based on regional relationships, can be estimated with reasonable certainty to be of Quaternary age.

In the sedimentary basin NW of the Leo Pargil gneiss dome, however, a rough age estimate can be made. The sedimentary fill is clearly related to transient basin

isolation, and we infer that normal faulting caused hydrologic isolation and the generation of accommodation space for sediments. The onset of basin filling therefore must have been simultaneous with the beginning of normal faulting, and the partially preserved paleo-surface provides a minimum time for the onset of normal faulting in this basin. Despite a lack of radiometric ages to further decipher these processes, the age of the sedimentary basin fill may be comparable to the fill units of the much larger Zada Basin on the SE side of the Leo Pargil dome, and a crude age estimate may be possible based on observations there. Saylor et al. (2009) suggest that the oldest sedimentary deposits in the Zada Basin are upper Miocene. Normal faults along the eastern flank of the Leo Pargil gneiss dome constitute the western border of this basin. Hence, if these normal faults are mechanically linked and are an integral part of the extensional structures that characterize this dome, the structures on the western flank of the dome and the sedimentary fills are coeval.

Soft-sediment deformation

Soft-sediment deformation features along the western flank of the Leo Pargil gneiss dome occur in lacustrine sediments that were deposited in a land-slide dammed lake (Bookhagen et al., 2005a). ^{14}C ages of the lowest part of these sediments show a consistent calibrated age of 28.5 ± 0.9 ka BP (Bookhagen et al., 2005a). Our OSL ages of sandy layers immediately above those strata affected by soft-sediment deformation provide similar ages within error, attesting to the recent nature of seismogenic movements in this region and to protracted activity along the Kaurik-Chango normal fault. Mohindra and Bagati (1996), and Banerjee et al. (1997) reported similar features in the Pare Chu Valley directly north of the area shown in Fig. 3.10. Based on OSL dating and sedimentary analysis, these authors inferred at least nine separate earthquakes with magnitudes large enough to produce soft-sediment deformation within the last 90 ka. Because the soft-sediment deformation features we observed are only a few kilometers from these lacustrine sediments, they all likely underwent soft-sediment deformation in the same tectonic environment. Thus, there is widespread evidence for seismic activity along the Kaurik-Chango normal fault indicating E-W extension since at least the Pleistocene.

3.6.2 Possible mechanisms for E-W extension in the Tethyan and Higher Himalaya

Models and interpretations of orogen-perpendicular grabens in the Central Himalaya can be separated into three major groups: (1) models linking the graben systems to escape tectonics in the course of the India-Eurasia collision process (e.g., Tapponnier and Molnar, 1976; Tapponnier et al., 1982); (2) models that relate the arc-perpendicular structures to the arcuate geometry of the Himalaya and/or the Indian subduction zone (e.g., Ratschbacher et al., 1994); and (3) models invoking processes such as slip partitioning resulting from oblique convergence (McCaffrey and Nabelek, 1998) or local extension due to metamorphic dome formation (e.g., Aoya et al., 2005). In Table 3.3, we summarize the major hypotheses as well as their implications for extensional structures in the NW Himalaya and consider if they are applicable to our region.

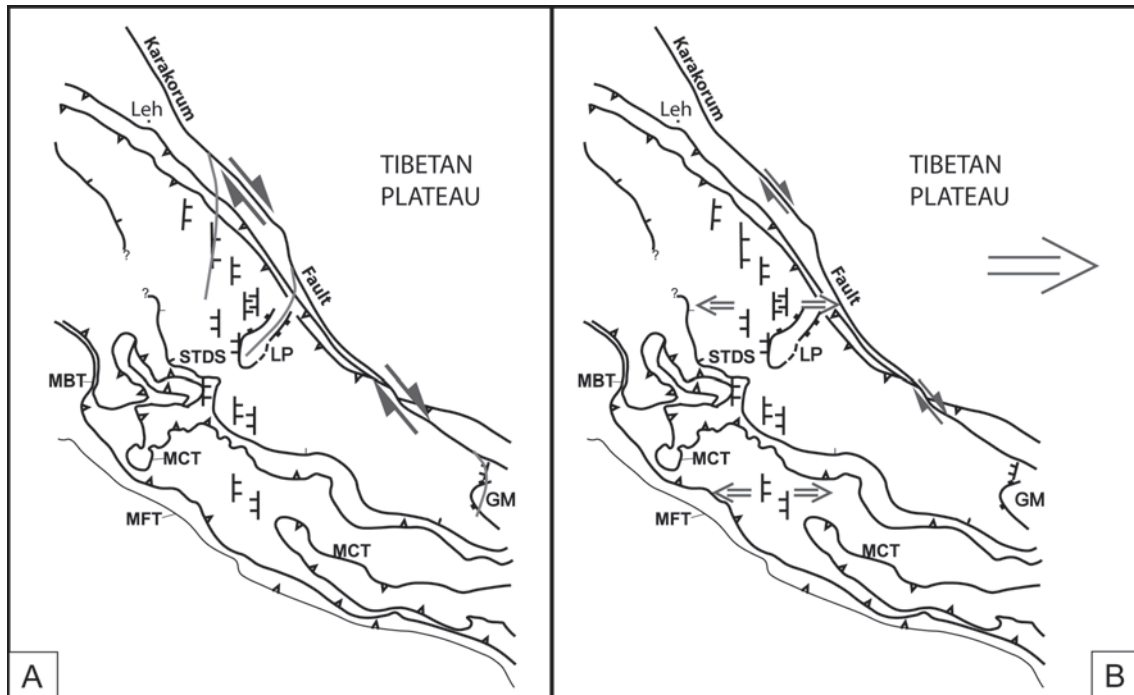


Figure 3.11: Models for E-W extension observed in the NW Indian Himalaya west of the Karakorum fault. (A) Horse-tail termination of the Karakorum fault. Gray lines show the inferred trend of the splays. Normal faults do not fit into this arrangement. (B) Transition of normal faulting from the Tibetan Plateau into the Himalayan realm. Arrows show the approximate extension direction observed in the Tibetan Plateau and in the NW Himalaya, as well as movement along the Karakorum fault. Major geological structures are from (DiPietro and Pogue, 2004). In the Higher and Lesser Himalaya, normal-fault symbols represent pervasive, closely spaced outcrop-scale normal faults. For abbreviations, see caption to Fig. 3.1.

Models explaining arc-parallel extension in the Central Himalaya based on the arcuate shape of the orogen predict normal faults that are generally perpendicular to the regional trend of the Himalaya. Due to the regional NW-SE trend of the NW Indian Himalaya, these models would predict a NW-SE oriented extension direction. This is inconsistent with our field observations as well as the results of our brittle-fault kinematic analysis, which show E-W directed extension. Furthermore, it is incompatible with the kinematic character derived from regional GPS measurements (Banerjee and Bürgmann, 2002) and extension directions obtained from focal mechanisms of larger earthquakes in the NW Indian Higher and Tethyan Himalaya (Molnar and Chen, 1983; Molnar and Lyon-Caen, 1989). These inconsistencies require that alternative mechanisms must be invoked to explain our observed E-W extension. Below, we assess three possible scenarios that could explain ongoing extension processes in this part of the mountain range.

The first, and rather local, explanation for the existence of brittle normal faults is their potential association with the Leo Pargil gneiss dome immediately east of our study area (see Fig. 3.1B). Similar to other active gneiss domes in the western Himalaya, it is associated with extensional structures at its flanks (Murphy et al.,

2002; Thiede et al., 2006; Saylor et al., 2009). The presence of normal faults in the vicinity of the gneiss dome would be related to accommodation of different exhumation rates between the buoyant gneiss dome and the surrounding region.

A second possible explanation for the normal faults involves a horse-tail termination of the neighboring dextral Karakorum Fault (Fig. 3.1). The eastward escape of central and northern Tibet is mainly accommodated along regional sinistral and dextral strike-slip faults at the northern and southern plateau margins, respectively (e.g., Peltzer and Tapponnier, 1988; Taylor et al., 2003). The southwestern margin of Tibet is bounded by the NW-SE striking Karakorum strike-slip fault system, which can be traced 1000 km from the Pamir in the northwest to the Gurla Mandhata dome in the southeast (Fig. 3.1A, Murphy et al., 2000). Close to this gneiss dome, the low-angle, west-dipping Gurla Mandhata Detachment Zone (GMDZ) is exposed. Geological field observations and $^{40}\text{Ar}/^{39}\text{Ar}$ chronology suggest a kinematic linkage of both faults (Murphy et al., 2000; Murphy and Burgess, 2006). If related, normal faults in the greater Sutlej region could be an integral part of such a horse-tail termination of this large strike-slip fault system (see Kim et al., 2004, and Fig. 3.11A)). Accordingly, the areas of localized normal faulting between the Tso Moriri dome in the north and the Zada Basin in the south could be interpreted as single branches of a horse-tail structure.

The third and final alternative explanation links normal faulting in the Himalaya to southward propagation of active extensional processes on the Tibetan Plateau (Fig. 3.11B). For example, fault-plane solutions of earthquakes in this region show dominant E-W extension (Molnar and Chen, 1983; Molnar and Lyon-Caen, 1989). If our observed E-W extension in the NW Himalaya is related to extension in the plateau, then the role of the Karakorum Fault as a first-order boundary between the tensional stress regime in the Tibetan Plateau and compression in the Himalaya would be of secondary importance. The ongoing controversy concerning the displacement rate of the Karakorum Fault (e.g., Lacassin et al., 2004; Chevalier et al., 2005; Searle and Phillips, 2007) underscores its ambiguous role in the recent deformation history of the Himalaya-Tibet region. If displacement rates are low (Searle et al., 1998; Murphy et al., 2000; Phillips et al., 2004, e.g.) normal faulting in the Sutlej-Spiti rivers region could indicate that the Karakorum Fault has not been able to fully accommodate the E-W extension generated in the Tibetan Plateau. In this scenario, the Karakorum Fault does not decouple the extensional processes in Tibet from the shortening regime in the Himalaya. Thus, extensional features in the NW Himalaya would be linked to southward propagation of normal faulting and graben formation that is currently observed in Tibet and the transition with the Central Himalaya.

Whereas the first hypothesis has only local significance relevant for the immediate surroundings of the Leo Pargil gneiss dome, the other two hypotheses could explain normal faulting affecting much more extensive regions. Both hypotheses represent regional-scale end-member scenarios. One of the crucial issues in correctly assessing the different factors producing normal faulting is the importance of the Karakorum Fault for recent deformation processes in the NW Himalaya. If the observed structures are indeed part of a horse-tail termination of the Karakorum Fault, this

structure would represent a first-order decoupling zone between the Tibetan Plateau and the Himalaya. Conversely, if normal faulting were related to the propagation of extensional faulting originating on the Tibetan Plateau, then the Karakorum Fault would be of secondary importance.

The three scenarios presented here may not be mutually exclusive. All present viable explanations for ongoing E-W oriented extension in the Higher Himalaya of NW India. However, the overall distribution and orientation of normal faults is inconsistent with the hypothesis of doming and tectonic exhumation of the Leo Pargil gneiss dome. If doming were the primary driver for extension, normal faults should be concentrated close to the flanks of the gneiss dome and not in a N-S striking swath of active faulting and seismicity that affects all pre-existing contractional structures. Furthermore, the normal faults should be oriented radially around the outline of the gneiss dome; however, this is not the case. The processes responsible for doming at the Leo Pargil gneiss dome may still contribute to the evolution of local normal faults. In particular, the rotation of the extensional axis from E-W to NW-SE in the vicinity of the gneiss dome could be a result of doming. Nonetheless, doming does not appear to be a viable mechanism to explain the regional extent of E-W extension observed in the NW Himalaya.

The two remaining end-member models that involve the Karakorum Fault may better reconcile the observed structural evolution of the NW Himalaya. In the model that relates the observed E-W extension with the horse-tail termination of the Karakorum Fault, single splays of normal faults perpendicular and south of this major structure would be expected. Our observations, however, did not reveal such single splays. Furthermore, the strike of such splay faults should rotate towards the Karakorum Fault into a NW-SE direction, i.e. parallel to the strike of the Karakorum fault, such as indicated by the grey lines in Fig. 3.11A. This should be particularly true for smaller-scale structures. This is not the case, as clearly shown by Epard and Steck (2008), who mapped Quaternary normal faults in the area between the Tso Morari and the Karakorum fault, immediately north of our study area. These faults do not show any change in strike direction closer to the Karakorum fault. In addition, if there were a kinematic linkage between the long-lived Karakorum Fault and E-W extension described here, the normal faults should have accrued higher total strain. This would imply that such faults would be more or at least equally pronounced as those normal faults observed around the Gurla Mandhata dome at the southernmost end of the Karakorum Fault and south of our study area (Murphy et al., 2002). Even if we cannot provide the exact amount of total normal displacement in the area, it is most likely less than the 35 to 66 km slip observed at the Gurla Mandhata dome (Murphy et al., 2002). This indicates that the mechanistic linkage between the N-S striking normal faults in the NW Indian Himalaya and the Karakorum fault is not likely. Therefore, we also discard this hypothesis as an explanation for E-W extension in the NW Himalaya.

The second end-member model predicts that E-W extension is transferred from the Tibetan Plateau into the NW Himalaya. In this scenario, the Karakorum Fault would be a second-order feature. If the Karakorum Fault indeed accommodated all of the E-W extension observed in the Tibetan Plateau, the level of seismic activity

should be much higher than the present-day level of activity. Globally recorded seismicity in this area shows that only a few earthquakes have occurred along this fault in the last 30 years (NEIC Catalog, 2009). We thus infer that the Karakorum Fault does not fully accommodate the bulk of E-W extension occurring in the Tibetan Plateau and therefore, part of this strain must be transferred SW of the Karakorum Fault into the NW Himalaya. This hypothesis explains why E-W extension in the NW Himalaya is a pervasive, ubiquitous phenomenon independent of local structures. The N-S striking normal faults would thus be an integral part of the same extensional processes that dominate the Tibetan Plateau and the transition to the Central Himalaya.

Among those models, there are two main differences: (1) models that assume the crust and mantle are decoupled, with eastward extrusion of Tibet either accommodated as a rigid block bounded by large fault systems such as the Karakorum and Altyn Tagh faults (e.g., Tapponnier et al., 1982) or through continuous deformation distributed over the whole area (Zhang et al., 2004; Taylor et al., 2003); and (2) models that assume the upper brittle crust is coupled to the mantle (e.g., Molnar and Chen, 1983) or there is a weak lower crustal level that decouples the mantle from the upper crust (Nelson et al., 1996, e.g.). Our data suggests that the transition of extensional tectonics from the Tibetan Plateau across the Karakorum Fault into the NW Himalaya may be related to a crust coupled to eastward-flowing mantle and continuous deformation not restricted to single larger structures. The question whether E-W extension in the Tibetan Plateau is triggered by the plate convection between India and Eurasia or is part of adjustment to a change of boundary conditions in eastern Asia (Yin, 2000; Yin and Harrison, 2000) is not possible to be resolved with the data presented here.

We thus conclude that predominant, pervasive and active E-W extension in the NW Indian Himalaya is a ubiquitous phenomenon and not restricted to the well known regions of focused extension (e.g., Leo Pargil dome, the Gurla Mandhata dome, the Thakkola Graben, the Ama Drime Massif, and the Yadong Graben). Our observations have clearly shown that E-W extension affects the entire mountain belt from the Indian-Eurasian suture zone to the footwall of the MCT in the Garhwal Himalaya. Importantly, extensional processes are not limited to regions north of the STDS, as previously thought. Although geochronologic data documenting the onset of normal faulting are still sparse, E-W extension has apparently been a protracted process that started at around 16 Ma and has continued until the present day. Based on the regional relationships documented in our study, we propose that E-W extension in the NW Himalaya is transferred from the Tibetan Plateau due to the inability of the Karakorum fault to accommodate all of the ongoing E-W extension on the Tibetan Plateau.

3.6. DISCUSSION AND CONCLUSIONS

Models	Observations from the NW Indian Himalaya						Migration of extensional structures from the TP into the Himalaya
	E-W extension oblique to the orogen	Extent of E-W extension	E-W extension not limited to larger structures	Role of the KF	Normal faulting south of the STDS		
Local explanations	Yes	Limited to the vicinity of the Leo Pargil gneiss dome	No, mainly focused to dome structures	Not predicted	Not predicted	No	
	Yes	SE of the KF	No, normal faults arranged in single splays originating at the KF	Large slip rate, greater impact	Not specified, but possible	No	
	No	Southern Tibet and Himalaya above the subducting plate	No, slip is mainly concentrated on KF	Large slip rate, taking up all shear	Not specified, but possible	No	
Tibetan extensional models	Yes	Whole Asia, including TP and Himalaya	Yes	Not specified	Not specified, but possible	Yes	
	Yes	Entire TP and Himalaya	Yes	Not a major feature	Not specified, but possible	Yes	
	Yes	Entire TP and Himalaya	Yes	Large slip rate, major feature	Not specified, but not likely	Yes	
	Yes	Entire TP and Himalaya	Yes	Not a major feature	Not specified	Yes	
	Yes	Entire TP and Himalaya	Yes	Not a major feature	Not specified, but not likely	Possible	

Table 3.3: Models for E-W extension in the Tibetan Plateau (TP) and the Himalaya, their implications and specifications for E-W extension in the NW Indian Himalaya and for the Karakorum Fault (KF)

Acknowledgements

We want to thank M.B. Bateman for providing the OSL data, Tashi Tsering for excellent logistical support, A. Yin, M. Murphy, and A. Webb for their constructive comments that helped to improve the paper, and K. Karlstrom for editorial support. This work was financially supported by the DFG Graduate School 1364 at the University of Potsdam, Germany.

Chapter 4

Active tectonics in the NW Indian Himalaya

In the following chapter, I will present additional geomorphic, sedimentological, and paleoseismological data from the Tethyan and Higher Himalaya (a) to show that the 1975 $M_w = 6.8$ Kinnaur earthquake was not a singular event, but the reflection of recurrent seismic activity in this area; (b) to document the impact of ongoing E-W extension on landscape evolution; and, finally, (c) to close the time gap between structures related to brittle deformation (chapters 2 and 3) and recent seismicity in a regime of active E-W extension in the NW Indian Himalaya. In order to provide a geodynamic context for these new data and observations presented in chapters 2 and 3, a summary of ongoing deformation within the Himalaya-Tibet region based on seismological and GPS records is given at first.

4.1 Present-day deformation in the Himalaya and Tibet based on earthquake and GPS records.

Due to the high convergence rate of approximately 55 mm/yr between India and Eurasia (Wang et al., 2001; Copley et al., 2010), GPS velocity records reflect well the first-order deformation patterns of the Himalayan-Tibet region and provide insight into the characteristics of the present-day deformation (Wang et al., 2001; Zhang et al., 2004). During the last decade, the collection of GPS velocity data has shown that deformation due to the protracted indentation of India into Eurasia is affecting a large region spanning from the Himalayas in the south to the Baikal rift in Siberia and associated zones of extension farther north (Wang et al., 2001; Zhang et al., 2004). However, the resultant deformation pattern is far from being uniformly distributed. Approximately half of India's northward motion is accommodated within the Himalayan range. Towards the east, the total amount of shortening across the Tibetan Plateau decreases from 4.7 mm/yr in the west to < 1 mm/yr in the east, while internal shortening observed within the Tibetan Plateau is accommodating 12 mm/yr (e.g. more than 30 % of the total amount of shortening, Zhang et al., 2004). In the Tien Shan of northwest China, about 20-22 mm/yr of north-directed movement have been measured, while 10 mm/yr are absorbed by structures across the Qaidam basin and the Qilian Shan at Tibet's NE margin (Zubovich et al., 2010). In addition, N-S shortening is compensated by of E-W extension within the Tibet Plateau, which mostly generates internal deformation, but also extension along distinctive N-S oriented rifts (Molnar and Tapponnier, 1978).

Due to the high velocity of the Indian plate, the Himalaya and the Tibetan Plateau are one of the seismically most active regions in the world (Ni and Barazangi, 1984; Molnar and Lyon-Caen, 1989; Bilham et al., 2001). Earthquakes within the Northern Tibetan Plateau are characterized by strike-slip faulting and extension, both compensating N-S shortening by accommodation of lateral motion and E-W extension. The observed earthquakes are concentrated at depths of < 15 km and have magnitudes of up to 7.0 (Molnar and Chen, 1983; Molnar and Lyon-Caen, 1989; Molnar, 1992). In the southern Tibetan Plateau, however, fault-plane solutions document pure normal faulting indicating E-W extension, both at shallow crustal levels (< 15 km) and at greater depths of 80 - 95 km (Molnar and Chen, 1983; Molnar and Lyon-Caen, 1989). In contrast, earthquakes along the southern Himalayan front with N-S oriented thrusting focal mechanisms and magnitudes of up to 8.0 are located at depths between 20 and 40 km, and are primarily related to the underthrusting of India beneath Eurasia (Seeber and Armbruster, 1981; Ni and Barazangi, 1984).

This dichotomy of shortening at the front of the orogen and extension in its interior is also observed within the NW Indian Himalaya, both in GPS and seismicity data (e.g., Molnar, 1992; Banerjee and Bürgmann, 2002). However, although the recent seismic activity has been well constrained since the installation of the worldwide seismic network during the 1960 (Fig. 3.1), historical seismic records are rare (Bilham, 2004). Despite this, increasing evidence from paleoseismological studies support the notion that the Himalayan frontal thrusts, and especially the MFT,

have been the source of mega-earthquakes with magnitudes $M > 8.0$ (e.g., Kumar et al., 2006; Malik et al., 2010). Less detailed information is available from the orogen interior. Despite this data gap, seismicity in the internal parts of the NW Indian Himalaya, especially between the Tso Morari and Leo Pargil gneiss domes, is ubiquitous. The 1975 Kinnaur ($M_w = 6.8$) earthquake and its aftershocks are prominent examples of this seismic activity (Singh et al., 1975; Khattri et al., 1978).

In the following sections, I will provide additional geomorphic and paleoseismological evidence that the Tibetan and Higher Himalaya of NW India is characterized by ongoing E-W extension, which might be reflected by the extensional seismicity in this part of the orogen. The geomorphic data comprises a set of disturbed longitudinal river profiles that cross an intermontane basin bounded by roughly N-S striking normal faults. The paleoseismological data is twofold and consists of a series of soft-sediment deformations, inferred to be seismites, in lake sediments close to the Kaurik-Chango-Normal fault, and observations concerning large displacements within paleo-lake sediments in the Baspa Valley.

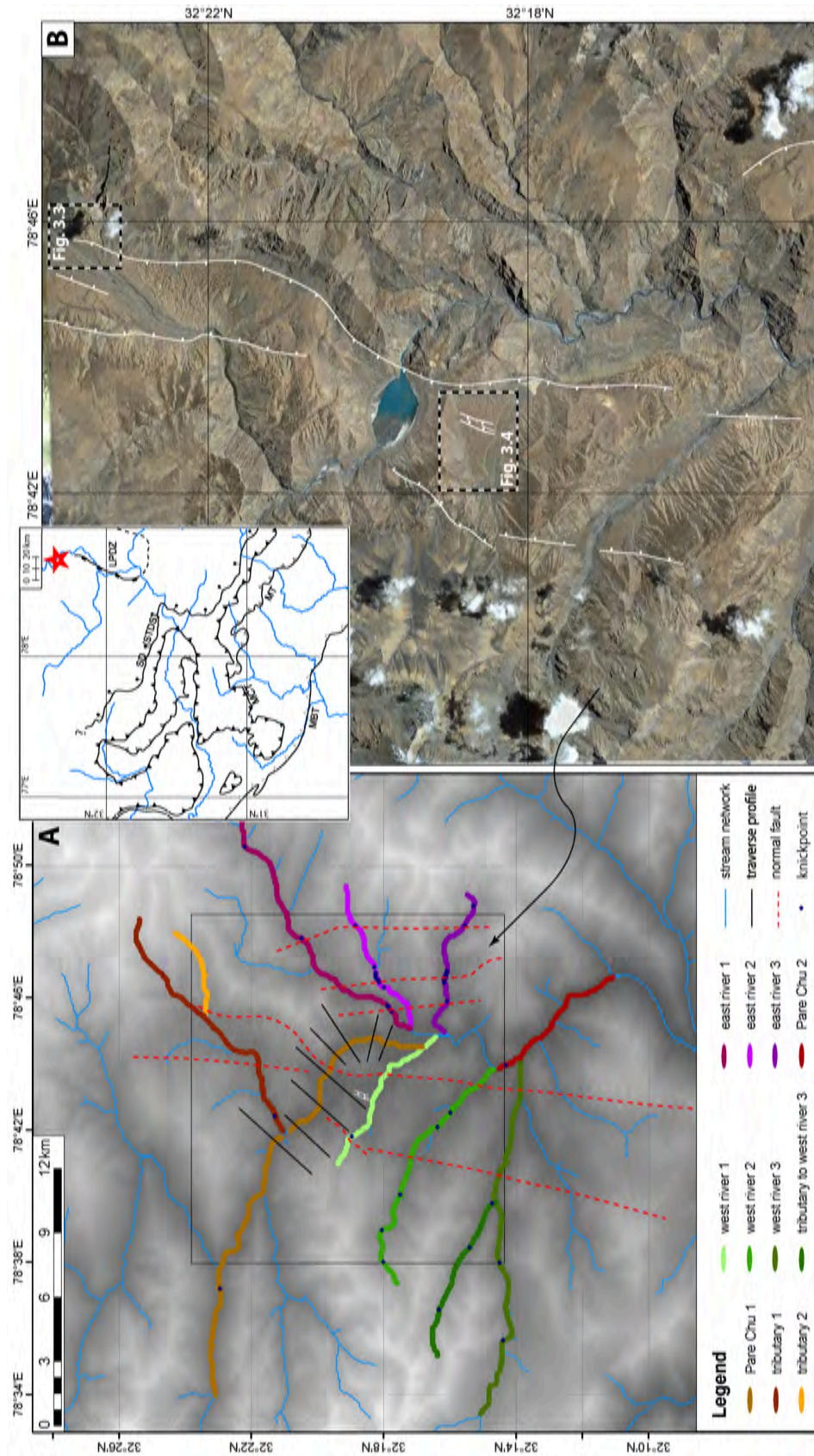


Figure 4.1: Overview of the normal fault-bounded basin NW of the Leo Pargil gneiss dome. (A) Stream network derived from the underlying DEM. Lineaments that were identified as normal faults are marked with red dashed lines. River profiles used for detailed analysis are color-coded. (B) Satellite image of area marked with the black box in (A). White lines mark normal faults, showing the movement of the hanging wall. Black and white dashed boxes show the locations of Figs. 3.3 and 3.4. Source: GoogleEarth. Location of the basin is marked with a red star in the inset showing the main geological structures of the NW Indian Himalaya (modified after Thiede et al. (2005) and references therein). Abbreviations: LPDZ - Leo Pargil detachment zone, MBT - Main Boundary thrust, MCT - Main Central thrust, MFT - Main Frontal thrust, MFT - Muniari thrust, SD - Sangla detachment, STDS - Southern Tibetan detachment system.

4.2 Disturbed river profiles in the intermontane basin NW of the Leo Pargil gneiss dome

In this section, I present river profiles of the Pare Chu River and its tributaries that are draining the intermontane basin NW of the Leo Pargil gneiss dome (described in section 3.4.1), which is located in a remote area within Chinese territory close to the Indian border, which is inaccessible for foreigners. Analysis of the river profiles, both longitudinal and transverse, are helpful to characterize fault activity in this basin and to understand basin development in this remote area.

Analysis of high-resolution satellite imagery (GoogleEarth and ASTER) as well as identification of lineaments on a DEM derived from SRTM data (resolution 90 m) provided the basis for a fault inventory shown in Fig. 4.1B. Since the basin has already been described in detail in section 3.4.1, only the main structural and geomorphic characteristics are repeated here:

The basin is bounded by E- and W-dipping normal faults. Movement along these faults created an approximately 10-km-wide accommodation space for sediments, which are now being incised and evacuated due to drainage capture by the Pare Chu River. Based on the degree of preservation of the fault scarps, the least preserved, and thus the oldest, normal faults occur at the eastern and western margins of the basin, respectively. Displaced alluvial fans, fan deltas, and fluvial terraces indicate recent faulting, at least in the central and northern parts of the basin (section 3.4.1). In addition, there are several N-S striking faults east of the basin, parallel to the eastern basin-bounding fault. These fault scarps are well visible in the satellite images as thin lines that traverse different lithological units.

In order to constrain the remote-sensing observations (see section 3.4.1), longitudinal profiles of 11 rivers across the basin were analyzed. In addition, 8 transverse profiles were extracted from the same DEM, describing the shape and width of the Pare Chu river valley in the central part of the basin (thin black lines in Fig. 4.1A).

4.2.1 Methodology

Under stable tectonic conditions, longitudinal river profiles tend to have an exponential concave shape and can be described by Flint's law (1974), a power-law relationship between local channel gradient S and upstream drainage area A

$$S = k_s A^{-\theta}$$

where k_s is the channel steepness index, and θ the concavity index (Hack, 1957; Flint, 1974). In general, such an ideal longitudinal profile depends on climate, bedrock lithology, and active tectonics (Fig. 4.2A). If one of those three components changes abruptly downstream, this ideal river profile is disturbed (Kirby and Whipple, 2001; Wobus et al., 2006; Harkins et al., 2007). The concavity index seems to be mostly influenced by changes in downstream discharge and channel width (Whipple and Tucker, 1999; Tucker, 2004); under steady-state conditions, it can be carefully considered as being independent of climate, lithology, and tectonics (Wobus et al., 2006). On the other hand, by using a referenced value for the concavity index θ_{ref} ,

4.2. DISTURBED RIVER PROFILES

the resultant normalized channel steepness k_{sn} is expected to reflect the landform response to those factors (Wobus et al., 2006).

Different bedrock lithologies may influence the channel steepness; i.e., steeper channels are associated with more resistant, less fractured rocks (e.g., Duvall et al., 2004), but it seems that the presence of even thin alluvial veneers within the channel decouples its steepness from the underlying bedrock (Kirby et al., 2003; Sklar and Dietrich, 2008). Climatic conditions are thought to play an important role in influencing erosion rates and thus channel steepness, i.e., a wetter climate may result in a high erosion rate, which in turn causes lower channel steepness (e.g., Aalto et al., 2006).

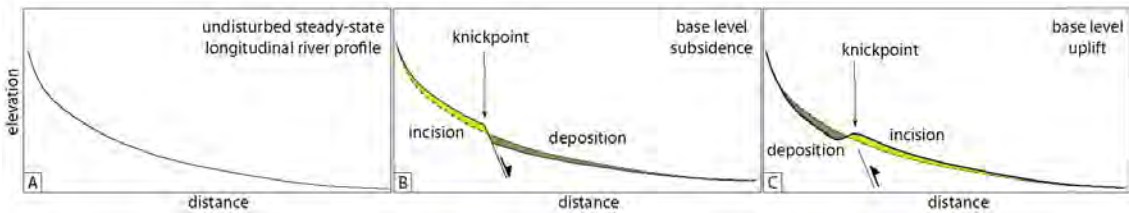


Figure 4.2: Longitudinal river profiles in case of steady state (A), base level subsidence (B) and uplift (C). Yellow areas indicate sections affected by incision, brown areas are sectors with deposition. Dashed lines in (B) and (C) indicate the steady stated river profile.

The best documented and studied factors on channel steepness, however, are rock uplift or subsidence relative to base level and erosion rates. The usually concave shape of longitudinal profiles of rivers crossing active faults (Fig. 4.2A) typically experiences channel steepening in case of downstream subsidence (Fig. 4.2B), or have a gentler profile in case of downstream uplift (Fig. 4.2C). Subsidence would cause steepening of the upstream level, leading to knickpoints that represent the transition between relict upstream areas and adjusting to downstream hydraulic topography.

The change of valley width and height may also reflect downstream changes. In the case of downstream subsidence, aggrading wide-floored valleys are observed, whereas deep, V-shaped valleys are typically associated with high incision rates, associated with footwall uplift (Bull, 1977).

All river profiles presented in this study are from an area where climatic conditions are invariably dry and the lithology consists of the sedimentary sequences of the Tibetan Himalaya with similar erodibility. Assuming such uniform climatic and lithologic conditions, the occurrence of knickpoints and change of valley width may be intimately linked with tectonics.

4.2.2 Longitudinal river profiles

In total, 11 longitudinal river profiles were extracted from the SRTM DEM. They can be grouped into the western rivers that cross the central part of the basin in the south (west rivers 1-3, the tributary to the west river 3, and Pare Chu 1, see left column on Fig. 4.3), and the eastern rivers that drain the eastern margin of the basin (east rivers 1-3 and Pare Chu 2, see right column in Fig. 4.3). Being the

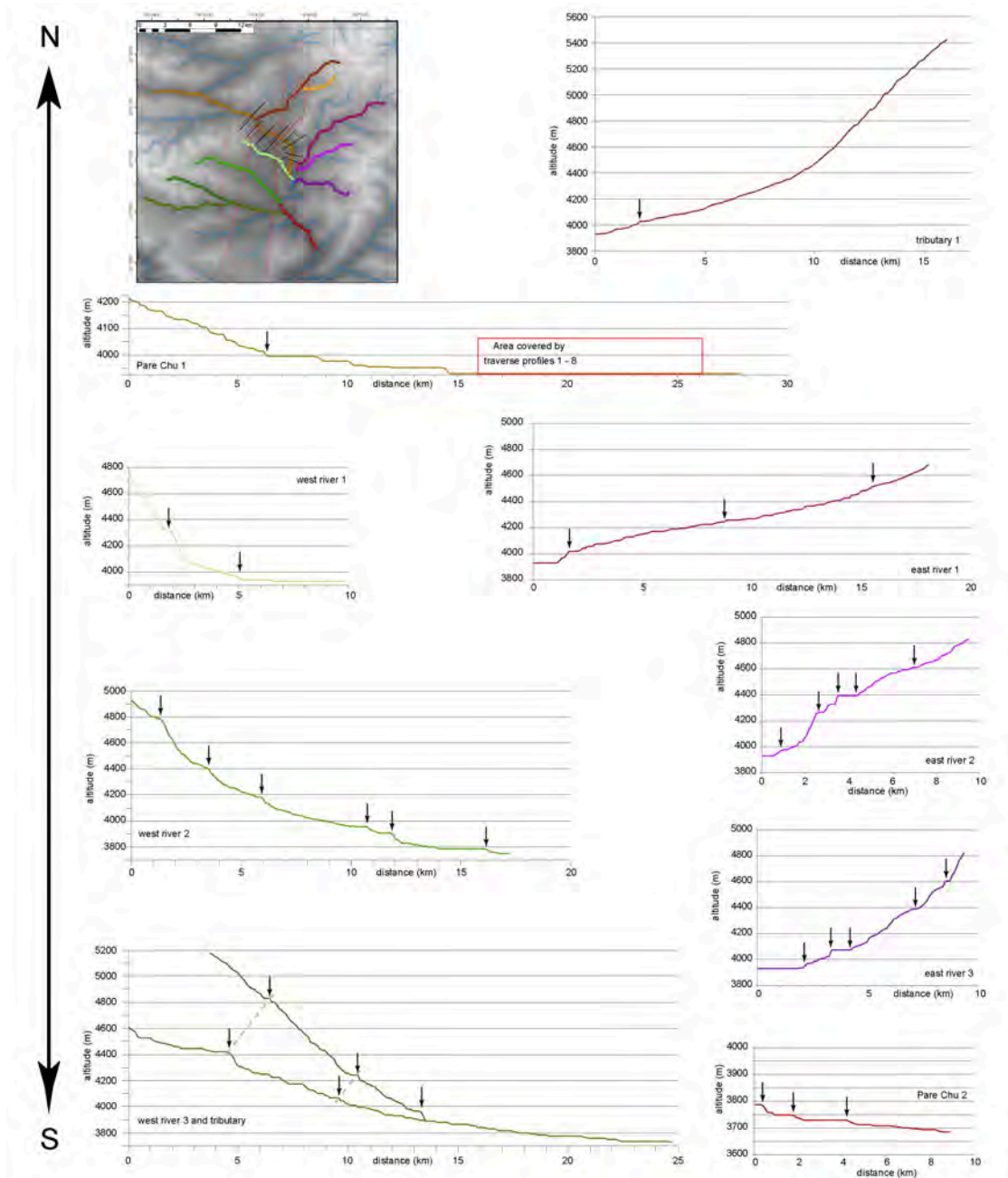


Figure 4.3: Longitudinal profiles of rivers crossing normal faults in the basin NW of the Leo Pargil. Arrangement of the profiles and the color code are in agreement with the stream network shown in the upper left inset and the legend shown in Fig. 4.1A.

only river that drains the northern and central part of the basin, “tributary 1” is considered separately.

The western rivers cross the central part of the basin and have eroded deep valleys into the basin fill. In general, they have concave longitudinal profiles. However, at closer inspection, all of those profiles are disturbed by several knickpoints. But

none of the identified knickpoints are directly related to either the eastern or the western basin-bounding faults. This might indicate that the basin-bounding faults are not active or less active than in the past, at least at the southern edges of the basin. However, knickpoints are found in the three southernmost rivers (west rivers 2, 3, and tributary to west river 3) at similar distances from the western fault. In addition, there are also knickpoints within the basin. All those knickpoints might be interpreted as being related to headward erosion away from the position of the respective faults. If true, the western knickpoint migration would indicate earlier activity along the western basin-bounding fault, and the eastern knickpoints may reflect activity along the eastern fault. The existence of more than one knickpoint either suggests that the rivers may have crossed more than one fault or that the different knickpoints are related to the deformation history of the faults. In the latter scenario, one might infer episodes with higher slip rates that may have been associated with earthquake surface ruptures. Alternatively, the knickpoints could reflect the incision and headward erosion of the river into the former basin and the subsequent lowered local base level.

In contrast, the eastern river profiles 1-3 are characterized by generally more convex longitudinal profiles. The knickpoints at the eastern rivers are much more pronounced compared to the western rivers (see right column in Fig. 4.3). In addition, the three major knickpoints in each of the eastern rivers coincide with the N-S trending lineaments visible in the satellite images (Fig. 4.1A). Taken together, the convex profiles and the pronounced knickpoints at the location of the lineaments suggest that the eastern faults are still active with relative uplift of the eastern blocks and subsidence towards the basin center.

“Tributary 1” is the only river of this data set that crosses the northern part of the central basin. It crosses two lineaments which may be the bounding active normal faults for the northern basin (see Fig. 4.1B). The western lineament seems not be related with a knickpoints, but is causing a southward bend of the course of the river. The eastern lineament crossed by the river is also the same lineament, where Quaternary terraces and alluvial fans are affected by normal faulting (see Fig. 3.3 and section 3.4.1). Here, the river seems to be influenced by faulting as it changes downstream from a steeper gradient sector to a more gentle part.

4.2.3 Transverse river profiles

Within the basin, the resolution of the longitudinal profile of the Pare Chu River (see section 3.4.1 and Fig. 3.2) is not high enough to decipher the course of the river across the basin and shows only a flat part (see box in Fig. 4.3). This might be the result of the existence of a temporary landslide-damed lake in the center of the basin (half-filled in Fig. 4.1B) which was catastrophically emptied in 2005, and resulted in a devastating flood that caused downstream damage and loss of lives in the Spiti and Sutlej river valleys (see appendix C). In order to further address the question as to whether the location of the lake is controlled by faulting, transverse profiles perpendicular to the course of the river were extracted from the SRTM DEM (Fig. 4.4). Profiles 1-4, marked in green, indicate a valley that widens towards the east, and the valley shoulders decrease towards the east. Interestingly, profiles 1 and 2 at the western margin of the basin have almost identical profiles, compared to the very open and wide profile 4 at the eastern margin. Profiles 5-8 showing the valley shape farther east exhibit the same characteristics, but less pronounced, starting from a very steep and narrow valley, with high valley shoulders to a somewhat more open valley.

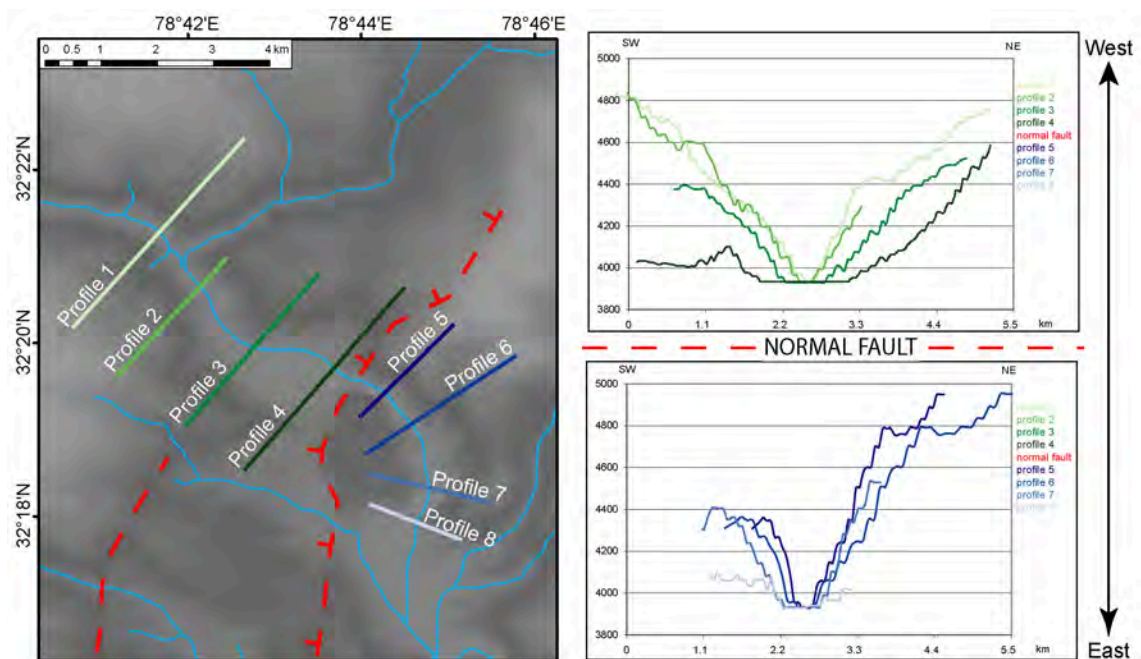


Figure 4.4: Change of valley width of the Pare Chu river crossing normal faults in the basin NW of the Leo Pargil. (A) Location of the transverse profiles across the valley, perpendicular to the river course. (B) Transverse valley profiles showing the change of valley width when crossing the normal faults that bound the intermontane basin. The color of the profiles is identical to the colors of the profiles in (A). For further explanations see text.

Even without further quantitative assessments, the following interpretation might explain the basin geometry. Profiles 1 and 2 are at the western margin of the basin. The river is cut deeply into resistant rock. Profile 3 and 4 are across the western

4.2. DISTURBED RIVER PROFILES

Figure 4.5: Central lake in the basin bounded by normal faults. Note the paleo-strand lines at higher levels than the present-day lake level. In addition, an alluvial fan is marked, which is adjusted to the highest paleo-strand line.



basin-bounding fault, within the basin, and therefore in the subsided hanging-wall block (relative to profiles 1 and 2). As soon as the river crosses the eastern basin-bounding fault, repeated faulting must have resulted in the stepwise uplift of the footwall and caused river incision (profiles 5 -7).

Together with the location of the knickpoints, and the evidence for active normal faulting in the northern and central parts of the basin (section 3.4.1), the transverse profiles indicate that the basin must have been active for a longer time span. Fault activity seems to have decreased or even stopped in the south, where channels have eroded again into the basin. However, in the central and northern parts, normal faulting seems to be still active, and may cause frequent landsliding and damming of the central lake. Furthermore, two well developed paleo-strandlines around this lake at higher elevations than today's lake level suggest a cycle of abandonment and refilling of the lake. In addition, alluvial fans adjusted to base levels higher than the recent one also suggest continuous downcutting. In summary, seismogenic faulting may have ultimately focused on the eastern bounding fault in the north of the basin and on at least three closely spaced, W-dipping normal faults east of the basin.

4.3 Paleoseismological records of active normal faulting

In addition to the tectonic landforms suggesting ongoing extension, soft-sediment deformation within lacustrine sediments is inferred to indicate seismogenically triggered deformation processes associated with nearby faults. Such data helps extend the seismological observation timeline for the faults under consideration. In the following section, I present two examples of paleoseismological records close to active normal faults. The first outcrop shows several layers of possible seismites in lacustrine sediments close to the Kaurik-Chango Normal fault (KCNF), and the second outcrop reveals evidence for large surface displacement preserved within sediments of an ancient lake in the Baspa Valley.

4.3.1 Soft-sediment records along the Kaurik-Chango Normal fault

Evidence for soft-sediment deformation of lacustrine sediments is observed along the lower Spiti River near the western flanks of the Leo Pargil gneiss dome, where lake deposits reach a thickness of up to 100 meters. Several discontinuous lacustrine sedimentary bodies extend along the valley for approximately 8 km and are located between 10 and 100 m above the recent river bed (Fig. 3.10). A road cut exposes one of these lacustrine sedimentary lenses with a total thickness of about 17 m, and provides access and excellent outcrop conditions. The outcrop location is shown in the inset of Fig. 4.6.

The sediments are mainly composed of lacustrine clay with intercalated thin sandy or silt layers of thicknesses between 0.5 and 10 cm. A NNE-SSW striking normal fault (dip direction/dip: 350/85) displaces the southern end of the outcrop by about 0.6 m (panel 3b in Fig. 4.6). While the upper part mainly consists of stable intercalations of sand and clay layers with wave ripples and cross-bedding, the lower part of the outcrop is dominated by intercalations of undisturbed clay/sand intercalation and layers with soft-sediment deformation (Fig. 4.7). The deformation structures include undulated/folded clay layers within sands, pseudo-nodules, fishtail-shaped intrusion, flame structures, and ball-and-pillow structures (see insets in Fig. 4.7). In total, there are 10 layers, where soft-sediment deformation can be observed. In Fig. 4.7, they are marked as E1 to E10 from bottom to top. In general, the deformed layers are between 10 to 20 cm, only layer E7 has a thickness of 75 cm. All layers are bounded by undeformed horizontal layers at their top and bottom layers, even the very thin clay layer between the layers affected by soft-deformations E3 and E4 do not show any macroscopic deformation.

The observed soft-sediment deformation may have been initiated by several different mechanisms, including glacial processes, rockfall and landsliding, instability of the sedimentary column due to overburden, and earthquakes (e.g., Ringrose, 1989). However, glacial processes can be excluded as a cause, because this part of the landscape has not been affected by glaciation. In addition, neither dropstones (as characteristic for glacial processes during lacustrine sedimentation) nor landslide deposits are observed within the outcrop. Finally, ripples and cross-bedding as well

4.3. PALEOSEISMOLOGICAL RECORDS OF ACTIVE NORMAL FAULTING

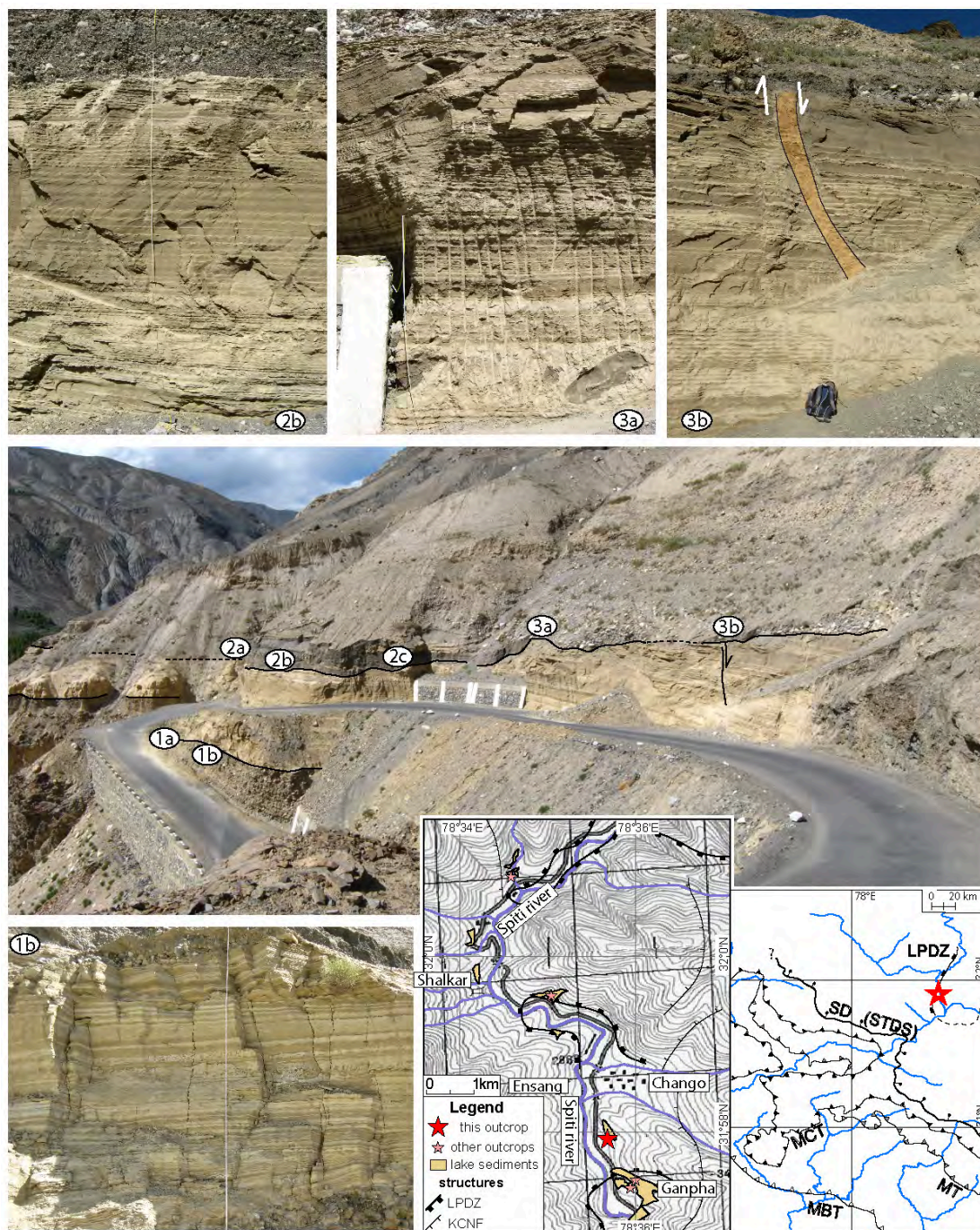


Figure 4.6: Lake sediments along the KCNF showing soft-sediment deformation. The sedimentary body is situated between two layers of coarse-grained fluvial sediments (black lines). Numbers from 1a to 3b show locations of profiles through the sediments described in fig. 4.7. At the right edge of the outcrop, a NNW-SSE striking normal fault displaces the sediments by about 0.6 m (Profile 3b). Outcrop location is marked with a red star in the insets showing the main geological structures of the NW Indian Himalaya (right inset, modified after Thiede et al. (2005) and references therein) and outcrop locations of lake sediments along the Spiti River (left inset, see Fig. 3.10 for details). Abbreviations: KCNF - Kaurik-Chango normal fault, LPDZ - Leo Pargil detachment zone, MBT - Main Boundary thrust, MCT - Main Central thrust, MFT - Main Frontal thrust, MT - Munsiri thrust, SD - Sangla detachment, STDS - Southern Tibetan detachment system.

as the onlap of lacustrine sediments on the underlying well rounded conglomerate clasts indicate a shallow water environment, thus instabilities due to overburden may be excluded as well.

Most of the observed flame structures, undulations and bed-and-pillow structures are similar to sedimentary structures that have been associated with earthquake-induced shaking of water-saturated lacustrine sediments (e.g., Seilacher, 1969; Sims, 1973, 1975; Mayall, 1983; Mohindra and Bagati, 1996). The Kaurik-Chango Normal fault (KCNF) is a seismogenic, steeply W-dipping normal fault crosscutting the Leo Pargil detachment zone at the western flanks of the Leo Pargil gneiss dome (Thiede et al., 2006). This fault zone has been inferred to be the source of the Kinnaur Earthquake (1975, $M_w = 6.8$) and associated aftershocks (Singh et al., 1975). Due to the vicinity of the lacustrine sediments to the KCNF, I hypothesize that the 10 layers of soft-sediment deformation (e.g., layers E1 to E10) observed within the outcrop may indicate separate single paleo-earthquakes triggered by this fault. Event E7 must have been an earthquake of larger magnitude compared to the others, since the affected layers are much thicker. Slip along the fault within the outcrop must have occurred after the abandonment of the lake, since growth strata were not observed and the gravels covering the lake sediments are also displaced. Because the fault strikes almost perpendicular to the local hill slope, gravitational sliding as a cause for faulting can be excluded.

Unfortunately, no datable material could be secured from these deposits. Therefore, only an approximate estimation can be made for the age of these sediments. Since this outcrop is located approximately at a similar height as the lacustrine sedimentary outcrops B and C shown in Fig. 3.9 which have been dated to 21.3 ± 1.1 ka and 29.2 ± 1.6 ka (see Table 3.2), it should be in the same age range. ^{14}C ages from the base of the lowest sediment bodies have a consistent calibrated age of 28.5 ± 0.9 ka BP (Bookhagen et al., 2005a), suggesting that the succession described above should be slightly older. In addition, 90 to 4.6-ka-old, extensive lacustrine sediment outcrops further north at the junction of the Pare Chu and the Spiti rivers also bear similar soft-sediment deformation phenomena (Mohindra and Bagati, 1996; Banerjee et al., 1997), suggesting a regional seismicity-related phenomenon rather than a local feature. These structures have been interpreted as evidence for 8 earthquakes with magnitudes $M > 5$ (Mohindra and Bagati, 1996; Banerjee et al., 1997).

The possible age of the sediments is in a similar age range between 90 ka and 20 ka, but this is only speculation and more rigorous assessment is needed. Additional field work and sampling will eventually provide the missing data for a more profound subsequent treatment of the data.

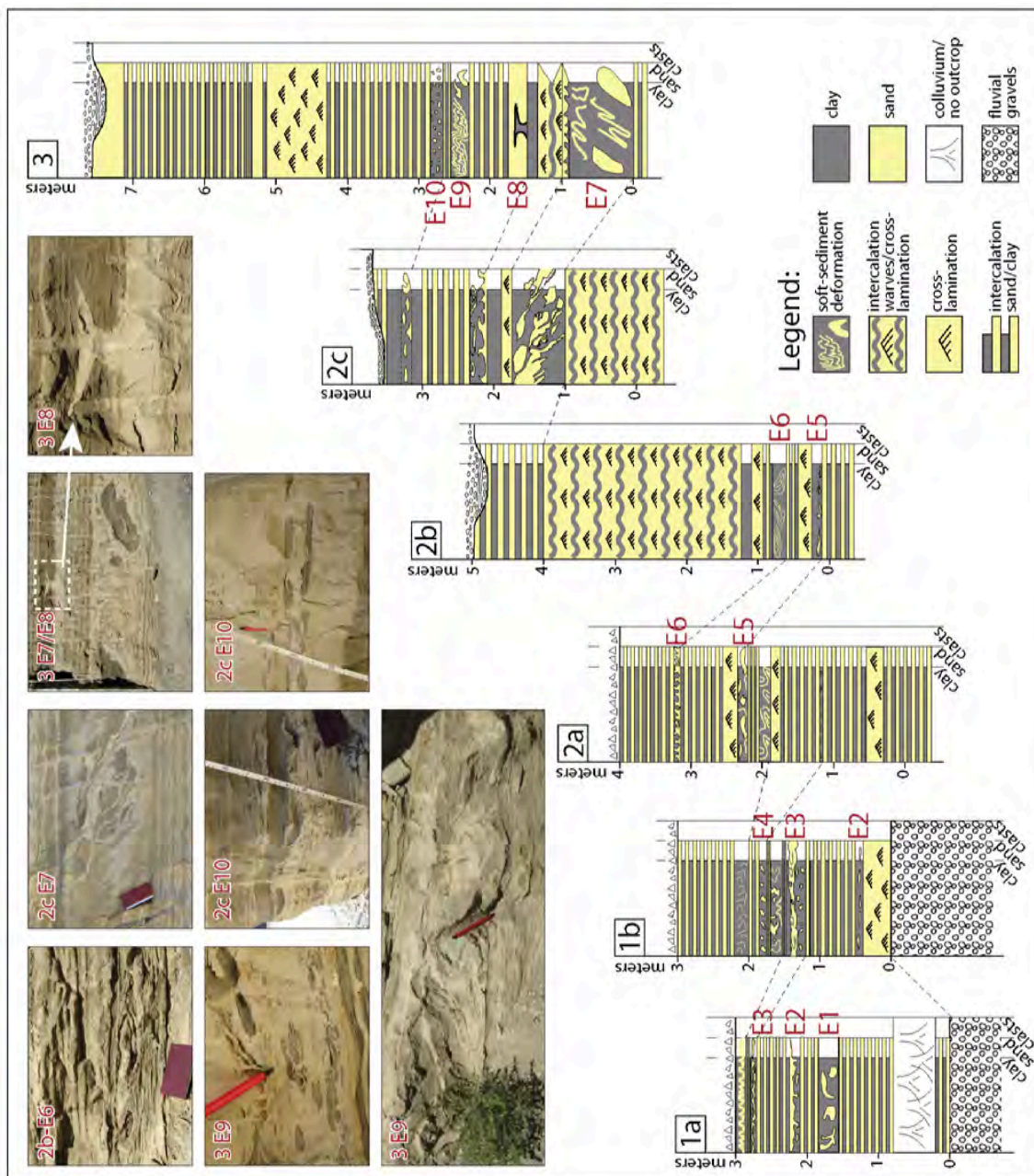


Figure 4.7: Soft-sediment deformation within lake sediments along the KCNF. The total strata of the lake sediments is presented in profiles 1a-3, profile locations are marked in Fig. 4.6. Correlation horizons between profiles are connected by dashed lines. Layers showing soft-sediment deformation events are marked with E1-E10. Inset pictures showing soft-deformation layers are labeled with profile and layer number, respectively.

4.3.2 Evidence for a paleo-earthquake in the Baspa Valley

Close to the village of Sangla in the northern catchment of the Baspa River (inset of Fig. 4.8), evidence for active tectonics was found in a construction pit (fig. 4.8). There, approximately 3 m of laminated lake sediments are exposed. These sediments are part of the vestiges of a landslide-dammed lake that existed between approximately 7.6 ± 0.3 ka BP and 5.2 ± 0.6 ka BP (Bookhagen et al., 2005b). The

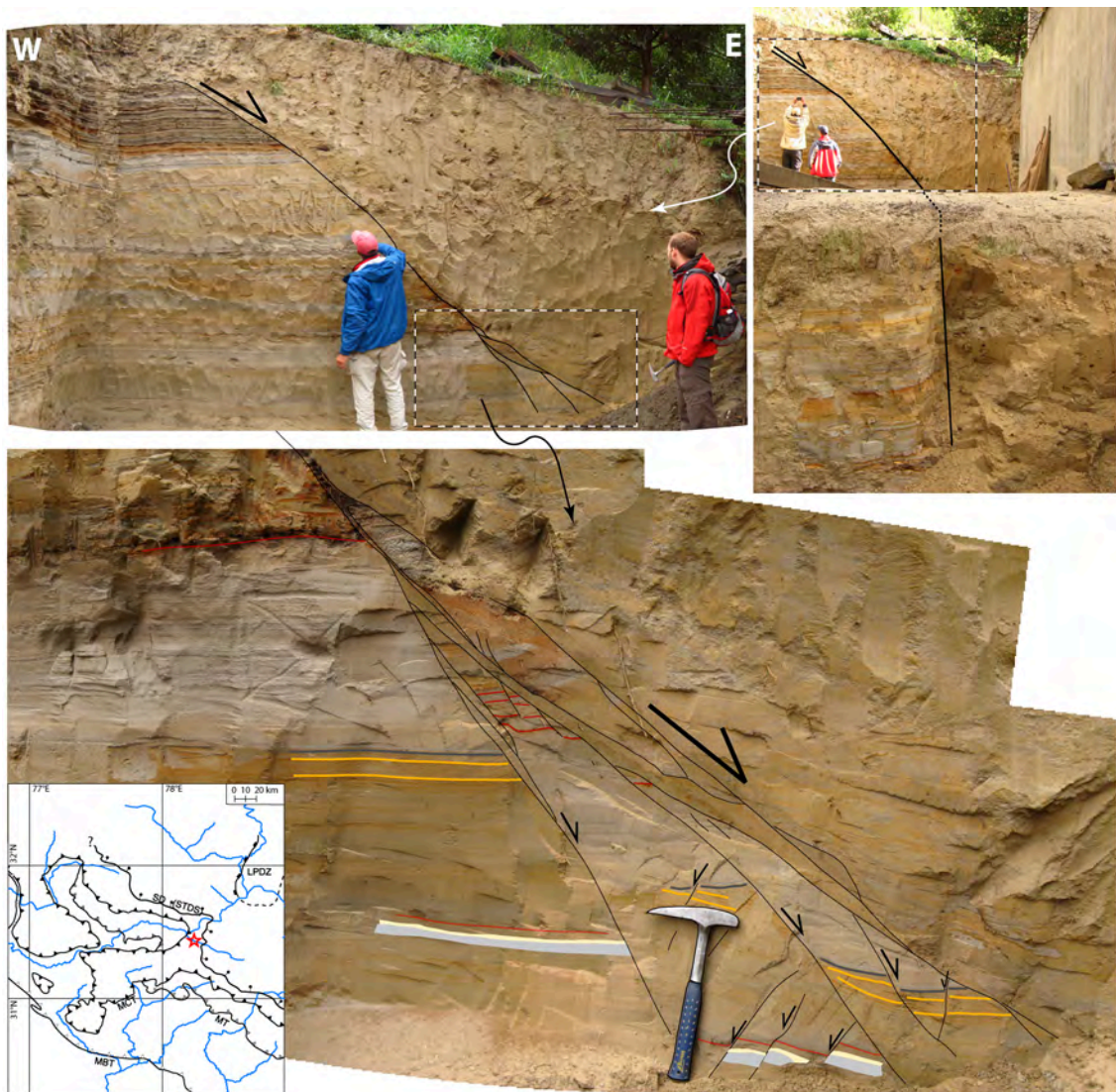


Figure 4.8: Lake deposits cut by a normal fault in a construction pit close to the village of Sangla in the Baspa Valley, view towards N. The laminated lake deposits on the western side of the outcrop are covered by unstratified sand. Within the sand unit, small laminated blocks are observed. In the lowermost part of the outcrop, however, displaced blocks are identified (see marked laminae in the lower inset) indicating normal faulting. Outcrop location is marked with a red star in the inset showing the main geological structures of the NW Indian Himalaya (right inset, modified after Thiede et al. (2005) and references therein).

lacustrine sediments are cut by a N-S striking normal fault, which displaces the lower part of the lake sediments by at least 40 cm along three parallel fault strands. The hanging wall of the fault consists of unstratified, loose sediments. Smaller blocks of cohesive sedimentary sequences with diameters of up to 10 cm are preserved within the hanging wall and suggest that the hanging wall consists of re-deposited foot-wall material. In addition, a small (~ 70 cm) block of reddish sediments covered by coarser grayish sediments is observed on top of the sequence affected by normal faulting. This block is clearly displaced by the main normal fault. A similar sequence of gray and red coarse sand layers are observed at the top of the sequence. If these layers and the block were once connected, the vertical displacement marked by the offset of these layers is approximately 2 m.

Two scenarios to explain these relationships are possible: (a) one earthquake displaced the lower part by approximately 40 cm. Subsequently, the upper part of the hanging wall collapsed, maybe due to erosion or fluvial undercutting. Scenario (b) would necessitate two earthquakes, starting with an earthquake generating the displacement of approximately 40 cm. Subsequently, during a second larger earthquake, the hanging wall was displaced by about 2 m and collapsed. Only small sedimentary blocks directly along the fault plane remained cohesive and were preserved. The very straight and linear contact between hanging and footwall deposits favors the latter version involving two earthquakes. In case of scenario (a) that erosion affects this setting, the contact would be expected to be more undulated.

In macroseismic studies, surface displacement can be used as (sometimes the only available) measurement for the determination of moment magnitude of an earthquake. Based on global observations of instrumentally recorded earthquakes, regressions provide correlations between average (or maximal) surface displacement measured in the field after the earthquake and instrumentally determined moment magnitude, such as the relationships of Wells and Coppersmith (1994). This regression has been established as a standard for magnitude estimates of paleo-earthquakes. Based on the regression for normal faults, the displacement of 40 cm would have been generated by an earthquake with a magnitude between $M_w = 6.5 \pm 0.5$ (average displacement) and $M_w = 6.3 \pm 0.1$ (maximum displacement). For the second earthquake, 2 m of offset would have been generated by an earthquake of $M_w = 7.0 \pm 0.7$ (average displacement) and $M_w = 6.8 \pm 0.1$ (maximum displacement). Interestingly, because both earthquakes occurred clearly after deposition and abandonment of the lake, both events should have happened after 5.2 ± 0.6 ka BP.

4.4 Conclusions

In this chapter I presented additional data for neotectonic E-W extension in the NW Indian Himalaya on different time scales. While my geochronologic results reveal that extension may have been ongoing since 14-16 Ma (chapter 3), the results of this chapter underscore that extensional processes have been sustained and continue until the present day. Longitudinal and transverse profiles of rivers crossing the basin NW of the Leo Pargil document normal faulting along approximately N-S striking faults. Knickpoints along the longitudinal river profiles at the western margin of the basin spatially coincide with mapped fault traces, indicating active faulting. At the eastern margin, however, knickpoints are identified at the same distance upstream of the fault traces, indicating less or no movement along these structures.

In addition, I document soft-sediment deformation in lake sediments close to the KCNF, which are best explained in terms of a succession of 10 paleo-earthquake with inferred magnitudes $M > 5$. Unfortunately, age control for these deposits is not available, but in comparison with other dated sedimentary bodies in close vicinity (Bookhagen et al., 2005*a*, and Table 3.2), the age of the sediments can be estimated to be between 90 ka and 20 ka. Interestingly, evidence for a paleo-earthquake is documented as far south as in the vicinity of the village of Sangla in the Baspa valley, where a N-S striking normal fault displaces lacustrine sediments by 40 cm and 2.0 m, respectively. Those displacements may correspond to earthquakes with magnitudes $M_w = 6.3 - 6.5$ and $M_w = 6.8 - 7.0$, respectively, which must have happened after the deposition of the lake sediments between 7.6 ± 0.3 ka BP and 5.2 ± 0.6 ka BP (Bookhagen et al., 2005*b*).

Finally, covering the last decades, GPS data and instrumental seismicity records also provide evidence for active E-W extension within the NW Indian Himalaya (e.g., Molnar, 1992; Banerjee and Bürgmann, 2002). I therefore provide evidence for active E-W extension on different timescales between at least 14-16 Ma and the present day, and a regional distribution spanning from the Tso Morari to the hangingwall of the STDS.

Chapter 5

General Conclusions

In this study, I have shown that strain patterns in the NW Indian Himalaya derived from a combination of fault-kinematic analysis, satellite imagery, geomorphic river-profile analysis, and neotectonic structures in the NW Indian Himalaya reflect regional deformation pattern very well. Extension processes are ubiquitous and emphasize the importance of active deformation processes in the NW Indian Himalaya and their role in providing a causal mechanism to generate destructive earthquake, mass movements and valley impoundments. In addition, I have documented and compiled the extent of E-W extension within the NW Indian Himalaya on different timescales, spanning millions of years to decades. These extension deformation patterns are recorded in brittle faults, affected sediments and landforms and are compatible with the most recent deformation documented in seismicity and geodetic data. These data sets are evaluated in time and space in comparison with existing models of normal faulting in orogens (see Table 3.3). Therefore, based on this study, I propose that E-W extension in the NW Indian Himalaya is linked to extension observed within the Tibetan Plateau.

I review the most important results by revisiting the research questions outlined in the introduction, which guided me through my study.

1. Is it possible to decipher several extension directions within the Himalaya? If so, which mechanisms govern the spatial and temporal evolution of those extensional directions?

It is possible to document different extension directions through time. In chapter 2, I have presented evidence mainly derived from brittle fault-kinematic analysis for several different deformation styles within the NW Indian Himalaya, among those also three major extension styles.

NE-SW (arc-normal) extension in the upper crust is not focused along the STDS but seems to be more widely distributed. This extension might be related to a ramp-like geometry of the underthrusting zone along the MHT and the southward motion of Himalayan rocks over such a ramp. The existence of a ramp-like structure below the Higher Himalaya has just been recently documented by Ps receiver functions

along a profile across the Garhwal Himalaya (Caldwell et al., 2012, 2013). Earlier documentation of a mid-crustal ramp include balanced cross-sections (e.g., Schelling and Arita, 1991; Seward and Manckelov, 1994), local changes in GPS velocities (Berger et al., 2004), and locally increased seismicity (Pandey et al., 1990).

Structures related to arc-parallel (NW-SE) extension are apparently younger than faults accommodating arc-normal extension. In addition, NW-SE extension is not only limited to large structures such as several dome and graben structures along the High Himalaya, but is rather linked with pervasive brittle, lower-order, closely spaced normal fault systems across the entire orogen. My field observations support the model of Murphy et al. (2009), where southward propagation of the active mountain front and the associated widening of the Himalayan arc are responsible for arc-parallel extension processes.

To sum up, the main driving force for both extensional directions is interpreted to be the southward propagation of the Himalayan thrust front. Due to the arc-shaped geometry of the orogen, a southward propagation of the thrust front implies also an increase in both, the length and the width of the orogen as a whole. This might be accommodated by extension parallel to the arc. As Murphy et al. (2009) have shown, the amount of extension increases towards the Himalayan mountain front, supporting such an interpretation. On the other hand, arc-normal extension, which is not limited to the close vicinity of the SDTS, might be produced by a ramp-like shape of the MHT below the Higher Himalaya. In such a scenario, as the thrust front moves southward, new rocks will be moved over the ramp and therefore produce localized extension at the surface.

The youngest extension phase is E-W oriented. While the differentiation of arc-parallel and arc-normal extension has been documented throughout the Himalaya (Ama Drime Massif, Thakkola Graben, Yadong-Graben ...), the conditions for geometrical differentiation between E-W and arc-parallel extension is only possible where the strike of the orogen is not E-W, i.e. in the NW Himalaya. However, (U-Th)/He zircon and apatite thermochronometric data from the Kung Co rift suggest at least for one of the Southern Tibetan graben systems that there might be two major episodes of extension in that region (Lee et al., 2011). The earlier phase might be related to the geometry of the Himalaya, and the later one related to the extensional processes within the Tibetan Plateau. If true, those studies support my point of view that arc-parallel extension and E-W extension are indeed related to two distinct deformation patterns with very different driving forces, which happen to be parallel in the Central Himalaya.

- 2. What is the nature of N-S striking normal faults in the internal part of the Himalaya? Are these structures**
- (a) related to tensional stresses related to the formation of the arc-shaped geometry of the orogen (McCaffrey and Nabelek, 1998);**
 - (b) explicable by the subduction process of the Indian plate beneath Eurasia (England and Molnar, 1993); or**
 - (c) kinematically linked to the observed E-W extension in the Tibetan Plateau (Chen and Yang, 2004)?**

N-S striking normal faults exist throughout in the study area. They are the youngest structures, superseding all older structures and influencing fluvial network evolution. These structures even displace late Pleistocene sediments, demonstrating ongoing E-W extension since at least 16 Ma. New U-Th-Pb geochronology data of the Leo Pargil gneiss dome suggest an even earlier onset of E-W extension possibly active at around 23 Ma (Langille et al., 2012). CHECK! They speak of orogen-parallel extension.

Most models for extension processes in the Himalaya are mainly based on observations from the central Himalaya. I present new data that provides additional information on the spatial characteristics of E-W extension in the NW Indian Himalaya and its relationship with other extensional styles. I analyzed this data in light of existing models and their implications for the NW Himalaya (see summary in Table 3.3).

Based on this evaluation, several suggested driving mechanisms for E-W extension can be excluded. For example, local doming of the Leo Pargil gneiss dome as the sole driving cannot explain the regional distribution and orientation of normal faults outside of the area affected by doming. Kinematic linkage of N-S striking faults with the Karakorum fault is also excluded based on the fact that these young faults do not correspond to the local stress field around the KF, as it would be expected in the case of kinematic linkage. Any linkage of E-W extension in the study area with the arc-shaped geometry is also unlikely (see above). I therefore conclude that the E-W extension observed within the Tibetan Plateau and the NW Indian Himalaya are of the same origin.

3. Does the Karakorum Fault form a strain boundary decoupling deformation in the Western Himalaya from the Tibetan Plateau or is this strike-slip fault system too small to separate deformation into two independent compartments?

The degree of activity of the Karakorum Fault plays a crucial role in the hypothesis for the transfer of extension from the Tibetan Plateau towards the NW Indian Himalaya. The ongoing controversy concerning the displacement rate of the Karakorum Fault (e.g., Lacassin et al., 2004; Chevalier et al., 2005; Searle and Phillips, 2007) underscores the problem of unambiguously defining the role of the Karakorum Fault in the recent deformation history of the Himalaya-Tibet region. If the Karakorum Fault is indeed a first-order structure that decouples the stress regimes of the Tibetan Plateau and the Himalaya, the level of seismic activity should be much higher than observed at present. For example, globally recorded seismicity in this area shows that only a few earthquakes have occurred along this fault in the last 30 years (NEIC Catalog, 2009). In addition, neither kinematic linkage between recent normal faults in the Western Himalaya with the KF nor rotation of the strike of faults towards the KF into a direction parallel to the KF can be observed (Epard and Steck, 2008). In addition, Robinson et al. (2012) document that the northern KF has most likely not moved during the last 200 ka, perhaps not even for the last 3 Ma. From these observations, I infer that the Karakorum Fault may be only of secondary importance and that it might not be able to fully accommodate the bulk of E-W extension occurring in the Tibetan Plateau. In such a scenario, part of this strain must be transferred southwestward of the Karakorum Fault into the NW Himalaya. I therefore suggest that the transition of extensional tectonics from the Tibetan Plateau across the Karakorum Fault into the NW Himalaya may be related to a crust coupled to eastward-flowing mantle and continuous deformation, which is not restricted to single larger structures.

Bibliography

- Aalto, R., Dunne, T. and Guyot, J.-L. (2006), 'Geomorphic controls on Andean denudation rates', *The Journal of Geology* **114**, 85–99.
- Ali, J. and Aitchison, J. (2005), 'Greater India', *Earth Science Reviews* **72**, 169–188.
- Allmendinger, R., Isacks, B., Jordan, T. and Kay, S. (1997), 'The Evolution of the Altiplano-Puna Plateau of the Central Andes', *Annual Review of Earth Sciences* **25**, 139–174.
- Anderson, T. (1998), 'Extensional tectonics in the Caledonides of Southern Norway, an overview', *Tectonophysics* **285**, 333–351.
- Aoya, M., Wallis, S., Terada, K., Lee, J., Kawakami, T., Wang, Y. and Heizler, M. (2005), 'North-South extension in the Tibetan crust triggered by granite emplacement', *Geology* **33**(11), 853–856.
- Arita, K. (1983), 'Origin of the inverted metamorphism of the Lower Himalayas, Central Nepal', *Tectonophysics* **95**, 43–60.
- Armijo, R., Tapponnier, P., Mercier, J. and Han, T. (1986), 'Quaternary extension in Southern Tibet: Field observations and tectonic implications', *Journal of Geophysical Research* **94**, 2787–2838.
- Avé Lallement, H. and Guth, L. (1990), 'Role of extensional tectonics in exhumation of eclogites and blueschists in an oblique subduction setting: Northeastern Venezuela', *Geology* **18**(10), 950–953.
- Banerjee, D., Singhvi, A., Bagati, T. and Mohindra, R. (1997), 'Luminescence chronology of seismites at Sumdo (Spiti valley) near Kaurik-Chango Fault, Northwestern Himalaya', *Current Science* **73**(3), 276–281.
- Banerjee, P. and Bürgmann, R. (2002), 'Convergence across the Northwest Himalaya from GPS Measurements', *Geophysical Research Letters* **29**(13).
- Bateman, M. and Catt, J. (1996), 'An absolute chronology for the raised beach deposits at Sewerby, E. Yorkshire, UK', *Journal of Quaternary Science* **11**, 389–395.
- Beaumont, C., Jamieson, R., Nguyen, M. and Lee, B. (2001), 'Himalayan tectonics explained by extrusion of a low-viscosity crustal channel coupled to focused surface denudation', *Nature* **414**, 738–742.
- Beaumont, C., Nguyen, M., Jamieson, R. and Ellis, S. (2004), Crustal flow modes in large hot orogens, in D. Law, M. Searle and L. Godin, eds, 'Channel Flow, Ductile Extrusion and Exhumation of lower-mid crust in Continental Collision Zones', Vol. 268, Geological Society of London Special Publications.
- Bendick, R. and Bilham, R. (2001), 'How perfect is the Himalayan Arc?', *Geology* **29**(9), 791–794.

BIBLIOGRAPHY

- Berger, A., Jouanne, F., Hassani, R. and Mugnier, J. L. (2004), 'Modelling the spatial distribution of present-day deformation in Nepal: how cylindrical is the Main Himalayan Thrust in Nepal?', *Geophysical Journal International* **156**(1), 94–114.
- Bhargava, O., Ameta, S., Gaur, R., Kumar, S., Agrawal, A., Jalote, P. and Sadhu, M. (1978), 'The Kinnaur (H.P., India) Earthquake of 19 January, 1975: summary of geoseismological observations', *Bulletin of the Indian Geological Association* **11**(1), 39–53.
- Bilham, R. (2004), 'Earthquakes in India and the Himalaya: tectonics, geodesy and history', *Annals of Geophysics* **47**(2), 839–858.
- Bilham, R., Gaur, V. and Molnar, P. (2001), 'Himalayan Seismic Hazard', *Science* **293**, 1442–1444.
- Bird, P. (1991), 'Lateral extrusion of lower crust from under high topography, in the isostatic limit', *Journal of Geophysical Research* **96**, 10275–10286.
- Blisniuk, P., Hacker, B., Glodny, J., Ratschbacher, L., Bi, S., Wu, Z., McWilliams, M. and Calvert, A. (2001), 'Extension in Central Tibet since at least 13.5 Myr', *Nature* **412**, 628–632.
- Blisniuk, P. and Sharp, W. (2003), 'Rates of late Quaternary Normal Faulting in Central Tibet from U-series dating of Pedogenic Carbonate in Displaced Fluvial Gravel Deposits', *Earth and Planetary Science Letters* **215**, 169–186.
- Bookhagen, B., Thiede, R. and Strecker, M. (2005a), 'Abnormal Monsoon Years and their control on erosion and sediment flux in the high, arid Northwest Himalaya', *Earth and Planetary Science Letters* **231**, 131–146.
- Bookhagen, B., Thiede, R. and Strecker, M. (2005b), 'Late Quaternary intensified monsoon phases control landscape evolution in the Northwest Himalaya', *Geology* **33**(2), 149–152.
- Bott, M. (1959), 'The mechanics of oblique slip faulting', *Geological Magazine* **96**, 109–117.
- Brookfield, M. (1993), 'The Himalayan passive margin from Precambrian to Cretaceous', *Sedimentary Geology* **84**, 1–35.
- Buck, W. R. and Sokoutis, D. (1994), 'Analog Model of Gravitational Collapse and Surface Extension During Continental Convergence', *Nature* **369**(6483), 737–740.
- Bull, W. (1977), 'The alluvial-fan environment', *Progress in Physical Geography* **1**(2), 222–270.
- Burbank, D., Beck, R. and Mulder, T. (1996), The Himalayan foreland basin, in A. Yin and T. Harrison, eds, 'The Tectonics of Asia', Cambridge University Press, New York, pp. 149–188.
- Burchfiel, B. C., Chen, Z., Hodges, K., Liu, Y., Royden, L. H., Deng, C. and Xu, J. (1992), *The South Tibetan Detachment System, Himalayan Orogen: Extension contemporaneous with and parallel to Shortening in a Collisional Mountain Belt*, Vol. 269, Geological Society of America Special Paper.
- Burchfiel, B. C., Chen, Z., Royden, L. H., Liu, Y. and Deng, C. (1991), 'Extensional development of Gabo Valley, Southern Tibet', *Tectonophysics* **194**, 187–193.
- Burchfiel, B. and Royden, L. (1985), 'North-South extension within the convergent Himalayan Region', *Geology* **13**, 678–682.
- Burg, J., Brunel, M., Gapais, D., Chen, G. and Liu, G. (1984), 'Deformation of Leucogranites of the Crystalline Main Central Sheet in Southern Tibet (China)', *Bulletin of the Seismological Society of America* **6**(5), 535–542.

BIBLIOGRAPHY

- Burg, J., Célérier, B., Chaudhry, N., Ghazanfar, M., Gnehm, F. and Schnellmann, M. (2005), 'Fault analysis and paleostress evolution in large strain regions: Methodological and geological discussion of the southeastern Himalayan fold-and-thrust belt in Pakistan', *Journal of Asian Earth Sciences* **24**, 445–467.
- Burg, J. and Chen, G. (1984), 'Tectonics and structural zonation of southern Tibet, China', *Nature* **311**, 219–223.
- Burtman, V. and Molnar, P. (1993), 'Geological and geophysical evidence for deep subduction of continental crust beneath the Pamir', *Special Paper of the Geological Society of America* **281**, 76.
- Caby, R., Pêcher, A. and Le Fort, P. (1983), 'Le grande chevauchement central himalayen: Nouvelles données sur le métamorphisme inverse à la base de la Dalle du Tibet', *Revue de Géographie Physique et Géologie Dynamique* **24**, 89–100.
- Caldwell, W., Klemperer, S., Lawrence, J., Rai, S. and Ashish, A. (2012), Geometry of the Main Himalayan Thrust and location of the locking line in the Garhwal Himalaya from receiver function CCP stacking, in 'AGU Fall Meeting', Vol. T23A-2633, American Geophysical Union.
- Caldwell, W., Klemperer, S., Lawrence, J., Rai, S. and Ashish, A. (2013), 'Localized flexure of the Indian plate and crustal-scale ramp beneath the High Himalaya of Garhwal, India', *Earth and Planetary Science Letters* . under review.
- Chemenda, A., Burg, J.-P. and Mattauer, M. (2000), 'Evolutionary model of the Himalaya-Tibet system: geopoem based on new modelling, geological and geophysical data', *Earth and Planetary Science Letters* **174**, 397–409.
- Chemenda, A., Mattauer, M., Malavieille, J. and Bokun, A. (1995), 'A mechanism for syn-collisional rock exhumation and associated normal faulting: results from physical modelling', *Earth and Planetary Science Letters* **132**, 225–232.
- Chen, W. and Yang, Z. (2004), 'Earthquakes beneath the Himalayas and Tibet: Evidence for strong lithospheric mantle', *Science* **304**, 1949–1952.
- Chevalier, M.-L., Fyerson, F., Tapponnier, P., Finkel, R., van der Word, J. and Qing, L. (2005), 'Slip-rate measurements on the Karakorum fault imply secular variations in fault motion', *Science* **307**, 411–414.
- Copley, A., Avouac, J.-P. and Royer, J.-Y. (2010), 'India-Asia collision and the Cenozoic slowdown of the Indian plate: Implications for the forces driving plate motions', *Journal of Geophysical Research* **115**(B03410).
- Cottle, J., Jessup, M., Newell, D., Horstwood, M., Noble, S., Parrish, R., Waters, D. and Searle, M. (2009), 'Geochronology of granulitized eclogite from the Ama Drime Massif: Implications for the tectonic evolution of the South Tibetan Himalaya', *Tectonics* **28**, doi: 10.1029/2008TC002256.
- Dahlen, F. (1984), 'Noncohesive Critical Coulomb Wedges: An Exact Solution', *Journal of Geophysical Research* **89**(B12), 10125–10134.
- Dalmayrac, B. and Molnar, P. (1981), 'Parallel Thrust and Normal Faulting in Peru and Constraints on the State of Stress', *Earth and Planetary Science Letters* **55**, 473–481.
- DeCelles, P., Gehrels, G., Quade, J., LaReau, B. and Spurlin, M. (2000), 'Tectonic implications of U-PL zircon ages of the Himalayan orogenic belt in Nepal', *Science* **288**, 497–499.
- DeCelles, P., Gehrels, G., Quade, J., Ojha, T., Kapp, P. and Upreti, B. (1998), 'Neogene foreland basin deposits, erosional unroofing, and the kinematic history of the Himalayan fold-thrust belt, western Nepal', *Geological Society of America Bulletin* **110**, 2–21.

BIBLIOGRAPHY

- Dèzes, P., Vannay, J.-C., Steck, A., Bussy, F. and Cosca, M. (1999), 'Synorogenic extension: Quantitative constraints on the age and displacement of the Zaskar shear zone (northwest Himalaya)', *Geological Society of America Bulletin* **111**(3), 364–374.
- DiPietro, J. A. and Pogue, K. R. (2004), 'Tectonostratigraphic subdivisions of the Himalaya: A view from the west', *Tectonics* **23**, 10.1029/2003TC001554.
- Draganits, E., Braddy, S. and Briggs, D. (2001), 'A Gondwana Coastal Arthropod Ichnofauna from the Muth Formation (Lower Devonian, Northern India): paleoenvironment and tracemaker behavior', *Palaios* **16**(2), 126–147.
- Duvall, A., Kirby, E. and Burbank, D. (2004), 'Tectonic and lithologic control on bedrock channel profiles and processes in coastal California', *Journal of Geophysical Research* **109**(F03002).
- Edwards, M. and Harrison, T. (1997), 'When did the roof collapse? Late Miocene north-south extension in the High Himalaya revealed by Th-Pb monazite dating of the Khula Kangri granite', *Geology* **25**, 543–546.
- England, P. (1982), Some numerical investigations of large-scale continental deformation, in K. Hs'ü, ed., 'Mountain building processes', Academic Press, London, pp. 129–139.
- England, P. and Houseman, G. (1989), 'Extension during Continental Convergence, with Application to the Tibetan Plateau', *Journal of Geophysical Research* **94**, 17561–17579.
- England, P. and Molnar, P. (1993), Cause and Effect among Thrust and Normal Faulting, Anatectic Melting and Exhumation in the Himalaya, in P. Treloar and M. Searle, eds, 'Himalayan Tectonics', Vol. 74, Geological Society of London Special Publications, pp. 401–411.
- Epard, J.-L. and Steck, A. (2008), 'Structural development of the Tso Moriri ultra-high pressure nappe of the Ladakh Himalaya', *Tectonophysics* **451**(1-4), 242–264.
- Fleitout, L. and Froidevaux, C. (1982), 'Tectonics and topography for a lithosphere containing density heterogeneities', *Tectonics* **1**, 21–56.
- Flint, J. (1974), 'Stream gradient as a function of order, magnitude, and discharge', *Water Resources Research* **10**, 969–973.
- Frank, W., Grasemann, B., Guntli, P. and Miller, C. (1995), 'Geological map of the Kishwar-Chamba-Kulu region (NW Himalayas India)', *Jahrbuch der Geologischen Bundesanstalt* **138**, 299–308.
- Froidevaux, C. and Isacks, B. (1984), 'The Mechanical State of the Lithosphere in the Altiplano-Puna Segment of the Andes', *Earth and Planetary Science Letters* **71**(2), 305–314.
- Fuchs, G. and Linner, M. (1996), 'On the Geology of the Suture Zone and Tso Moriri Dome in Eastern Ladakh (Himalaya)', *Jahrbuch der Geologischen Bundesanstalt, Vienna/A* **139**, 191–207.
- Gaetani, M., Casnedi, R., Fois, E., Garzanti, E., Jadoul, F., Nicora, A. and Tintori, A. (1986), 'Stratigraphy of the Tethys Himalaya in Zaskar, Ladakh, Initial report', *Rivista Italiana di Paleontologie e Stratigraphia* **91**, 443–478.
- Gansser, A. (1964), *Geology of the Himalayas*, London, Wiley Interscience.
- Garzzone, C., Dettman, D., Quade, J., DeCelles, P. and Butler, R. (2000), 'High times on the Tibetan Plateau: Paleoelevation of the Thakkhola graben, Nepal', *Geology* **28**, 339–342.

BIBLIOGRAPHY

- Garzione, C. N., DeCelles, P. G., Hodkinson, D., Ojha, R. and Upreti, B. (2003), 'E-W Extension and Miocene Environmental Change in the Southern Tibetan Plateau: Thakkhola graben, Central Nepal', *Geological Society of America Bulletin* **115**(1), 3–20.
- Grasemann, B. and Vannay, J. (1999), 'Flow controlled inverted metamorphism in shear zones', *Journal of Structural Geology* **21**, 450–743.
- Grujic, D., Casey, M., Davidson, C., Hollister, L. S., Kündig, R., Pavlis, T. and Schmid, S. (1996), 'Ductile Extrusion of the Higher Himalayan Crystalline in Bhutan: Evidence from Quartz Microfabrics', *Tectonophysics* **260**, 21–43.
- Guillot, S., de Sigoyer, J., Lardeaux, J. M. and Mascle, G. (1997), 'Eclogitic Metasediments from the Tso Morari area (Ladakh, Himalaya): Evidence for Continental Subduction during India-Asia convergence', *Contributions to Mineralogy and Petrology* **128**, 197–212.
- Guo, L., Zhang, J. and Zhang, B. (2008), 'Structures, kinematics, thermochronology and tectonic evolution of the Ramba gneiss dome in the northern Himalaya', *Progress in Natural Science* **18**, 851–860.
- Hack, J. (1957), 'Studies of longitudinal stream profiles in Virginia and Maryland', *U.S. Geological Survey Professional Paper* **294-B**, 45–97.
- Harkins, N., Kirby, E., Heimsath, A., Robinson, R. and Reiser, U. (2007), 'Transient fluvial incision in the headwaters of the Yellow River, northeastern Tibet, China', *Journal of Geophysical Research* **F03S04**.
- Hayden, H. (1904), 'The geology of Spiti with parts of Bushahr and Rupshu', *Memoir Geological Survey India* **6**, 1–121.
- Heim, A. and Gansser, A. (1939), 'Central Himalaya', *Geological Observations of Swiss* pp. 1–246.
- Hintersberger, E., Thiede, R., Strecker, M. and Hacker, B. (2010), 'East-west extension in the NW Indian Himalaya', *Geological Society of America Bulletin* **122**(9–10), 1499–1515.
- Hodges, K., Bowring, S., Davidek, K., Hawkins, D. and Krol, M. (1998), 'Evidence for rapid displacement on Himalayan normal faults and the importance of tectonic denudation in the evolution of mountain ranges', *Geology* **26**, 483–486.
- Hogdes, K., Parrish, R. R. and Searle, M. P. (1996), 'Tectonic Evolution of the Central Annapurna Range, Nepalese Himalayas', *Tectonics* **15**, 1264–1291.
- Hogdes, K. V. (2000), 'Tectonics of the Himalaya and Southern Tibet', *Geological Society of America Bulletin* **112**(3), 324–350.
- Hogdes, K. V., Hurtado, J. M. and Whipple, K. X. (2001), 'Southward Extrusion of Tibetan Crust and its Effect on Himalayan Tectonics', *Tectonics* **20**(6), 799–809.
- Hurtado, J. M., Hodges, K. V. and Whipple, K. X. (2001), 'Neotectonics of the Thakkhola Graben and Implications for Recent Activity on the South Tibetan Fault System in the central Nepal Himalaya', *Geological Society of America Bulletin* **113**(2), 222–240.
- Jain, A., Kumar, D., Singh, S., Kumar, A. and Lal, N. (2000), 'Timing, Quantification and Tectonic Modelling of Pliocene-Quaternary Movements in the NW Himalaya: Evidence from Fission Track Dating', *Earth and Planetary Science Letters* **179**(3/4), 437–451.
- Janda, C., Hager, C., Grasemann, B., Draganits, E., Vannay, J.-C., Bookhagen, B. and Thiede, R. (2002), 'The Karcham Normal Fault: Implications for an active extruding wedge, Sutlej Valley, NW Himalaya', *Journal of Asian Earth Sciences* **20**, 19–20.

BIBLIOGRAPHY

- Jessup, M., Newell, D., Cottle, J., Berger, A. and Spotila, J. (2008), 'Orogen-parallel extension and exhumation enhanced by denudation in the trans-Himalayan Arun River gorge, Ama Drime Massif, Tibet-Nepal', *Geology* **36**(7), 587–590.
- Kapp, P. and Guynn, J. (2004), 'Indian Punch Rifts Tibet', *Geology* **32**(11), 993–996.
- Kapp, P. and Yin, A. (2001), 'Unbending of the lithosphere as a mechanism for active rifting in Tibet: Insight from elastic modelling, AGU Fall Meeting.
- Kayal, J., Kamble, V. and Rastogi, B. (1992), 'Aftershock sequence of Uttarkashi earthquake of October 20, 1991', *Geological Survey of India Special Publications* **30**, 203–217.
- Khattari, K., Rai, K., Jain, A., Sinval, H., Gaur, V. and Mithal, R. (1978), 'The Kinnaur earthquake, Himachal Pradesh, India, of 19 January, 1975', *Tectonophysics* **49**(1-2), 1–21.
- Kim, Y.-S., Peacock, D. and Sanderson, D. (2004), 'Fault damage zones:', *Journal of Structural Geology* **26**, 503–517.
- Kirby, E. and Whipple, K. (2001), 'Quantifying differential rock-uplift rates via stream profile analysis', *Geology* **29**(5), 415–418.
- Kirby, E., Whipple, K., Tang, W. and Chen, Z. (2003), 'Distribution of active rock uplift along the eastern margin of the Tibetan Plateau: Inferences from bedrock channel longitudinal profiles', *Journal of Geophysical Research* **108**(2217).
- Klootwijk, C., Conaghan, P. and Powell, C. (1985), 'The Himalayan arc: large-scale continental subduction, oroclinal bending, and back-arc spreading', *Earth and Planetary Science Letters* **75**, 316–319.
- Klootwijk, C., Gee, J., Peirce, J., Smith, G. and McFadden, P. (1992), 'An early India-Asia contact: Paleomagnetic constraints from the Ninetyeast Ridge, ODP Leg 121', *Geology* **20**, 395–398.
- Kumar, A., Lal, N., Jain, A. and Sorkhabi, R. (1995), 'Late Cenozoic-Quaternary thermo-tectonic history of Higher Himalayan Crystalline (HC) in Kishtwar-Padar-Zaskar region, NW Himalayan: evidence from fission ages', *Journal of Geological Society of India* **45**, 375–391.
- Kumar, S., Wesnousky, S., Rockwell, T., Briggs, R., Thakur, V. and Jayangondaperumal, R. (2006), 'Paleoseismic evidence of great surface rupture earthquakes along the Indian Himalaya', *Journal of Geophysical Research* **111**(B03304), 10.1029/2004JB003309.
- Kwatra, S., Singh, S., Singh, V., Sharma, R., Rai, B. and Kishor, N. (1999), 'Geochemical and geochronological characteristics of the Early Paleozoic granitoids from Sutlej-Baspa Valleys, Himachal Himalayas', in A. Jain and R. Manickavasagam, eds, 'Geodynamics of the NW Himalaya', Vol. 6, Gondwana Research Group Memoirs, pp. 145–158.
- Lacassin, R., Valli, F., Arnaud, N., Leloup, P., Paquette, J., Haibing, L., Tapponnier, P., Chevalier, M.-L., Guillot, S., Maheo, G. and Zhiqin, X. (2004), 'Large-scale geometry, offset and kinematic evolution of the Karakorum fault, Tibet', *Earth and Planetary Science Letters* **219**, 255–269.
- Lal, N., Mehta, Y., Kumar, D., Kumar, A. and Jain, A. (1999), 'Cooling and exhumation history of the Mandi granite and adjoining units, Himachal Pradesh, and estimation of closure temperature from external surface of zircon', in A. Jain and R. Manickavasagam, eds, 'Geodynamic of the NW Himalaya', Vol. 6, Gondwana Research Group Memoirs, pp. 485–509.
- Langille, J., Jessup, M., Cottle, J., Lederer, G. and Ahmad, T. (2012), 'Timing of metamorphism, melting and exhumation of the Leo Pargil dome, northwest India', *Journal of metamorphic geology* **30**(8), 769–791.

BIBLIOGRAPHY

- Lavé, J. and Avouac, J. (2001), 'Fluvial incision and tectonic uplift across the Himalayas of central Nepal', *Journal of Geophysical Research* **106**(B11), 26561–26591.
- Le Fort, M., Freytet, P. and Colchen, M. (1982), 'Structural and Sedimentological Evolution of the Thakkhola-Mustang Graben (Nepal Himalayas)', *Zeitschrift für Geomorphologie* **42**, 75–98.
- Le Fort, P. (1975), 'Himalaya: the collided range. Present knowledge of the continental arc', *American Journal of Science* **275A**, 1–44.
- Le Pichon, X., Fournier, M. and Jolivet, L. (1992), 'Kinematics, topography, shortening, and extrusion in the India-Eurasia collision', *Tectonics* **11**, 1085–1098.
- Lee, J., Hager, C., Wallis, S., Stoeckli, D., Whitehouse, M., Aoya, M. and Wang, Y. (2011), 'Middle to late Miocene extremely rapid exhumation and thermal reequilibration in the Kung Co rift, southern Tibet', *Tectonics* **30**.
- Leloup, P., Mahéo, G., Arnaud, N., Kali, E., Boutonnet, E., Liu, D., Liu, X. and Li, H. (2010), 'The South Tibet detachment shear zone in the Dinggye area: time constraints on extrusion models of the Himalayas', *Earth and Planetary Science Letters* **292**, 1–16.
- Liebke, U., Appel, E., Ding, L., Neumann, U., Antolin, B. and Xu, Q. (2010), 'Position of the Lhasa terrane prior to India-Asia collision derived from palaeomagnetic inclinations of 53 Ma old dykes of the Linzhou Basin: constraints on the age of collision and post-collisional shortening within the Tibetan Plateau', *Geophysical Journal International* **182**(3), 1199–1215.
- Liu, M., Yang, Y., Stein, S. and Klosko, E. (2002), Crustal Shortening and Extension in the Andes from a Viscoelastic Model, in S. Stein and J. Freymueller, eds, 'Plate Boundary Zones', Vol. 30 of *Geodynamic Series*, AGU, Washington, D.C. 15 pages.
- Malik, J., Sahoo, A., Shah, A., Shinde, D., Juyal, N. and Singhvi, A. (2010), 'Paleoseismic evidence from trench investigation along Hajipur fault, Himalayan Frontal Thrust, NW Himalaya: Implications of the faulting pattern on landscape evolution and seismic hazard', *Journal of Structural Geology* **32**, 350–361.
- Mayall, M. (1983), 'An earthquake origin for synsedimentary deformation in a late Triassic (Rhaetian) lagoonal sequence, southwest Britain', *Geological Magazine* **120**, 613–622.
- McCaffrey, R. (1996), 'Estimates of Modern Arc-parallel Strain Rates in Fore-arcs', *Geology* **24**(1), 27–30.
- McCaffrey, R. and Nabelek, J. (1998), 'Role of Oblique Convergence in the Active Deformation of the Himalayas and Southern Tibet Plateau', *Geology* **26**, 691–694.
- McNulty, B. (1995), 'Pseudotachylyte generated in the semi-brittle and brittle regimes, Bench Canyon shear zone, central Sierra Nevada', *Journal of Structural Geology* **17**, 1507–1521.
- Meigs, A., Burbank, D. and Beck, R. (1995), 'Middle – late Miocene (> 10 Ma) Initiation of the Main Boundary Thrust in the Western Himalaya', *Geology* **23**, 423–426.
- Metcalfe, M. (1993), Pressure, temperature and time constraints on metamorphism across the Main Central Thrust zone and high Himalayan slab in the Garhwal Himalaya, in P. Treloar and M. Searle, eds, 'Himalayan Tectonics', Vol. 74, Geological Society of London Special Publication, pp. 485–509.
- Michard, A., Chopin, C. and Henry, C. (1993), 'Compression versus Extension in the Exhumation of the Dora-Maira coesite-bearing unit, Western Alps, Italy', *Tectonophysics* **221**, 173–193.

BIBLIOGRAPHY

- Middlemiss, C. (1910), 'The Kangra earthquake of 4th April, 1905', *Geological Survey of India Memoir* **38**, 1–409.
- Miller, C., Klötzli, U., Frank, W., Thöni, M. and Grasemann, B. (2000), 'Proterozoic crustal evolution in the NW Himalaya (India) as recorded by circa 1.80 Ga mafic and 1.84 Ga granitic magmatism', *Precambrian Research* **103**, 191–206.
- Mohindra, R. and Bagati, T. (1996), 'Seismically Induced Soft-sediment Deformation Structures (Seismites) around Sumdo in the lower Spiti Valley (Tethys Himalaya)', *Sedimentary Geology* **101**, 69–83.
- Molnar, P. (1984), 'Structure and Tectonics of the Himalaya: Constraints and Implications of Geophysical Data', *Annual Review of Earth and Planetary Sciences* **12**, 489–518.
- Molnar, P. (1992), 'A Review of Seismicity, Recent Faulting and Active Deformation of the Tibetan Plateau', *Journal of Himalayan Geology* **31**(1), 43–78.
- Molnar, P. and Chen, W.-P. (1983), 'Focal Depths and Fault Plane Solutions of Earthquakes under the Tibetan plateau', *Journal of Geophysical Research* **88**, 1180–1196.
- Molnar, P. and Lyon-Caen, H. (1988), Some simple physical aspects of the support, structure, and evolution of mountain belts, *in* S. Clark, B. Burchfiel and J. Suppe, eds, 'Processes in continental lithospheric deformation', Vol. 218, Geological Society of America Special Paper, pp. 179–207.
- Molnar, P. and Lyon-Caen, H. (1989), 'Fault Plane Solutions of Earthquakes and Active Tectonics of the Tibetan Plateau and its Margins', *Geophysical Journal International* **99**, 123–153.
- Molnar, P. and Tapponnier, P. (1975), 'Cenozoic tectonics of Asia: Effects of a continental collision', *Science* **189**, 419–426.
- Molnar, P. and Tapponnier, P. (1977), 'The collision between India and Eurasia', *Scientific American* **236**(4), 30–42.
- Molnar, P. and Tapponnier, P. (1978), 'Active tectonics of Tibet', *Journal of Geophysical Research B: Solid Earth* **83**, 5361–5375.
- Montero Lopez, M., Hongn, F., Strecker, M., Marrett, R., Seggiaro, R. and Sudo, M. (2010), 'Late Miocene-early Pliocene onset of N-S extension along the southern margin of the Central Andean Puna Plateau: Evidence from magmatic geochronological and structural observations', *Tectonophysics* **494**, 48–63.
- Murphy, M. and Burgess, W. (2006), 'Geometry, kinematics, and landscape characteristics of an active transtension zone, Karakorum fault system, Southwest Tibet', *Journal of Structural Geology* **28**, 268–283.
- Murphy, M. and Copeland, P. (2005), 'Transtensional deformation in the central Himalaya and its role in accommodating growth of the Himalayan orogen', *Tectonics* **24**, 10.1029/2004TC001659.
- Murphy, M., Saylor, J. and Ding, L. (2009), 'Late Miocene topographic inversion in southwest Tibet based on integrated paleoelevation reconstructions and structural history', *Earth and Planetary Science Letters* **282**, 1–9.
- Murphy, M., Yin, A., Kapp, P., Harrison, T. M., Lin, D. and Jinghui, G. (2000), 'Southward Propagation of the Karakoram Fault System, Southwest Tibet: Timing and Magnitude of Slip', *Geology* **28**(5), 451–454.

BIBLIOGRAPHY

- Murphy, M., Yin, A., Kapp, P., Harrison, T. M., Manning, C., Ryerson, F., Ding, L. and Guo, J. (2002), 'Structural Evolution of the Gurla Mandhata Detachment System, Southwest Tibet: Implications for the Eastward Extent of the Karakoram Fault System', *Geological Society of America Bulletin* **114**(4), 428–447.
- Murray, A. and Wintle, A. (2000), 'Luminescence dating of quartz using an improved single-aliquot regenerative-dose protocol', *Radiation Measurements* **32**, 57–73.
- Najman, Y., Garzanti, E., Pringle, M., Bickle, M., Stix, J. and Khan, I. (2003), 'Early-middle Miocene paleodrainage and tectonics in the Pakistan Himalaya', *Geological Society of America Bulletin* **115**, 1265–1277.
- Nelson, K. D., Zhao, W., Brown, L. D., Kuo, J., Che, J., Liu, X., Klemperer, S., Makovsky, Y., Meissner, R., Mechie, J., Kind, R., Wenzel, F., Ni, J., Nabelek, J., Chen, L., Tan, H., Wei, W., Jones, A., Booker, J., Unsworth, M., Kidd, W., Hauck, M., Alsdorf, D., Ross, A. and Cogan, M., Wu, C., Sandvol, E. and Edwards, M. (1996), 'Partially Molten Middle Crust Beneath Southern Tibet: Synthesis of Project INDEPTH Results', *Science* **274**(5293), 1684–1688.
- Neumayer, J., Wiesmayr, G., Janda, C., Grasemann, B. and Draganits, E. (2004), 'Eohimalayan fold and thrust belt in the NW-Himalaya (Lingti-Pin Valleys): Shortening and depth to detachment calculation', *Austrian Journal of Earth Sciences* **95/96**, 28–36.
- Ni, J. and Barazangi, M. (1984), 'Seismotectonics of the Himalaya Collision Zone: Geometry of the Underthrusting Indian Plate Beneath the Himalaya', *Journal of Geophysical Research* **89**(B2), 1147–1163.
- Ortner, H., Reiter, F. and Acs, P. (2002), 'Easy handling of tectonic data: the programs TectonicVB for Mac and TectonicsFP for Windows', *Computers & Geosciences* **28**, 1193–1200.
- Pandey, M., Tandukar, R., Avouac, J., Vergne, J. and Héritier, T. (1990), 'Seismotectonics of the Nepal Himalaya from a local seismic network', *Journal of Asian Earth Sciences* **17**, 703–712.
- Parrish, R. and Hodges, V. (1996), 'Isotopic constraints on the age and provenance of the Lesser and Greater Himalayan sequences, Nepalese Himalaya', *Geological Society of America Bulletin* **108**(7), 904–911.
- Patriat, P. and Achache, J. (1984), 'India-Eurasia collision chronology has implications for crustal shortening and driving mechanism of plates', *Nature* **311**, 615–621.
- Pêcher, A. (1989), 'The metamorphism in the central Himalaya', *Journal of Metamorphic Geology* **7**, 31–41.
- Pêcher, A. (1991), 'The contact between the Higher Himalaya crystallines and the Tibetan sedimentary series: miocene large scale dextral shearing', *Tectonics* **10**, 587–598.
- Pêcher, A. and Scaillet, B. (1989), 'La structure du Haut-Himalaya au Garhwal (Indes)', *Eclogae Geologicae Helvetiae* **82**, 655–668.
- Pêcher, A., Seeber, L., Guillot, S., Jouanne, F., Kausar, A., Latif, M., Majid, A., Mahéo, G., Mugnier, J., Rolland, Y., van der Beek, P. and Van Melle, J. (2008), 'Stress field evolution in the northwest Himalayan syntaxis, northern Pakistan', *Tectonics* **27**.
- Peltzer, G. and Tapponnier, P. (1988), 'Formation and Evolution of Strike-slip Faults, Rifts and Basins during the India-Asia Collision: An Experimental Approach', *Journal of Geophysical Research* **93**, 15095–15117.

BIBLIOGRAPHY

- Phillips, R., Parrish, R. and Searle, M. (2004), 'Age constraints on ductile deformation and long-term slip rates along the Karakorum fault zone, Ladakh', *Earth and Planetary Science Letters* **226**, 305–319.
- Rastogi, B. (2000), 'Chamoli earthquake of magnitude 6.6 on 29 March 1999', *Geological Society of India* **55**, 505–515.
- Ratschbacher, L., Frisch, W., Liu, G. H. and Chen, C. S. (1994), 'Distributed Deformation in Southern and Western Tibet during and after the India-Asia Collision', *Journal of Geophysical Research (Solid Earth)* **99**(B10), 19917–19945.
- Rey, P., Vanderhaeghe, O. and Teyssier, C. (2001), 'Gravitational Collaps of the Continental Crust: Definition, Regimes and Modes', *Tectonophysics* **342**, 435–449.
- Ringrose, P. (1989), 'Paleoseismic (?) liquifaction event in late Quaternary lake sediment at Glen Roy, Scotland', *Terra Nova* **1**, 57–62.
- Robinson, A., Yin, A., Manning, C., Harrison, T., Zhang, S. and Wang, X. (2007), 'Cenozoic evolution of the eastern Pamir: Implications for strain-accommodation mechanisms at the western end of the Himalayan-Tibetan orogen', *Geological Society of America Bulletin* **119**(7-8), 882–896.
- Rosenberg, C., Brun, J.-P. and Gapais, D. (2004), 'Indentation Model of the Eastern Alps and the Origin of the Tauern Window', *Geology* **32**, 997–1000.
- Rowley, D. (1996), 'Age of collision between India and Asia: a review of the stratigraphic data', *Earth Planetary Science Letters* **145**, 1–13.
- Royden, L. and Burchfiel, B. C. (1987), Thin-skinned N-S extension within the convergent Himalayan Region: Gravitational collapse of a Miocene topographic front, in 'Continental Extensional Tectonics', Blackwell Scientific Publications, pp. 611–619.
- Royden, L., Burchfiel, B., King, R., Wang, E., Chen, Z., Shen, F. and Liu, Y. (1997), 'Surface deformation and lower crustal flow in eastern Tibet', *Science* **96**, 788–790.
- Saylor, J. and Quade, J., Dettman, D., DeCelles, P., Kapp, P. and Ding, L. (2009), 'The late Miocene through Present paleoelevation history of southwestern Tibet', *American Journal of Science* **309**, 1–42.
- Schärer, U., Xu, R. and Allègre (1986), 'U-(Th)-Pb systematics and ages of Himalayan leucogranites, south Tibet', *Earth and Planetary Science Letters* **77**, 35–48.
- Schelling, D. (1992), 'The tectonostratigraphy and structure of the eastern Nepal Himalaya', *Tectonics* **11**, 925–943.
- Schelling, D. and Arita, K. (1991), 'Thrust tectonics, crustal shortening and the structure of the far-eastern Nepal Himalayas', *Tectonics* **10**, 851–862.
- Schulmann, K., Kroner, A., Hegner, E., Wendt, I., Konopasek, J., Lexa, O. and Stipska, P. (2005), 'Chronological constraints on the pre-orogenic history, burial and exhumation of deep-seated rocks along the eastern margin of the Variscan Orogen, Bohemian Massif, Czech Republic', *Journal of Geophysical Research* **305**(5), 407–448.
- Searle, M. (1996), 'Geological evidence against large-scale pre-Holocene offsets along the Karakorum Fault: Implications for the limited extrusion of the Tibetan Plateau', *Tectonics* **15**, 171–186.

- Searle, M., Parrish, R., Hodges, K., Hurford, A., Ayres, M. and M.J. W. (1997), 'Origin of the inverted metamorphism of the Lower Himalayas, Central Nepal', *Journal of Geology* **105**, 295–317.
- Searle, M. and Phillips, R. (2007), 'Relationships between right-lateral shear along the Karakoram fault and metamorphism, magmatism, exhumation and uplift: Evidence from the K2-Gasherbrum-Pangong Ranges, north Pakistan and Ladakh', *Journal of the Geological Society of London* **164**, 439–450.
- Searle, M., Simpson, R., Law, R., Parrish, R. and Waters, D. (2003), 'The structural geometry, metamorphic and magmatic evolution of the Everest massif, High Himalaya of Nepal-South Tibet', *Journal of the Geological Society* **160**, 345–366.
- Searle, M., Weinberg, R. and Dunlap, W. (1998), Transpressional tectonics along the Karakoram fault zone, northern Ladakh: Constraints on Tibetan extrusion, in R. Holdsworth, R. Strachan and J. Dewey, eds, 'Continental Transpressional and Transtensional Tectonics', Vol. 135, Geological Society of London Special Publication, pp. 307–326.
- Seeber, L. and Arbuster, J. (1981), Great detachment earthquakes along the Himalayan arc and the long term forecasts, in E. Simpson and P. Richards, eds, 'Earthquake Prediction: An International Review', Vol. 4 of *Maurice Ewing Series*, American Geophysical Union, pp. 259–277.
- Seeber, L. and Arbuster, J. (1984), 'Some elements of continental subduction along the Himalayan front', *Tectonophysics* **105**, 263–278.
- Seilacher, A. (1969), 'Fault-grade beds interpreted as seismites', *Sedimentology* **13**, 155–159.
- Silverstone, J. (2005), 'Are the Alps Collapsing?', *Annual Review of Earth Sciences* **33**, 2.1–2.20.
- Seward, D. and Manckelw, N. (1994), 'Neogene Kinematics of the Central and Western Alps: Evidence from Fission-track dating', *Geology* **22**(9), 803–806.
- Sims, J. (1973), 'Earthquake Induced Structures in Sediments of Van Norman Lake, San Fernando, California', *Science* **182**, 161–163.
- Sims, J. (1975), 'Determining Earthquake Recurrence Intervals from Deformational Structures in young Lacustrine Sediments', *Tectonophysics* **29**, 141–152.
- Singh, S., Sinha, P., Jain, A., Singh, V. and Srivastava, L. (1975), 'Preliminary Report on the January 19, 1975 Kinnaur Earthquake in Himachal Pradesh', *Earthquake Engineering Studies* **75**, 1–32.
- Sklar, L. and Dietrich, W. (2008), 'Implications of the saltation-abrasion bedrock incision model for steady-state river longitudinal profile relief and concavity', *Earth Surface Processes and Landforms* **33**, 1129–1151.
- Sorkhabi, R., Stump, E., Foland, K. and Jain, A. (1996), 'Fission-track and $^{40}\text{Ar}/^{39}\text{Ar}$ evidence for episodic denudation of the Gangotri granites in the Garhwal Higher Himalaya, India', *Tectonophysics* **260**, 187–199.
- Spang, J. (1972), 'Numerical method for dynamic analysis of calcite twin lamellae', *Geological Society of America Bulletin* **83**, 467–472.
- Sperner, B. (1996), 'Computer programs for the kinematic analysis of brittle deformation structures and the Tertiary tectonic evolution of the Western Carpathians Slovakia', *Tübinger Geowissenschaftliche Arbeiten A* **27**, 120.

BIBLIOGRAPHY

- Srivastava, P. and Mitra, G. (1994), 'Thrust geometries and deep structure of the outer and Lesser Himalaya, Jumoan and Garhwal (India): implications for evolution of the Himalayan fold and thrust belt', *Tectonics* **13**, 89–109.
- Stampfli, G. and Borel, G. (2002), 'A plate tectonic model for the Paleozoic and Mesozoic constrained by dynamic plate boundaries and restored synthetic oceanic isochrons', *Earth and Planetary Science Letters* **196**, 17–33.
- Steck, A., Spring, L., Vannay, J.-C., Masson, H., Bucher, H., Stutz, E., Marchant, R. and Tiede, J.-C. (1993), The tectonic evolution of the Northwestern Himalaya in eastern Ladakh and Lahul, India, in P. Treloar and M. Searle, eds, 'Himalayan Tectonics', Vol. 74, Geological Society of London Special Publication, pp. 265–276.
- Strecker, M., Alonso, R., Hilley, G., Sobel, E. and Trauth, M. (2007), 'Tectonics and climate of the southern central Andes', *Annual Reviews in Earth and Planetary Sciences* . in revision.
- Sue, C., Delacou, B., Champagnac, J.-D., Allanic, C. and Burkhard, M. (2007), 'Aseismic deformation in the Alps: GPS vs. seismic strain quantification', *Terra Nova* **19**, 182–188.
- Tapponnier, P. and Molnar, P. (1976), 'Slip-Line Field-Theory and Large-Scale Continental Tectonics', *Nature* **264**(5584), 319–324.
- Tapponnier, P., Peltzer, G., Ledain, A., Armijo, R. and Cobbold, P. (1982), 'Propagating Extrusion Tectonics in Asia - New Insights from Simple Experiments with Plasticine', *Geology* **10**(12), 611–616.
- Taylor, M., Yin, A., Ryerson, F., Kapp, P. and Ding, L. (2003), 'Conjugate strike-slip faulting along the Bangong-Nujiang suture zone accommodates coeval east-west extension and north-south shortening in the interior of the Tibetan Plateau', *Tectonics* **22**, doi: 10.1029/2002TC001361.
- Thakur, V. (1998), 'Structure of the Chamba nappe and position of the Main Central Thrust in Kashmir Himalaya', *Journal of Asian Earth Sciences* **2/3**, 269–282.
- Thiede, R., Arrowsmith, J., Bookhagen, B., McWilliams, M., Sobel, E. and Strecker, M. (2005), 'From tectonically to erosionally controlled development of the Himalayan Orogen', *Geology* **33**(8), 689–692.
- Thiede, R., Arrowsmith, J., Bookhagen, B., McWilliams, M., Sobel, E. and Strecker, M. (2006), 'Dome formation and extension in the Tethyan Himalaya, Leo Pargil, northwest India', *Geological Society of America Bulletin* **118**, 635–650.
- Thiede, R., Bookhagen, B., Arrowsmith, J., Sobel, E. and Strecker, M. (2004), 'Climatic Control on Rapid Exhumation along the Southern Himalayan Front', *Earth and Planetary Science Letters* **222**, 791–806.
- Tucker, G. (2004), 'Drainage basin sensitivity to tectonic and climatic forcing: Implications of a stochastic model for the role of entrainment and erosion thresholds', *Earth Surface Processes and Landforms* **29**, 185–205.
- Turner, F. (1953), 'Nature and dynamic interpretation of deformation lamellae in calcite of three marbles', *American Journal of Science* **251**, 276–298.
- Valdiya, K. (1980), *Geology of the Kumaon Lesser Himalaya*, Wadia Institute of Himalaya, Dehra Dun, India. 291 p.
- Vannay, J.-C. and Grasemann, B. (1998), 'Inverted Metamorphism in the High Himalaya of Himachal Pradesh (NW India): Phase Equilibria versus Thermobarometry', *Schweizerische Mineralogische und Petrographische Mitteilungen* **78**, 107–132.

BIBLIOGRAPHY

- Vannay, J.-C. and Grasemann, B. (2001), 'Himalayan inverted metamorphism and syn-convergence extension as a consequence of a general shear extrusion', *Geological Magazine* **138**(3), 253–276.
- Vannay, J.-C., Grasemann, B., Rahn, M., Frank, W., Carter, A., Baudraz, V. and Cosca, M. (2004), 'Miocene to Holocene Exhumation of Metamorphic Crustal Wedges in the NW Himalaya: Evidence for Tectonic Extrusion coupled to Fluvial Erosion', *Tectonics* **TC1014**, 10.1029/2002TC001429.
- Wang, Q., P.-Z., Z., Freymueller, J., Bilham, R., Larson, K., Lai, X., You, X., Niu, Z., Wu, J., Li, Y., Liu, J., Yang, Z. and Chen, Q. (2001), 'Presentday crustal deformation in China constrained by Global Positioning System (GPS) measurements', *Science* **294**, 574–577.
- Webb, A., Yin, A., Harrison, T., Célérier, J. and Burgess, W. (2007), 'The leading edge of the Greater Himalayan Crystalline complex revealed in the NW Indian Himalaya: Implications for the evolution of the Himalayan orogen', *Geology* **35**(10), 955–958.
- Wells, D. and Coppersmith, K. (1994), 'New empirical relationships among magnitude, rupture length, rupture width, rupture area, and surface displacement', *Bulletin of the Seismological Society of America* **84**, 974–1002.
- Wesnousky, S., Kumar, S., Mohindra, R. and Thakur, V. (1999), 'Uplift and Convergence along the Himalayan Frontal Thrust of India', *Tectonics* **18**(6), 967–976.
- Wheeler, J. and Butler, R. (1993), 'Evidence for Extension in the Western Alpine Orogen: the Contact between the Oceanic Piemonte and overlying Continental Sesia Units', *Earth and Planetary Science Letters* **117**, 457–474.
- Whipple, K. and Tucker, G. (1999), 'Dynamics of the stream-power river incision model: Implications for height limits of mountain ranges, landscape response timescales, and research needs', *Journal of Geophysical Research* **104**(B8), 17661–17674.
- Wiesmayr, G. and Grasemann, B. (2002), 'Eohimalayan Fold and Thrust Belt: Implications for the Geodynamic Evolution of the NW-Himalaya (India)', *Tectonics* **21**(6).
- Wobus, C., Whipple, K., Kirby, E., Snyder, N., Johnson, J., Spyropoulou, K., Crosby, B. and Sheehan, D. (2006), 'Tectonics from topography: Procedures, promise, and pitfalls', *Geological Society of America Special Paper* **398**, 55–74.
- Wu, C., Nelson, K., Wortman, G., Samson, S., Yue, Y., Li, J., Kidd, W. and Edwards, M. (1998), 'Yadong Cross Structure and South Tibetan Detachment in the East Central Himalaya (8990E)', *Tectonics* **17**, 28–45.
- Yeats, R. and Lillie, S. (1991), 'Contemporary tectonics of the Himalayan front fault system: folds, blind thrusts and 1905 Kangra earthquake', *Journal of Structural Geology* **13**, 215–225.
- Yin, A. (1989), 'Origin of regional, rooted low-angle normal faults: a mechanical model and its tectonic implications', *Tectonics* **8**(3), 469–482.
- Yin, A. (2000), 'Mode of Cenozoic east-west extension in Tibet suggests a common origin of rifts in Asia during Indo-Asian collision', *Journal of Geophysical Research* **105**(3), 21,745–21,759.
- Yin, A. (2006), 'Cenozoic tectonic evolution of the Himalayan orogen as constrained by along-strike variation of structural geometry, exhumation history, and foreland sedimentation', *Earth-Science Reviews* **76**(1-2), 1–131.
- Yin, A. and Harrison, T. (2000), 'Geological Evolution of the Himalayan-Tibetan Orogen', *Annual Reviews of Earth and Planetary Sciences* **28**, 211–280.

BIBLIOGRAPHY

- Yin, A., Kapp, P., Murphy, M., Manning, C., Harrison, T., Grove, M., Lin, D., Xi-Guang, D. and Cun-Ming, W. (1999), 'Significant late Neogene East-West Extension in Northern Tibet', *Geology* **27**(9), 787–790.
- Zeilinger, G., Burg, J., Chaudhry, N., Dawood, H. and Hussain, S. (2000), 'Fault systems and paleo-stress tensors in the Indus Suture Zone (NW Pakistan)', *Journal of Asian Earth Sciences* **18**(5), 547–559.
- Zhang, P., Shen, Z., Wang, M., Gan, W., Bürgmann, R., Molnar, P., Wang, Q., Niu, Z., Sun, J., Wu, J., Hanrong, S. and Xinzhao, Y. (2004), 'Continuous Deformation of the Tibetan Plateau from Global Positioning System data', *Geology* **32**(9), 809–812.
- Zhu, B., Kidd, W., Rowley, D., Currie, B. and Shafique, N. (2005), 'Age of initiation of the India-Asia collision in the East-Central Himalaya', *The Journal of Geology* **113**, 265–285.
- Zubovich, A., Wang, X., Scherba, Y., Schelochkov, G., Reilinger, R., Reigber, C., Mosienko, O., Molnar, P., Michajljow, W., Makarov, V., Li, J., Kuzikov, S., Herring, T., Hamburger, M., Hager, B., Dang, Y., Bragin, Y. and Beisenbaev, R. (2010), 'GPS velocity field for the Tien Shan and surrounding regions', *Tectonics* **29**(TC6014).

Appendix A

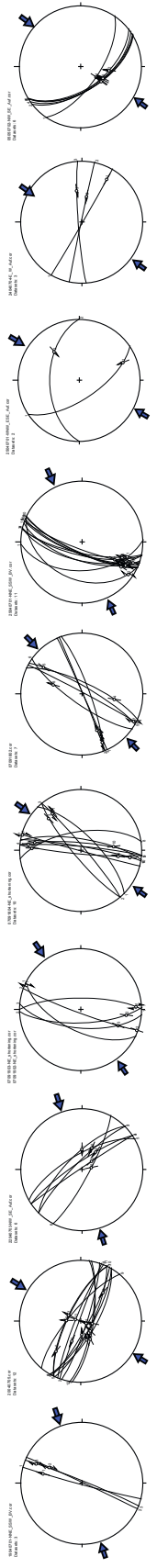
Overview of paleostrain data

A.1 Examples of kinematic field information derived from brittle faults as base for paleo-strain calculations

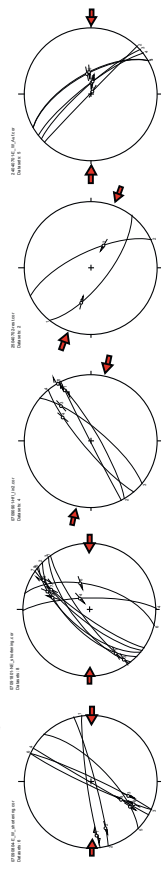
Exemplary stereo plots for the kinematic information derived from brittle faults are shown in the following Fig. A.1. Those data are the base for paleo-strain calculations as described in section 2.3 and shown in Figs. 2.2-2.8. Data shown in one stereo plot represent congenetic faults and associated lineations for one single outcrop, projected in a lower hemisphere Schmidt stereogram. Arrows indicate horizontal projection of either the shortening (pointing towards the center of the stereo plot) or extensional direction (pointing away from the center of the stereo plot) that result from paleo-strain calculations using the numeric dynamic analysis (NDA Spang, 1972; Sperner, 1996) and carried out with the program TectonicsFP (Ortner et al., 2002). Lineations are marked in the same way as mentioned in Fig. 2.1.

EXAMPLES OF BRITTLE-FAULT KINEMATIC INFORMATION AS BASE FOR THE PALEOSTRAIN CALCULATIONS (sorted after deformation phases)

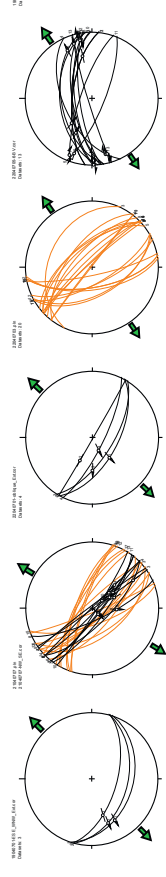
NE-SW shortening (D1)



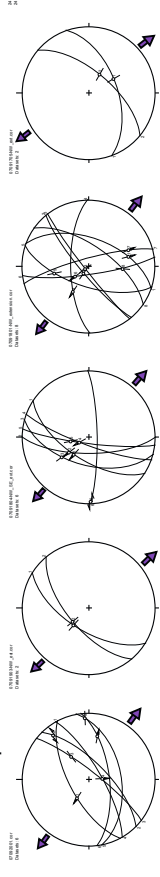
E-W shortening (D2)



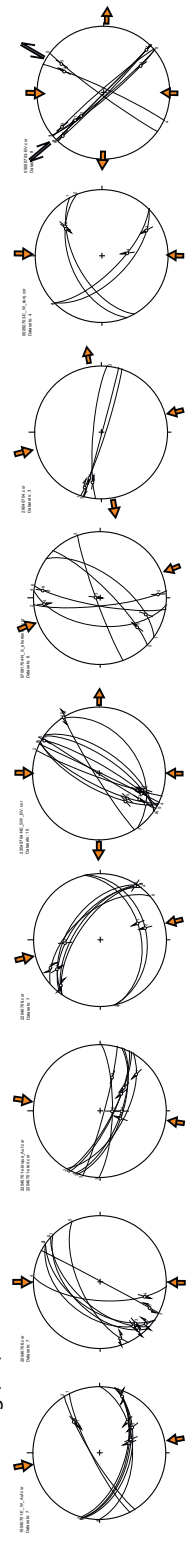
NE-SW (arc-perpendicular) Extension (D3)



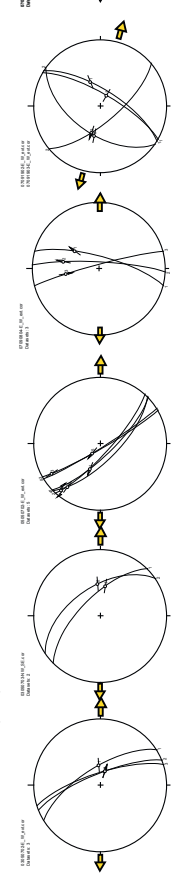
NW-SE (arc-parallel) Extension (D4)



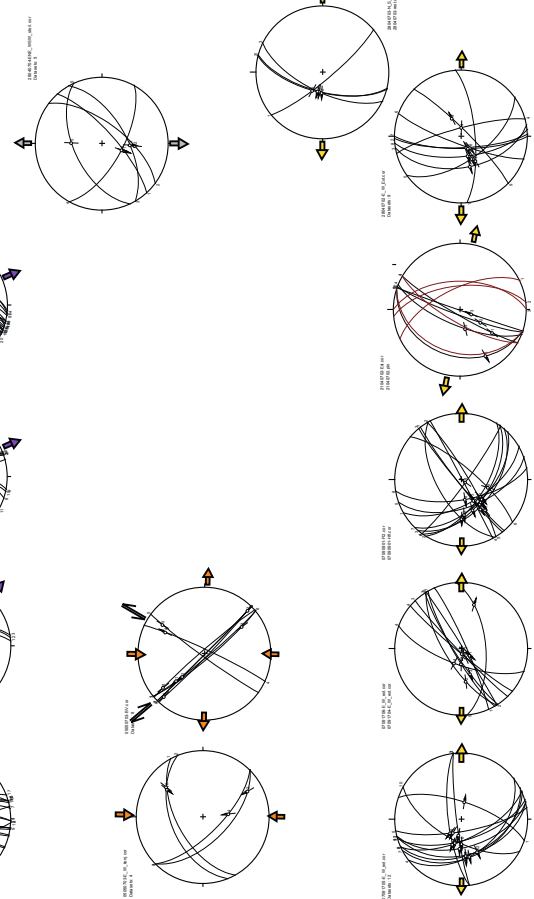
N-S shortening (D5)



E-W Extension (D6)



N-S Extension (D7)



lineations in the stereo plots

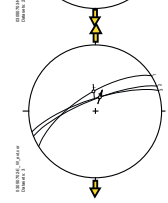
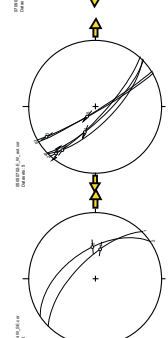
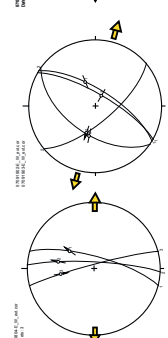
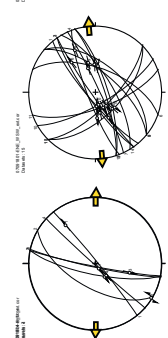
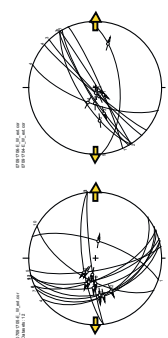
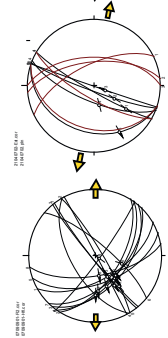
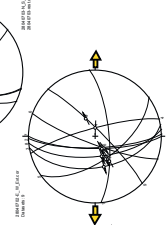
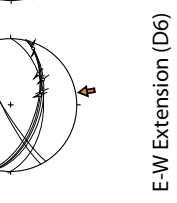
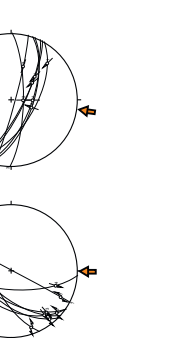
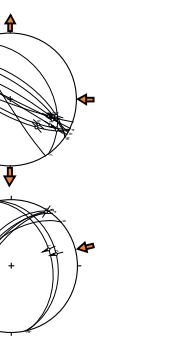
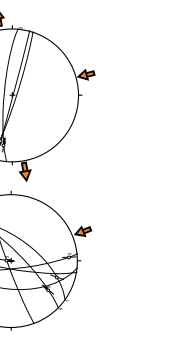
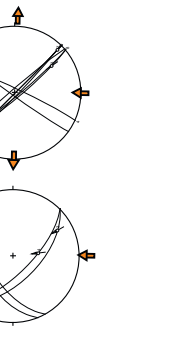
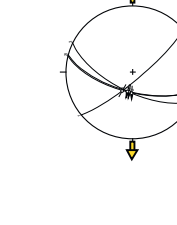
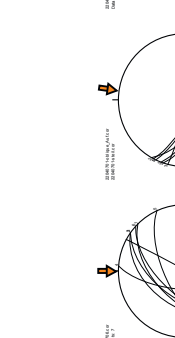
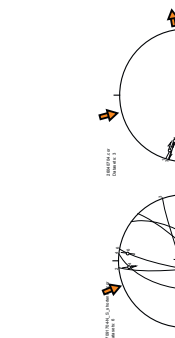
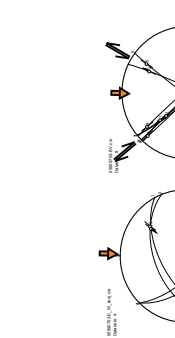
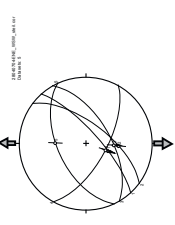
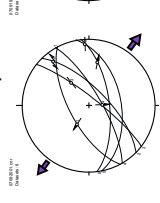
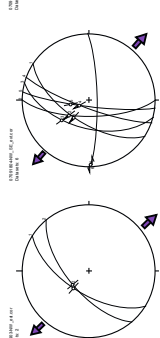
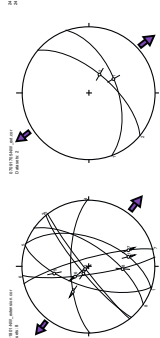
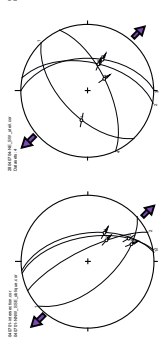
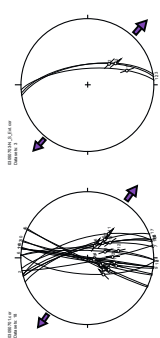
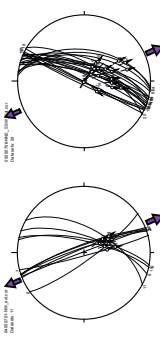
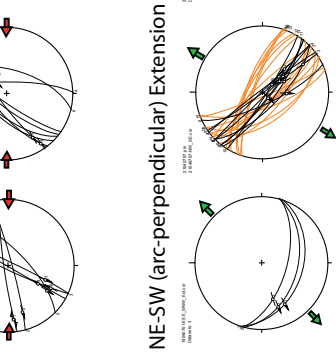
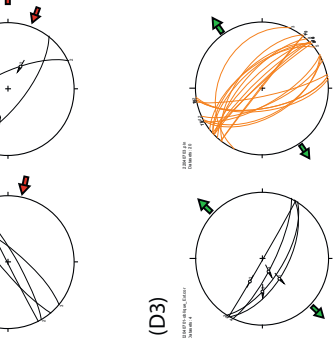
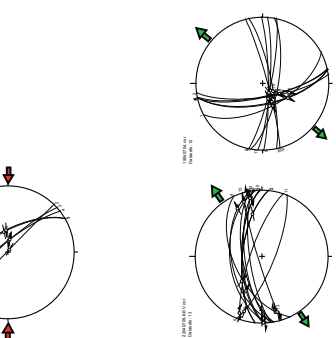
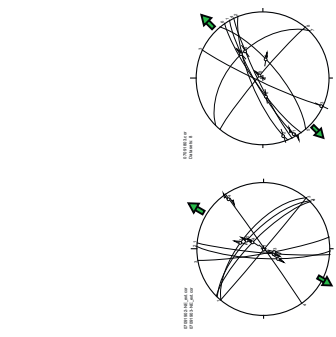
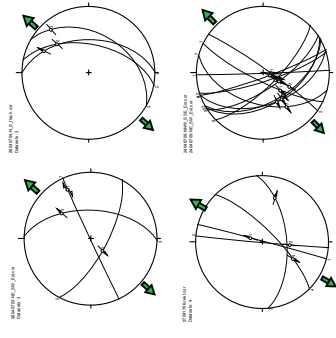
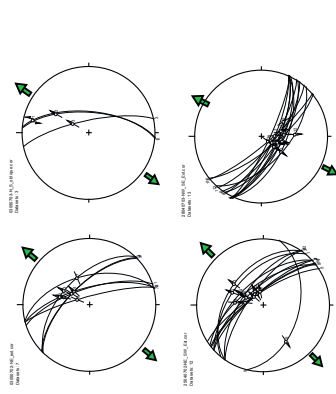
normal/reverse strike - slip quality

(hanging block) very good
good
weak

shear sense not known

orientation of strain axes

shortening extension



A.2 Overview of obtained paleo-strain axes

In the following table, the results of paleo-strain calculations are shown. Outcrop numbers (first row) are identical with those shown in Fig. A.1.

outcrop#	longitude	latitude	D1 #	p axes	t axes	D2 #	p axes	t axes	D3 #	t axes	p axes	D4 #	t axes	p axes	D5 #	p axes	t axes	D6 #	t axes	D7#	p axes	t axes
19040701	78.12070	30.45481	3	71 / 21	331 / 22	0	73 / 16	192 / 50	3	44 / 10	294 / 63	3	331 / 22	71 / 21	7	350 / 9	87 / 51	0	/	0	/	/
19040702	78.27606	30.41508	0	/	/	3	/	/	0	/	/	0	/	/	0	/	/	0	/	0	/	/
19040703	78.37057	30.46882	0	/	/	0	/	/	0	/	/	0	/	/	0	/	/	0	/	3	260 / 81	11 / 5
19040704	78.33035	30.62893	0	/	/	0	/	/	12	230 / 35	/	0	/	/	0	/	/	0	/	0	/	/
20040701	78.45407	30.74397	0	/	/	0	/	/	4	223 / 0	134 / 44	0	/	/	0	/	/	0	/	0	/	/
20040702	78.52449	30.74001	0	/	/	0	/	/	6	20 / 29	218 / 56	0	/	/	0	/	/	0	/	0	/	/
20040703	78.59775	30.77062	0	/	/	0	/	/	6	20 / 29	218 / 56	0	/	/	0	/	/	0	/	0	/	/
20040704	78.61714	30.80161	0	/	/	0	/	/	14	29 / 19	233 / 65	0	/	/	0	/	/	0	/	0	/	/
20040705	78.61859	30.82540	12	212 / 38	/	0	/	/	0	/	/	0	/	/	0	/	/	0	/	0	/	/
20040706	78.69511	30.96257	0	/	/	0	/	/	0	/	/	0	/	/	7	179 / 33	83	7	83	0	/	/
20040709	78.71358	31.01626	0	/	/	0	/	/	0	/	/	5	316 / 17	/	0	/	/	0	/	3	307 / 71	177 / 12
21040702	78.87030	31.02289	0	/	/	0	/	/	0	/	/	9	274 / 4	/	0	/	/	5	101 / 33	0	/	/
21040703	78.85961	31.03503	0	/	/	0	/	/	3	228 / 7	/	7	325 / 21	/	0	/	/	0	/	0	/	/
21040707	78.68610	30.94033	0	/	/	0	/	/	11	211 / 35	/	0	/	/	0	/	/	0	/	0	/	/
21040708	78.67980	30.90364	0	/	/	4	80 / 13	346 / 16	0	/	/	0	/	/	0	/	/	1	283 / 24	4	80 / 13	346 / 16
22040701	78.62694	30.83848	0	/	/	0	/	/	4	223 / 19	/	0	/	/	7	188 / 15	/	0	/	0	/	/
22040703	78.32114	30.61915	0	/	/	6	72 / 25	203 / 55	0	/	/	0	/	/	0	/	/	0	/	0	/	/
22040704	78.28276	30.72437	0	/	/	0	/	/	0	/	/	0	/	/	10	165 / 17	262 / 19	10	290	5	130 / 44	13 / 24
22040705-6	78.26900	30.75800	0	/	/	2	83 / 26	224 / 56	13	236 / 20	/	0	/	/	0	/	/	0	/	0	/	/
22040708	78.25985	30.78649	0	/	/	0	/	/	0	/	/	0	/	/	7	166 / 3	/	0	/	0	/	/
24040702	78.40493	30.93905	0	/	/	0	/	/	0	/	/	0	/	/	0	/	/	8	266 / 19	0	/	/
24040704	78.32721	30.90135	3	35 / 31	/	0	/	/	0	/	/	0	/	/	0	/	/	0	/	0	/	/
24040705	78.26129	30.83654	0	/	/	0	/	/	11	244 / 22	/	0	/	/	0	/	/	0	/	0	/	/
25040701	78.16975	30.79552	13	217 / 12	/	0	/	/	0	/	/	0	/	/	0	/	/	0	/	0	/	/
25040702	78.10778	30.82047	0	/	/	0	/	/	12	42 / 7	261 / 81	0	/	/	0	/	/	0	/	0	/	/
25040703	78.08165	30.87191	0	/	/	0	/	/	0	/	/	0	/	/	0	/	/	0	/	0	/	/
26040703	78.09777	30.94393	0	/	/	0	/	/	3	220 / 3	/	0	/	/	0	/	/	0	/	0	/	/
26040704	78.09184	30.95903	0	/	/	0	/	/	0	/	/	0	/	/	3	345 / 10	/	3	251 / 21	0	/	/
26040706	78.07370	31.04616	0	/	/	0	/	/	0	/	/	2	309 / 7	/	6	190 / 26	/	6	70 / 35	0	/	/
27040701	78.19961	31.07089	0	/	/	0	/	/	3	237 / 26	/	0	/	/	5	194 / 6	/	5	102 / 22	0	/	/
27040702	78.03793	31.01366	5	244 / 12	/	0	/	/	0	/	/	0	/	/	0	/	/	0	/	0	/	/
27040706	77.92197	30.96547	5	48 / 27	/	0	/	/	0	/	/	5	142 / 8	/	0	/	/	0	/	0	/	/
28040701	77.78670	31.09574	0	/	/	5	282 / 9	26 / 50	0	/	/	0	/	/	0	/	/	0	/	0	/	/
28040702	77.73131	31.18885	0	/	/	0	/	/	0	/	/	0	/	/	0	/	/	0	/	2	253 / 36	158 / 6
28040703	77.98569	31.25810	0	/	/	0	/	/	13	206 / 21	/	0	/	/	0	/	/	9	267 / 2	5	248 / 70	173 / 2
28040704	77.96377	31.25299	0	/	/	0	/	/	3	235 / 8	/	0	/	/	0	/	/	4	285 / 21	0	/	/
28040705	77.91067	31.23785	0	/	/	7	63 / 18	173 / 5	0	/	/	3	321 / 8	/	0	/	/	3	104 / 7	5	311 / 71	175 / 21
29040705	77.56186	31.10986	0	/	/	0	/	/	0	/	/	6	333 / 2	242 / 62	8	190 / 36	69 / 37	0	/	0	/	/
30040701	77.40797	31.35506	0	/	/	9	112 / 9	1 / 18	0	/	/	0	/	/	0	/	/	0	/	9	112 / 9	1 / 18
30040702	77.38814	31.38626	0	/	/	0	/	/	7	247 / 22	/	0	/	/	0	/	/	5	288 / 0	0	/	/
30040704	77.43003	31.45116	0	/	/	0	/	/	0	/	/	0	/	/	6	15 / 12	269 / 49	5	88 / 29	0	/	/
1050701	77.36878	31.55654	0	/	/	9	253 / 19	335 / 1	6	42 / 27	236 / 68	0	/	/	0	/	/	0	/	0	/	/
1050702	77.30112	31.66866	0	/	/	8	270 / 25	15 / 30	0	/	/	0	/	/	0	/	/	0	/	0	/	/
1050704	77.25708	31.70962	0	/	/	0	/	/	0	/	/	0	/	/	4	355 / 25	/	4	261 / 7	0	/	/
1050705	77.21844	31.72493	0	/	/	3	280 / 46	163 / 23	0	/	/	0	/	/	0	/	/	0	/	3	280 / 46	163 / 23
2050701	77.15237	31.90291	0	/	/	4	105 / 39	6 / 9	6	233 / 36	8 / 44	0	/	/	0	/	/	0	/	4	105 / 39	6 / 9
2050702	77.17778	31.91356	4	50 / 16	309 / 54	0	/	/	0	/	/	0	/	/	4	356 / 38	98 / 15	4	98 / 15	0	/	/
2050703	77.17681	31.93284	0	/	/	0	/	/	5	220 / 38	76 / 38	0	/	/	0	/	/	0	/	0	/	/
2050704	77.21518	31.97569	0	/	/	0	/	/	5	54 / 32	235 / 57	0	/	/	0	/	/	0	/	0	/	/
2050705	77.22130	31.98230	0	/	/	0	/	/	6	216 / 14	341 / 59	0	/	/	0	/	/	0	/	0	/	/
2050706	77.28911	32.00659	0	/	/	0	/	/	0	/	/	0	/	/	0	/	/	7	284 / 24	0	/	/
2050707	77.34034	32.02325	0	/	/	0	/	/	8	48 / 30	250 / 57	0	/	/	0	/	/	0	/	0	/	/

outcrop#	longitude	latitude	D1 #	p axes	t axes	D2 #	p axes	t axes	D3 #	t axes	p axes	D4 #	t axes	p axes	D5 #	p axes	t axes	D6 #	t axes	D7#	p axes	t axes
3050701	77,40971	32,00523	0	/	/	0	/	/	0	/	/	18	115 / 37	248 / 43	0	/	/	0	/	0	/	/
3050702	77,39313	32,00574	0	/	/	0	/	/	7	50 / 3	/	0	/	/	0	/	/	4	77 / 30	0	/	/
3050703	77,36820	32,01985	0	/	/	0	/	/	3	61 / 11	313 / 48	4	109 / 2	207 / 45	0	/	/	2	88 / 0	0	/	/
3050704	77,35488	32,02622	7	54 / 27	312 / 27	0	/	/	2	41 / 22	266 / 60	7	312 / 27	54 / 27	0	/	/	0	/	0	/	/
3050706	77,34242	32,02627	10	41 / 34	240 / 53	0	/	/	0	/	/	0	/	/	0	/	/	3	91 / 18	0	/	/
4050701	77,48505	32,00190	0	/	/	0	/	/	0	/	/	11	148 / 0	/	0	/	/	11	100 / 31	0	/	/
5050702	77,25379	32,03003	6	225 / 12	/	0	/	/	0	/	/	0	/	/	7	6 / 34	264 / 10	7	264 / 10	0	/	/
5050703	77,25123	32,02530	0	/	/	0	/	/	0	/	/	0	/	/	12	192 / 5	/	0	/	0	/	/
5050704	77,24702	32,02317	0	/	/	0	/	/	0	/	/	0	/	/	2	7 / 23	272 / 13	2	272 / 13	0	/	/
5050706	77,24570	32,01802	0	/	/	0	/	/	0	/	/	17	119 / 5	223 / 67	0	/	/	3	283 / 41	0	/	/
6050701	77,12543	32,08238	0	/	/	0	/	/	11	217 / 31	78 / 50	0	0 / 0	/	6	158 / 25	297 / 58	0	/	0	/	/
6050703	77,17968	32,17817	0	/	/	7	82 / 40	196 / 26	0	/	/	0	/	/	0	/	/	0	/	7	196 / 26	82 / 40
6050704	77,18020	32,26508	0	/	/	4	85 / 15	309 / 69	16	256 / 42	127 / 35	0	/	/	0	/	/	0	/	0	/	/
6050706	77,17158	32,13167	0	/	/	0	/	/	0	/	/	7	128 / 33	5 / 46	0	/	/	0	/	0	/	/
7050701	77,13293	32,36426	4	226 / 0	315 / 49	0	/	/	0	/	/	0	/	/	0	/	/	0	/	0	/	/
7050702	77,14959	32,32464	0	/	/	0	/	/	9	39 / 13	307 / 7	0	/	/	0	/	/	0	/	0	/	/
7050704	77,17669	32,30814	2	75 / 36	225 / 50	0	/	/	0	/	/	0	/	/	0	/	/	9	91 / 11	0	/	/
7050705	77,17587	32,27122	0	/	/	0	/	/	0	/	/	8	117 / 23	299 / 68	0	/	/	0	/	0	/	/
8050701	77,23490	32,36088	0	/	/	0	/	/	10	246 / 12	55 / 77	0	/	/	0	/	/	6	260 / 0	0	/	/
8050703	77,22262	32,35806	0	/	/	0	/	/	12	216 / 12	273 / 83	0	/	/	0	/	/	0	/	0	/	/
9050701	77,20133	32,33563	0	/	/	0	/	/	7	34 / 31	249 / 54	0	/	/	0	/	/	0	/	0	/	/
9050702	77,18810	32,31638	0	/	/	0	/	/	0	/	/	0	/	/	0	/	/	0	/	0	/	/
7090804	78,05158	32,25156	0	/	/	0	/	/	0	/	/	0	/	/	0	/	/	8	260 / 6	6	77 / 2	165 / 61
7090901	78,06435	32,26617	0	/	/	4	102 / 14	6 / 19	14	235 / 11	33 / 79	0	/	/	0	/	/	3	265 / 1	6	276 / 26	176 / 21
7091001	78,24001	32,15294	0	/	/	0	/	/	0	/	/	4	143 / 35	306 / 56	0	/	/	2	267 / 10	0	/	/
7091704	78,23032	32,04775	0	/	/	0	/	/	0	/	/	0	/	/	5	354 / 3	99 / 9	0	/	0	/	/
7091705	78,19108	32,09968	0	/	/	0	/	/	0	/	/	0	/	/	0	/	/	12	93 / 2	0	/	/
7091802	78,09633	32,04679	7	229 / 8	318 / 10	0	/	/	0	/	/	7	318 / 10	229 / 8	0	/	/	0	/	0	/	/
7091803	78,13397	32,06894	0	/	/	0	/	/	0	/	/	0	/	/	0	/	/	0	/	0	/	/
7091804	77,92581	32,32887	0	/	/	0	/	/	0	/	/	5	298 / 20	79 / 66	0	/	/	4	278 / 22	0	/	/
7091804	77,92581	32,32887	0	/	/	0	/	/	0	/	/	12	117 / 3	29 / 2	0	/	/	0	/	0	/	/
7091902	77,93864	32,42567	2	234 / 8	145 / 1	0	/	/	4	38 / 29	230 / 60	2	145 / 1	234 / 8	0	/	/	4	103 / 6	0	/	/
7092001	77,99229	32,36305	0	/	/	0	/	/	0	/	/	6	314 / 3	33 / 59	0	/	/	0	/	0	/	/
6042401	78,27573	31,52461	0	/	/	0	/	/	0	/	/	0	/	/	0	/	/	0	/	0	/	/
6042402	78,27968	31,52348	0	/	/	0	/	/	0	/	/	0	/	/	0	/	/	0	/	0	/	/
6042403	78,28447	31,53138	0	/	/	0	/	/	0	/	/	0	/	/	0	/	/	0	/	0	/	/
6042404	78,28546	31,53533	0	/	/	0	/	/	0	/	/	0	/	/	0	/	/	0	/	0	/	/
60424	78,28133	31,52870	0	/	/	0	/	/	0	/	/	0	/	/	0	/	/	18	101 / 35	0	/	/
6052501	78,27037	31,56521	4	55 / 24	323 / 5	0	/	/	0	/	/	4	323 / 5	55 / 24	0	/	/	2	269 / 20	0	/	/
6052502	78,27023	31,57058	0	/	/	0	/	/	0	/	/	0	/	/	7	155 / 24	272 / 45	5	106 / 27	0	/	/
6052503	78,27601	31,57198	0	/	/	0	/	/	0	/	/	20	125 / 17	243 / 56	0	/	/	0	/	0	/	/
6052504	78,27911	31,57589	0	/	/	0	/	/	0	/	/	17	127 / 9	230 / 55	0	/	/	0	/	0	/	/
6051702	78,33158	31,60380	0	/	/	0	/	/	0	/	/	28	112 / 8	219 / 64	10	161 / 20	258 / 4	11	279 / 5	0	/	/
6051701	78,31432	31,60029	0	/	/	0	/	/	0	/	/	35	291 / 1	204 / 66	0	/	/	0	/	0	/	/
6052004	78,44144	31,60186	0	/	/	0	/	/	0	/	/	0	/	/	0	/	/	0	/	0	/	/
6052001	78,44582	31,57812	0	/	/	0	/	/	0	/	/	0	/	/	0	/	/	0	/	0	/	/
6052002	78,44863	31,58187	0	/	/	0	/	/	0	/	/	0	/	/	0	/	/	0	/	0	/	/
6052003	78,44850	31,58645	0	/	/	0	/	/	0	/	/	0	/	/	0	/	/	0	/	0	/	/
60520	78,44610	31,58707	0	/	/	16	83 / 13	176 / 9	0	/	/	21	155 / 12	272 / 65	0	/	/	0	/	16	83 / 13	176 / 9
6052101	78,44826	31,59093	0	/	/	0	/	/	0	/	/	0	/	/	0	/	/	0	/	0	/	/
6052102	78,44651	31,59528	0	/	/	0	/	/	0	/	/	0	/	/	0	/	/	0	/	0	/	/
60521	78,44739	31,59311	0	/	/	0	/	/	6	238 / 0	151 / 7	18	321 / 1	224 / 74	0	/	/	0	/	0	/	/

outcrop#	longitude	latitude	D1 #	p axes	t axes	D2 #	p axes	t axes	D3 #	t axes	p axes	D4 #	t axes	p axes	D5 #	p axes	t axes	D6 #	t axes	D7 #	p axes	t axes
6043002	78.58364	31.98882	0	/	/	0	/	/	0	/	/	0	/	/	2	154 / 35	/	0	/	0	/	/
6043005	78.57695	31.99153	0	/	/	7	285 / 8	192 / 16	0	/	/	0	/	/	0	/	/	0	/	7	285 / 8	192 / 16
6050803	78.60229	31.92807	0	/	/	3	253 / 21	152 / 27	4	242 / 30	114 / 48	13	301 / 13	41 / 33	0	/	/	0	/	3	253 / 21	152 / 27
6051303	78.59737	31.93947	0	/	/	0	/	/	0	/	/	5	296 / 29	/	0	/	/	0	/	0	/	/
6051501	78.59373	31.87714	0	/	/	3	261 / 25	159 / 23	6	244 / 8	334 / 5	0	/	/	0	/	/	5	282 / 16	3	261 / 25	159 / 23
6051502	78.59613	31.87346	0	/	/	6	293 / 3	24 / 22	0	/	/	0	/	/	0	/	/	7	274 / 25	6	293 / 3	24 / 22
6051503	78.59700	31.87200	0	/	/	0	/	/	0	/	/	0	/	/	0	/	/	4	105 / 15	0	/	/
6051504	78.59804	31.87046	0	/	/	5	75 / 24	168 / 5	0	/	/	0	/	/	0	/	/	4	104 / 14	5	75 / 24	168 / 5
8082001	78.46018	30.99477	7	59 / 9	169 / 59	0	/	/	0	/	/	0	/	/	0	/	/	0	/	0	/	/
8082002	78.45680	30.99078	7	32 / 18	201 / 71	0	/	/	2	256 / 12	158 / 35	0	/	/	0	/	/	3	260 / 0	0	/	/
8082003	78.43171	30.97142	0	/	/	0	/	/	6	58 / 13	235 / 77	0	/	/	0	/	/	0	/	0	/	/
8082102	78.41328	30.95250	0	/	/	0	/	/	3	56 / 7	160 / 65	0	/	/	0	/	/	0	/	0	/	/
8082201	78.18127	30.80038	0	/	/	0	/	/	0	/	/	0	/	/	2	164 / 12	261 / 30	2	261 / 30	7	133 / 80	16 / 3
8082202	78.16958	30.79580	0	/	/	0	/	/	0	/	/	0	/	/	8	346 / 8	61 / 35	8	61 / 35	0	/	/
8082203	78.11713	30.78120	5	54 / 8	148 / 3	0	/	/	0	/	/	5	148 / 3	54 / 8	0	/	/	0	/	0	/	/
8082204	78.10062	30.76225	3	34 / 56	213 / 34	0	/	/	3	230 / 25	345 / 46	0	/	/	0	/	/	0	/	0	/	/
8082205-6	78.07407	30.70088	0	/	/	0	/	/	3	246 / 25	337 / 2	0	/	/	3	343 / 9	252 / 22	3	252 / 22	0	/	/
RT02-93	78.63748	31.77606	0	/	/	0	/	/	0	/	/	0	/	/	0	/	/	32	99 / 13	0	/	/
RT02-91	78.53986	31.70875	0	/	/	0	/	/	0	/	/	23	326 / 4	61 / 81	0	/	/	0	/	0	/	/
RT02-87	78.44545	31.66744	0	/	/	0	/	/	0	/	/	19	129 / 1	231 / 86	0	/	/	3	103 / 6	0	/	/
Jakhri_2oct	77.72832	31.50849	0	/	/	0	/	/	15	17 / 15	235 / 71	0	/	/	0	/	/	7	260 / 14	0	/	/
Lingti_28sept	78.17899	32.11821	0	/	/	0	/	/	0	/	/	0	/	/	0	/	/	8	89 / 1	3	45 / 69	192 / 18
Luhri_2oct	77.42825	31.34403	0	/	/	4	298 / 24	32 / 10	4	54 / 25	238 / 65	0	/	/	0	/	/	11	261 / 2	4	298 / 24	32 / 10
NARK1_2oct	77.35648	31.35287	0	/	/	0	/	/	13	220 / 16	42 / 74	0	/	/	0	/	/	5	277 / 2	0	/	/
Shim_1oct	77.17933	31.10402	0	/	/	0	/	/	19	46 / 4	180 / 86	0	/	/	0	/	/	0	/	0	/	/

Appendix B

$^{40}\text{Ar}/^{39}\text{Ar}$ data

The complete data set for $^{40}\text{Ar}/^{39}\text{Ar}$ ages presented in Fig. 3.7 and Table 3.1 is given in the following table. Both samples have been taken at the same location in order to assure the reproductibility of the resultant ages (see Fig. 3.8B for sample location). They yield both well-constrained plateau ages of 16.3 and 16.9 Ma, respectively (Fig. 3.7). The whole $^{40}\text{Ar}/^{39}\text{Ar}$ dating procedure was carried out by B. Hacker at the University of California in Santa Barbara. Details of the procedure are given in section 3.3.3.

Abbreviations: T: Temperature ($^{\circ}\text{C}$); t: heating time (minutes); 40/39: ratio corrected for blanks, decay, and interference; 37/39: corrected ratio; 36/39: corrected ratio; $^{40}\text{Ar}^*$: moles ($\times 10^{-13}$), radiogenic ^{40}Ar ; ^{39}K : (moles ($\times 10^{-13}$) inferred from ^{39}Ar ; %rad: radiogenic fraction of corrected ^{40}Ar ; K/Ca: inferred K/Ca ratio.

T	t	40/39	37/39	36/39	40Ar*	39K	%rad	K/Ca	Age (Ma)	$\pm 1\sigma$
600	15	100.3733	0.002	0.3238	0.149	0.032	4.7	248	17.1	1.40
650	15	64.6432	0.0036	0.2028	0.344	0.073	7.3	136	17.2	0.67
700	15	88.46	0.0051	0.2823	0.667	0.132	5.7	97	18.4	1.41
700	15	35.7989	-0.0008	0.1057	0.379	0.083	12.7	>10000	16.6	0.41
750	15	48.6781	0.0064	0.1488	1.023	0.218	9.7	76	17.1	0.81
760	12	18.6204	0.0006	0.0472	0.723	0.154	25.2	824	17.1	0.23
790	12	16.727	-0.0003	0.041	1.981	0.431	27.5	>10000	16.8	0.11
820	12	7.755	-0.0005	0.0111	4.959	1.105	57.9	>10000	16.4	0.10
820	12	5.2819	0.0002	0.0027	2.75	0.613	84.9	2343	16.4	0.04
850	12	5.4128	-0.0001	0.0032	3.957	0.885	82.6	>10000	16.3	0.03
880	12	5.4571	0.0002	0.0034	3.753	0.841	81.8	2729	16.3	0.03
910	12	5.9128	-0.0002	0.0049	2.966	0.664	75.5	>10000	16.3	0.04
940	12	6.5113	-0.0003	0.0069	2.117	0.474	68.7	>10000	16.3	0.05
970	12	6.6363	-0.0005	0.0074	1.601	0.359	67.2	>10000	16.3	0.06
1000	12	6.6281	0.0003	0.0073	1.497	0.335	67.3	1929	16.3	0.07
1020	12	6.5286	-0.0002	0.0069	1.337	0.299	68.6	>10000	16.3	0.07
1050	12	6.4259	0.0001	0.0066	1.791	0.401	69.6	3283	16.3	0.06
1090	12	5.997	-0.0001	0.0051	3.249	0.723	75.0	>10000	16.4	0.03
1130	12	4.9619	0	0.0017	1.33	0.299	89.7	16749	16.2	0.06
1160	12	4.7207	0.0007	0.0009	0.559	0.126	94.3	739	16.2	0.12
1190	12	4.6272	-0.0005	0.0005	0.313	0.07	96.8	>10000	16.3	0.20
1230	12	4.6636	-0.0015	0.0008	0.194	0.044	95.2	>10000	16.2	0.33
1300	12	4.5595	-0.0073	0.0004	0.129	0.029	97.3	>10000	16.2	0.49

Table B.1: Complete $^{40}\text{Ar}/^{39}\text{Ar}$ data set for sample B270901-3, $J=0.002031 \pm 0.1\%$

T	t	40/39	37/39	36/39	40Ar*	39K	%rad	K/Ca	Age (Ma)	$\pm 1\sigma$
720	14	29.743	0.003	0.084	0.328	0.067	16.6	166	17.9	0.45
740	14	17.9216	0.0042	0.0444	0.387	0.081	26.8	118	17.5	0.31
760	14	15.4229	0.0052	0.036	0.679	0.141	31.1	94	17.5	0.21
790	14	8.0728	0.0006	0.0113	2.543	0.536	58.8	887	17.3	0.06
820	14	5.6367	0.0007	0.0032	4.495	0.96	83.0	700	17	0.03
850	14	5.065	0.0007	0.0014	3.478	0.749	91.7	703	16.9	0.02
880	14	5.0979	0.0003	0.0016	2.404	0.518	91.0	1500	16.9	0.03
910	14	5.3357	0.0011	0.0024	1.578	0.341	86.7	456	16.8	0.05
940	14	5.5874	0.0006	0.0032	1.118	0.241	83.2	849	16.9	0.07
960	14	5.532	0	0.003	0.811	0.175	83.8	>10000	16.9	0.09
980	14	5.5167	-0.0008	0.003	0.734	0.158	84.0	>10000	16.9	0.10
1000	14	5.4825	0.0012	0.003	0.715	0.155	84.1	406	16.8	0.10
1020	14	5.4358	0.002	0.0027	0.773	0.167	85.1	243	16.8	0.10
1050	14	5.381	0.0014	0.0026	1.219	0.265	85.5	357	16.8	0.06
1080	14	5.1338	-0.0001	0.0017	1.611	0.349	90.0	>10000	16.8	0.05
1110	14	4.881	0.0007	0.0009	0.799	0.173	94.6	729	16.8	0.09
1140	14	4.7997	-0.0002	0.0005	0.385	0.083	96.8	>10000	16.9	0.18
1170	14	4.7937	0.0024	0.0003	0.237	0.05	98.4	201	17.2	0.29
1200	14	4.821	0.0103	0.0002	0.172	0.036	98.7	48	17.3	0.39

Table B.2: Complete $^{40}\text{Ar}/^{39}\text{Ar}$ data set for sample B270901-4, $J=0.002029 \pm 0.1\%$

Appendix C

Reports on flash floods in the Sutlej Valley

The following excerpts of reports on natural disasters in the Kinnaur describe the flash floods that occurred in the Sutlej Valley in 2000 and 2005. In addition, damages and losses are also reported. Finally, the known cause for the 2005 flash flood, a outburst of a landslide-dammed lake along the Pare Chu River, a tributary of the Spiti River, is documented.

The reports are downloaded from the following webpages:

- Himachal Pradesh State Disaster Management Authority
<http://hpsdma.nic.in/disastermanagement/KNRDDMPfinal.pdf>
- United Nations Development Programme in corporation with the European Commission of Humanitarian Aid
<http://www.managingclimaterisk.org/document/India-Preparatory-Assessment-Report-GLOF-Initiative.pdf>



*Empowered lives.
Resilient nations.*

DISTRICT DISASTER MANAGEMENT PLAN
OF
DISTRICT KINNAUR, HIMACHAL PRADESH

PREPARED BY: -

**DISTRICT DISASTER MANAGEMENT AUTHORITY
(DDMA) KINNAUR**

UNDER

**{The Government of India-UNDP Disaster Risk Reduction
(DRR) Programme (2009-12)}**

District Disaster Management Plan 2012, Kinnaur (H. P.)

IV. Flash Floods, Cloudburst and GLOFs

Some of the important floods in the District: -

- i) **31st July and 1st August 2000 in Satluj valley.** Increase in water level of Satluj up to 60 feet above the normal level. The flash flood was termed as the one that occurs once in 61,000 years. Widespread damage in the valley right from its confluence with Spiti river near Khab to downstream areas. Extensive damage to 200 Km of NH-22, washed away 20 bridges, 22 Jhulas and badly damaged 12 bridges. About 1,000 irrigation, sewerage, flood protection and water supply schemes were badly damaged. 135 people and 1673 cattle lost their lives. The total estimated loss was to the tune of Rs. 1466.26 crore.

ii) **Pareechhu Lake Outburst, 2005**

- Flash flood in Satluj river due to breach in the Parechu lake in Tibetan catchment on 26th June 2005
- Washed away the NH-22 at a number of places, 10 bridges, 11 ropeways washed away, 15 motor able bridges and 8 jeep able and footbridges damaged/affected, 10 Km stretch of NH-22 between Wangtoo and Samdo was washed away, and various link roads were damaged.
- Total loss estimated to the government as well as public property was some Rs. 610 crore.

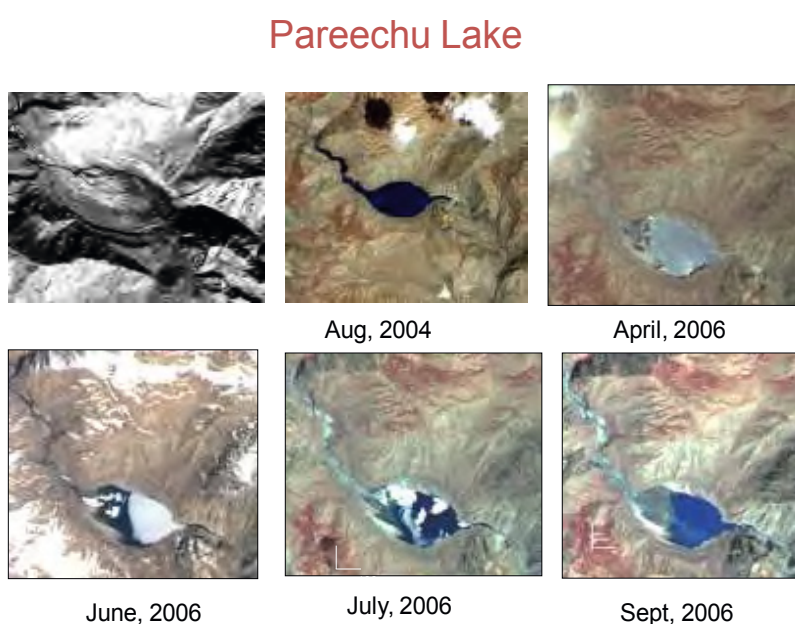


Figure 17: Pareechu 2005

Table 9: Some of the devastating Floods, which caused heavy damage to Private as well as Public Property in Kinnaur District.

Prominent Flash Floods.	History of Damage Occurred
8 July 1973	Lake formed by the blockage of Satluj river due to Nathpa rock fall damaged Sanjay powerhouse, loss of about Rs. 45 million estimated.
19 Jan. 1975	In Satluj basin two blockages were observed in Spiti valley. One on Parechu River between Sumdo and Kaurik due to landslide created by 19 Jan. 1975 earthquake, which occurred along the Sumdo-Kaurik fault. Blockage was 60m in height and 150m in length created temporary lake. In march this lake burst causing flash floods in Spiti valley

District Disaster Management Plan 2012, Kinnaur (H. P.)

<p>On 29th Sept. 1988 (2.30 a.m.) a flash flood occurred due to cloud burst in Soldang Khad.</p>	<p>Caused heavy loss of life and property in the Soldng village.</p> <ul style="list-style-type: none"> • Washed away the Bhabanagar water works. • Washed away 2 Km of NH-22 across Soldan Khad. • Created landslides along the eastern slopes of Soldan Khad and damaged road to Ponda. • Lake was formed on the Satluj river near conference. • Block stopped the flow of Satluj river for about 30 minutes and created a temporary lake having dimensions roughly about 6000 m long. 200-250 m wide and 25-30 m deep extending up to Wangtoo Bridge. • Lake water entered Sanjay Vidut Pariyojna and damaged the Power House.
<p>31 July and 2 August 1991</p> <p>24 Feb 1993</p> <p>4th and 5th September</p>	<p>Cloudburst and flash flood along Soldan Khad in Satluj valley killed 32 people, 15 houses, 35 bigha agriculture land, 600 apple trees, 2Km of road of NH 22 and 20 m bridge on Soldan Khad washed away. Agriculture land along Leo village situated downstream.</p> <p>Flood washed away 15 houses, 35 bigha of agriculture land and about 600 apple trees in Soldang village.</p> <p>Satluj river blocked twice due to major landslide and rock fall near Jhakri and Nathpa, damaging NH-22.</p> <p>Another flash flood occurred in two phases along Duling Khad on 4th and 5th September causing extensive damage in Tapri, district Kinnaur.</p>
<ul style="list-style-type: none"> • First flash flood occurred on 4th September 1954 at 2 p.m. After cloudbursts in the upper catchments of Duling and damaged the PWD rest house. • Another flood came at 6 a.m. and 9 a.m. on 5th Sept. 1995 bursting the lake formed during the previous cloudbursts. 	<ul style="list-style-type: none"> • 32 people and 35 cattle lost their lives. • Huge debris formed a fan along Satluj and formed a take partially blocking the Satluj • Flash flood caused heavy damage due to change in course of Satluj from left to right bank increased the tow and lateral erosion at Tapri. • Washed away 19 houses, HRTC workshop along with 3 buses. • Change in course is still causing tow erosion to NH-22.
<p>4-5 Sept. 1995</p>	<p>Flash flood along Panwi Khad in Satluj valley washed away 19 houses, 3 buses, HRTC workshop and damaged HPPWD rest house at Tapri.</p>
<p>August 1997</p>	<p>Cloudburst and flash flood along Satluj river killed 19 people, 464 cattle, 105 houses damaged, 10 cattle sheds and 39-hectare agriculture land. Total loss was estimated Rs.672.9 million.</p>
<p>Flash floods in the night of 31st July and 1st August 2000 in Satluj valley.</p>	<p>Flash floods in the Satluj valley resulting in the increase in water level of Satluj an up to 60 feet above the normal level. The flash flood was termed as the one that occurs once in 61,000 years. Widespread</p>

District Disaster Management Plan 2012, Kinnaur (H. P.)

	<p>damage in the valley right from its confluence with Spiti river near Khab to downstream areas. Extensive damage to 200 Km of NH-22, washed away 20 bridges, 22 Jhulas and badly damaged 12 bridges. About 1000 irrigation, sewerage, flood protection and water supply schemes were badly damaged. Expensive damage to hydel projects including NJPC. 135 people and 1673 cattle lost their lives. The total estimated loss was to the tune of Rs. 1466.26 crore.</p>
<p>Flash flood in Satluj river due to breach in the Parachoo lake in Tibetan catchment on 26th June 2005</p>	<p>Extensive damage as a result of risen water level of Satluj river due to breach in Parachoo lake formed in Tibet catchments. Washed away the NH-22 at a number of places, 10 bridges, 11 ropeways washed away, 15 motor able bridges and 8 jeep able and footbridges damaged/affected, 10 Km stretch of NH-22 between Wangtoo and Samdo was washed away, and various link roads were damaged. Total loss estimated to the government as well as public property was some Rs. 610 crore.</p>

(Source: Bhandari, 1988; Sah et al, 1996; Sah and Mazari 1998; Sah and Bist, 1988; Paul et al, 2000, Revenue Department, Govt. of Himachal Pradesh).



Figure 18: Picture showing damage to roads



Figure 19: 2005 Floods- Loss of Kharo Bridge



Figure 20: 2005 Flood: Damage to Leo Village



Figure 21: Loss of road and landslides

Capacity Building for Disaster Risk Reduction Regional Glacial Lake Outburst Floods (GLOF) Risk Reduction in the Himalayas

Preparatory Assessment Study Report Sutlej Basin - Himachal Pradesh India

EUROPEAN COMMISSION



Humanitarian Aid





GLOF/FLASH FLOOD INCIDENTS IN THE SUTLEJ VALLEY

The Sutlej Basin is a densely populated river basin in Himachal Pradesh. It is the lifeline for the state in terms of economic activity, power generation, agriculture, horticulture, livestock and vegetable produce.

In the last two decades, the Sutlej valley in eastern Himachal Pradesh has witnessed a substantial increase in the number of flash flood events. The accentuating impact of these events can be attributed to many reasons, including cases of river damming outburst, frequent cloud burst incidents or suspected cases of GLOFs. Increasing anthropogenic pressure, including population growth, seasonal migration to the valleys, exploitation of hydropower potential and changing land use patterns, are some of the other reasons for an increase in the impact from recent flash floods. The combination of natural hazards and anthropogenic changes in the area has resulted in increased incidents of inter-related landslides and flash floods.

These flash floods cause massive devastation in downstream areas in terms of loss of human life, livestock, horticultural and agricultural land, and damage to roads, bridges and houses. Sometimes complete communities get washed away, as happened in the year 2000 when the Sutlej washed people along with their possessions downstream into the Govind Sagar Reservoir.

Formation and dimension

Though flash floods in the Sutlej basin are a recurrent feature, two of them stand out

because of the sheer volume of water that suddenly discharged and the socio-economic impact it had. These were the flash floods that occurred in 2000 and 2005.

Flash flood of 2000

On the night of 1st August, 2000, a 50-foot high wall of water in the Sutlej River swept away around 200 people from Kinnaur and Shimla districts. There was extensive damage caused by the sudden surge of water. Roads and bridges, some of them dating back at least 60 years, were washed away with the waters. There was substantial loss to human life and livelihoods. The Naptha-Jhakri Power Corporation (NJPC) suffered huge losses as a result of the flash floods and there was a substantial delay in the commissioning of the power project.⁷

In the last two decades, the Sutlej valley in eastern Himachal Pradesh has witnessed a substantial increase in the number of flash flood events. The accentuating impact of these events can be attributed to many reasons

Kinnaur was the worst affected district in Himachal Pradesh in this flash flood and relief had to be air lifted in to the cut off district for a period of time. According to a UN OCHA report dated 22nd August, 2000,⁸ the Central Government in India conducted an assessment of the situation on 7th and 8th August,

2000 and released INR 1 billion to the state government in relief funds.

Flash flood of 2005

Parechu, a tributary of the Sutlej enters Himachal Pradesh from Tibet. At the beginning of August 2004, a 230 hectare size lake was formed on the river, inside Tibet, 35 km from the Himachal Pradesh border. China claimed

⁷ HP seeks 1500 cr for flood damage, The Tribune; <http://www.tribuneindia.com/2000/20000812/himachal.htm#1>

⁸ <http://www.reliefweb.int/rw/rwb.nsf/AllDocsByUNID/0c32c79dd3e9a542852569430067da52>



that this lake was formed due to a sudden landslide leading to blockage of the river, at an inaccessible and high altitude site.⁹ Early warning of the formation of the lake was given by China, unlike the lack of information exchanged in the year 2000 flash floods which were also trans-boundary in nature.

The lake finally burst in June 2005. Reports claimed that around 5,000 people were evacuated by the government along the 200 km long stretch of the Sutlej as a precautionary measure.¹⁰ The press also claimed that the dam might have burst due to the increased water pressure which accumulated due to snow melting caused by above normal temperatures in that period.¹¹

River dam outbursts, such as the Parechu incident of 2005, have led to widespread destruction. There were complete tracts of land, including horticultural fields that were washed away by the surge of water, which at places was more than 25 metres in height.¹²

Differential impact

In comparative terms of damage, the 2005 flash flood was less harmful from the one in the year 2000. This was even though the volume of water was higher in 2005 and led to the destruction of roads, bridges and houses in Himachal Pradesh with an estimated US\$186 million worth of damage.¹³ The reason behind this, as evident from our interactions in the region, is because the year 2000 flash flood paved a wider basin for

the flow of water that came in the 2005 flood. Moreover, the 2000 flash flood came without any prior warning and in the middle of the night, created a greater impact. In the 2005 situation, the flash flood was expected, though the exact time and date was unknown. As it happened, the flood came in the middle of the day and that too when local people were tired of waiting for it to come for almost a year. As a result the national, state and district administration's state of preparedness was much greater in 2005 as they had the previous experience of the 2000 flash flood.

The satellite images below show the reduced size of Parechu lake one month after the flood, in July 2005, and size of the lake before it burst in September 2004.



July 2, 2005



September 1, 2004

Source: NASA; Images of the Parechu River damming in Tibet¹⁴

⁹ http://www.ipcs.org/China_east_asia_articles2.jsp?action=showView&kValue=1582&keyArticle=1009&issue=1009&status=article&mod=a

¹⁰ AFP; <http://www.terradaily.com/news/india-05zb.html>

¹¹ AFP; <http://www.terradaily.com/2005/050627184318.juof4o4e.html>

¹² <http://www.mapsofindia.com/maps/mapinnews/2005/flood-in-sutlej-himachal-pradesh.html>

¹³ IRI-Columbia; <http://iri.columbia.edu/climate/cid/Jul2005/impacts.html>

¹⁴ http://earthobservatory.nasa.gov/Newsroom/NewImages/images.php3?img_id=16973

Hiermit versichere ich an Eides Statt, diese Arbeit selbständig verfasst und keine anderen als die angegebenen Quellen und Hilfsmittel benutzt zu haben.

Potsdam, den 03. Januar 2013